A first look: understanding the ground reaction forces experienced by pectoral fins of *Polypterus senegalus* during terrestrial locomotion

Gurjit Bhamra

Thesis submitted to the University of Ottawa
in partial fulfillment of the requirements for the
Master of Science degree in Biology.

Department of Biology
Faculty of Science
University of Ottawa

ABSTRACT

Polypterus senegalus, an extant member of the ray-finned fishes, can both swim in water and walk overland. Both environments impose different locomotor requirements on *Polypterus* fins. In an aquatic environment, forward propulsion is largely generated through oscillations of the pectoral fins working in sync with each other. On land, the pectoral fins are engaged in a contralateral gait, and are involved in lifting the body off the ground while simultaneously balancing the body. *Polypterus* have been shown to undergo behavioural, anatomical, and physiological changes during both short- and long-term exposure to land. Differences in force environments and locomotor behaviour between aquatic and terrestrial environments are hypothesized to be the cause of these plastic changes observed in the musculoskeletal tissues of *Polypterus*. Despite these observable changes, it is unclear exactly how the pectoral fins are experiencing ground reaction forces (GRF) during terrestrial locomotion. By measuring and quantifying force production during walking in *Polypterus*, this thesis provides a first look at the relationship between GRFs produced and experienced during walking and the pectoral fins of the amphibious fish, *Polypterus.* The kinematics of the pectoral fins and fore body were analyzed during terrestrial locomotion, and strategic points across both pectoral fins and body were digitized. Kinematics were compared with GRFs in the thrust (X), stabilizing (Y) and lifting (Z) planes to understand how impact forces travel through the fin tissues. Further analysis, using inverse dynamics, is required to determine how these impact forces travel through the musculature of the pectoral fins, perhaps providing potential hypotheses as to the effects of GRFs and their role in not only how terrestrial locomotion affects the behavioural, anatomical, and physiological plasticity observed in *Polypterus,* but also the limbs of tetrapods during the evolutionary transition from aquatic to terrestrial environments.

ACKOWLEDGEMENTS

I would like to express my deepest thanks to my supervisor Emily Standen for giving me this opportunity. Thank you for the constant guidance and advice you've provided me, and for always being there for me when I faced difficulties with my research. I am sincerely grateful to have had a patient, supportive, and inspiring supervisor like yourself, to guide me through this experience. To my thesis committee members, John Lewis, Jeff Dawson, and Vincent Careau, thank you for the amazing feedback you've provided throughout my research. To John and Jeff, thank you for taking me on as a student and teaching me the necessary skills in biomechanics and dynamic modelling. Both classes taught me to think critically and were incredibly helpful when writing my thesis. To Vincent Careau, thank you for all of your stats advice. It was an honour to have you all in my committee. To Keegan Lutek, Trina Du, and Cassandra Donatelli, thank you for the constant feedback and reassurance you've provided me throughout this journey. This was a new experience for me, but you always found the time to answer my questions and concerns. To the Standen Lab, thank you for the support these past couple of years. It was an honour to have worked alongside each of you. Lastly, I'd like to thank my family for their ongoing and unconditional love and support. I could not have done this without your help.

TABLE OF CONTENTS

LIST OF TABLES

LIST OF FIGURES

the tip of the nose. Point 4 is placed above the pectoral girdle, and represents the center of mass (CoM) of the fish.

Figure 2.6 Kinematic variables. Body elevation during both the stance phase and the swing phase of the stroke cycle was calculated via (A) the nose, and (B) the CoM.

Figure 2.7 Kinematic variables. Fin abduction angle was calculated as the angle created between the nose, CoM, and the tip of the pectoral fin.

Figure 2.8 Kinematic motion and corresponding raw force signals obtained. *Polypterus* were allowed to freely walk across the force plate (A), which captured the raw force sigals across all six transducers in three axes (B). Force transducers were numbers 1-6 for identification.

Figure 2.9 Representative force trace. The force trace represents each force component: anteroposterior (Fx) (red), mediolateral (Fy) (light green), vertical (Fz) (black) produced during a single stance phase, as well as the resultant GRF magnitude, depicted by the dark blue colour. Each coloured vertical line corresponds to a specific kinematic timepoint during the stance phase. The trace is composed of forces produced by both the pectoral fin and the anterior body as it was difficult to differentiate between the two and their contributions to the force production.

Figure 2.10 Significant kinematic and force temporal variables within whole group analysis. The entire stroke is represented from 0-360 °, with the stance phase beginning at 0° and ending at 180°, and swing phase beginning from 180° and ending at 0° or 360°. The variables that show directionality are minimum abduction angular velocity (yellow); maximum nose elevation during stance (orange); minimum nose elevation during stance (blue); minimum nose velocity during swing phase (red); maximum lateral (Fy) force (purple); and minimum lateral (Fy) force (green).

Figure 2.11 Differences in maximum GRF magnitudes measured during walking. Force components are differentiated by colour as indicated in the associated legend. Individual data points are represented by the respective coloured dots. Forces were measured in its component force directions: (A) Anteroposterior (Fx) versus mediolateral (Fy); (B) Anteroposterior (Fx) versus vertical (Fz); and (C) Mediolateral (Fy) versus vertical (Fz). Mean and 95% CI are indicated by the black bars. Asterisks indicate significant differences between the force components. P-values are reported in Table A9 in the Appendix.

Figure 2.12 Differences in GRF magnitudes measured at the onset of the stance phase during walking. Force components are differentiated by colour as indicated in the associated legend. Individual data points are represented by the respective coloured dots. Forces were measured in its component force directions: (A) Anteroposterior (Fx) versus mediolateral (Fy); (B) Anteroposterior (Fx) versus vertical (Fz); and (C) Mediolateral (Fy) versus vertical (Fz). Mean and 95% CI are indicated by the black bars. Asterisks indicate significant differences between the force components. P-values are reported in Table A9 in the Appendix.

Figure 2.13 Significant kinematic and force temporal variables grouped by category *slip.* The entire stroke is represented from 0-360^o, with the stance phase beginning at 0^o and ending at 180^o, and swing phase beginning from 180^o and ending at 0^o or 360^o. Thick dark blue lines are used to distinguish subgroups from each other. The variables that show directionality are minimum abduction angle (dark blue); maximum nose velocity during swing phase (cyan); maximum nose elevation during stance (orange); minimum nose velocity during swing phase (red); minimum nose elevation during stance (light blue); and maximum lateral (Fy) force (purple).

Figure 2.14 The effects of slip duration on kinematic and kinetic variables within whole group analysis (n=10). The duration of the slip phase within a step was found to have no significant correlation to (A) total nose distance; (B) total CoM distance; (C) total fin distance; (D) maximum anteroposterior (Fx) force production; (E) maximum mediolateral (Fy) force production; or (F) maximum vertical (Fz) force production. The linear relationship is indicated in the top right corner of each plot. The marginal R^2 value, along with the corresponding p-values are also indicated in the top right corner of each plot. Marginal and conditional R^2 values, as well as p-values are recorded in Table A10 in the Appendix.

Figure 2.15 The effects of stance duration on kinematic and kinetic variables within whole group analysis (n=10). Significant correlations are indicated by the asterisks. Stance duration was found to have positive correlations with (A) nose distance, (B) CoM distance, and (C) fin distance. The duration of stance was found to have no correlation with peak GRF production (D-F). The linear relationship is indicated in the top right corner of each plot. The marginal R^2 value, along with the corresponding p-values are also indicated in the top right corner of each plot. Marginal and conditional R^2 values, as well as p-values are recorded in Table A10 in the Appendix.

Figure 2.16 Significant kinematic and force temporal variables within the category *motion*. The entire stroke is represented from 0-360 ^{o}, with the stance phase beginning at 0^o and ending at 180^o, and swing phase beginning from 180^o and ending at 0^o or 360^o. Thick dark blue lines are used to distinguish subgroups from each other. The variables that show directionality are minimum CoM velocity during swing phase (dark green), maximum lateral (Fy) force (purple), minimum abduction angular velocity (yellow), maximum nose elevation during stance (orange), minimum nose elevation during stance (light blue), minimum nose velocity during swing phase (red), and minimum lateral (Fy) force (green).

Figure 2.17 The effects of fin motion on kinematic and kinetic variables during walking. Two different motions of the pectoral fin were employed by *Polypterus* during walking. *Tucked* fin steps are indicated in red; *untucked* fin steps are indicated in blue. Individual data points are represented by the respective coloured dots. Asterisks indicate significant differences between the fin motions. Significant differences were found in (B) total CoM distance; (E) maximum mediolateral (Fy) force production; and (G) total stance duration. There were no differences found in (A) total nose distance; (C) total fin distance; (D) maximum anteroposterior (Fx) force

production; (F) maximum vertical (Fz) force production; or (H) total slip duration. Mean and 95% CI are indicated by the black bars. P-values are reported in Table A11 in the Appendix.

Figure 2.18 Representative force trace (A) and illustrations depicting kinematic motion, force components, and predicted resultant force vector (B-D) of step 2 (Table 2.2). Step 2 belongs to the '*mid-slip*' subgroup of category *slip.* (A) Stance duration is depicted as percent stance. Anteroposterior (Fx), mediolateral (Fy), and vertical (Fz) force components are indicated by the red, green, and black lines, respectively. The resultant force magnitude is displayed by the dark blue line. This step contains a single slip phase, indicated by the pink box. Objective kinematic timings are indicated by the vertical lines and include maximum nose elevation (yellow), minimum nose elevation (dark green), minimum abduction angle (light blue), and minimum abduction angular velocity (brown). (B-D) The kinematic motions illustrated were observed at the midpoint between the timings of interest, and include the onset of loading to the onset of the slip phase (B); the onset of the slip phase to the end of the slip phase (C); the end of the slip phase to the end of the stance (D). The mean magnitudes of forward (Fx) (blue), lateral (Fy) (green), and vertical (Fz) (purple) forces are recorded in the tables. Arrows in orange depict the resultant force vector, and arrows in yellow illustrate the straightest path of motion as determined by the kinematics measured from the CoM.

Figure 2.19 A representative force trace (A) and kinematic images (B-E) used to illustrate common kinematic and force patterns observed during walking. Stance duration is depicted as percent stance. Forward (Fx), lateral (Fy), and vertical (Fz) force components are indicated by the red, green, and black lines, respectively. The resultant force magnitude is displayed by the dark blue line. This step contains a single slip phase, indicated by the pink box. Objective kinematic timings are indicated by the vertical lines and include maximum nose elevation (yellow), minimum nose elevation (dark green), minimum abduction angle (light blue), and minimum abduction angular velocity (brown). The kinematic images (B-E) illustrate the motion of the pectoral fin (yellow) across a single step. (B) represents the fin at the onset of loading; (C) and (D) represent the start and end of the slip phase, respectively; and (E) represents the end of the stance phase.

Figure 3.1 Axis of reference (A); front view (B) and rear view (C). In this single segmented model, the contact point between the medial radials and fin rays act as the sole joint, and CoP point. (A) Motion can occur linearly and angularly in two directions along and about the horizontal (x) and vertical (y) axes. Force transfer originates at the CoP point and can travel in two directions, as depicted by the direction of the arrows (B & C).

Figure 3.2 Free body diagrams taken from Fig. 3.1. (A) A diagram illustrating angular motion about each joint. J_1 is located at the shoulder joint of the pectoral fin and is the proximal-most joint; J_2 is located where the medial radials meet the fin rays, and represents the distal-most joint. The net joint torque is represented by τ. The mass of each segment is indicated by m_1 and m_2. (B) A diagram illustrating the reaction forces and moments about each joint within the musculoskeletal system.

LIST OF APPENDICES

Table A4.2 Statistically significant variables, as indicated using Rayleigh's test for directionality for category *motion,* subgroup *lateral fin.* This group categorizes the steps depending on the motion of the fin during the stance phase. Subgroup *lateral fin* contains steps in which the planted fin remains to the side of the anterior body at all times during the step. Significant temporal variables have been plotted along a circular plot, also known as a polar plot. Variables were found to have directionality if their Rayleigh's test value was less than 0.05. Each colour corresponds to a specific variable, as indicated in the table.

Table A5 Means, standard deviation, and s.e.m. of all variables analyzed within whole group analysis for stance duration and slip duration.

Table A6 Means, standard deviation, and s.e.m. of all variables analyzed within whole group analysis. A total of twelve (12) kinematic and force variables were analyzed during the stance phase. Variable names can be found in column 1.

Table A7 Means and s.e.m. of all variables analyzed within category *slip*. A total of thirty-three (33) kinematic and force variables were analyzed during the stance phase. Variable names can be found in column 1. Columns 2-4 represent each subgroup, and their respective means and s.e.m. of each variable analyzed.

Table A8 Means and s.e.m. of all variables analyzed within category *motion*. A total of thirty-three (33) kinematic and force variables were analyzed during the stance phase. Variable names can be found in column 1. Columns 2-3 represent each subgroup, and their respective means and s.e.m. of each variable analyzed.

Table A9 Results from paired T-tests used to compare differences between GRF components. Maximum GRFs were measured in three planes: anteroposterior (Fx), mediolateral (Fy), and vertical (Fz). The magnitudes of GRFs produced at the onset of the stance phase were also measured. The corresponding p-values are listed in column 2. Asterisks indicate the that significant difference exists between the two force components.

Table A10 Results from a Linear Mixed Effects (LME) model. Dependent variables are listed in column 1. Fixed variables include slip duration and stance duration. P values, as well as marginal (*m*) and conditional (*c*) R^2 values are reported. Asterisks indicate the existence of significant correlations between the corresponding dependent variable and the fixed effect.

Table A11 Results from unpaired T-tests used to compare differences between fin motions. Two fin motions were observed during walking and were defined at *tucked* and *untucked* fin steps. The corresponding p-values are listed in column 2. Asterisks indicate the that significant difference exists between the two force components.

Figure A1 Force trace (A) and illustrations depicting kinematic motion, force components, and predicted resultant force vector (B-F) of step 1 (Table 2.2). Step 1 belongs to the '*special slip*'

subgroup of category *slip* as it contained two periods of slip within a single step. Stance duration is depicted as percent stance. Forward (Fx), lateral (Fy), and vertical (Fz) force components are indicated by the red, green, and black lines, respectively. The resultant force magnitude is displayed by the dark blue line. This step contains a single slip phase, indicated by the pink box. Objective kinematic timings are indicated by the vertical lines and include maximum nose elevation (yellow), minimum nose elevation (dark green), minimum abduction angle (light blue), and minimum abduction angular velocity (brown). The kinematic motions illustrated were observed at the midpoint between the timings of interest, and include the onset of loading to the onset of the first slip phase (B); the onset of the first slip phase to the end of the first slip phase (C); the end of the first slip phase to the onset of the second slip phase (D); the onset of the second slip phase to the end of the second slip phase (E); and lastly, the end of the second slip phase to the end of the stance (F). The mean magnitudes of forward (Fx) (blue), lateral (Fy) (green), and vertical (Fz) (purple) forces are recorded in the tables.

Figure A2 Force trace (A) and illustrations depicting kinematic motion, force components, and predicted resultant force vector (B-D) of step 2 (Table 2.2). Step 2 belongs to the '*mid-slip*' subgroup of category *slip.* Stance duration is depicted as percent stance. Forward (Fx), lateral (Fy), and vertical (Fz) force components are indicated by the red, green, and black lines, respectively. The resultant force magnitude is displayed by the dark blue line. This step contains a single slip phase, indicated by the pink box. Objective kinematic timings are indicated by the vertical lines and include maximum nose elevation (yellow), minimum nose elevation (dark green), minimum abduction angle (light blue), and minimum abduction angular velocity (brown). The kinematic motions illustrated were observed at the midpoint between the timings of interest, and include the onset of loading to the onset of the slip phase (B); the onset of the slip phase to the end of the slip phase (C); the end of the slip phase to the end of the stance (D). The mean magnitudes of forward (Fx) (blue), lateral (Fy) (green), and vertical (Fz) (purple) forces are recorded in the tables.

Figure A3 Force trace (A) and illustrations depicting kinematic motion, force components, and predicted resultant force vector (B-D) of step 3 (Table 2.2). Step 3 belongs to the '*mid-slip*' subgroup of category *slip.* Stance duration is depicted as percent stance. Forward (Fx), lateral (Fy), and vertical (Fz) force components are indicated by the red, green, and black lines, respectively. The resultant force magnitude is displayed by the dark blue line. This step contains a single slip phase, indicated by the pink box. Objective kinematic timings are indicated by the vertical lines and include maximum nose elevation (yellow), minimum nose elevation (dark green), minimum abduction angle (light blue), and minimum abduction angular velocity (brown). The kinematic motions illustrated were observed at the midpoint between the timings of interest, and include the onset of loading to the onset of the slip phase (B); the onset of the slip phase to the end of the slip phase (C); the end of the slip phase to the end of the stance (D). The mean magnitudes of forward (Fx) (blue), lateral (Fy) (green), and vertical (Fz) (purple) forces are recorded in the tables.

Figure A4 Force trace (A) and illustrations depicting kinematic motion, force components, and predicted resultant force vector (B-D) of step 4 (Table 2.2). Step 4 belongs to the '*variable slip*' subgroup of category *slip.* Slip occurs after 50% stance. Stance duration is depicted as percent stance. Forward (Fx), lateral (Fy), and vertical (Fz) force components are indicated by the red, green, and black lines, respectively. The resultant force magnitude is displayed by the dark blue line. This step contains a single slip phase, indicated by the pink box. Objective kinematic timings are indicated by the vertical lines and include maximum nose elevation (yellow), minimum nose elevation (dark green), minimum abduction angle (light blue), and minimum abduction angular velocity (brown). The kinematic motions illustrated were observed at the midpoint between the timings of interest, and include the onset of loading to the onset of the slip phase (B); the onset of the slip phase to the end of the slip phase (C); the end of the slip phase to the end of the stance (D). The mean magnitudes of forward (Fx) (blue), lateral (Fy) (green), and vertical (Fz) (purple) forces are recorded in the tables.

Figure A5 Force trace (A) and illustrations depicting kinematic motion, force components, and predicted resultant force vector (B) of step 5 (Table 2.2). Step 5 belongs to the '*special slip*' subgroup of category *slip.* Stance duration is depicted as percent stance. Forward (Fx), lateral (Fy), and vertical (Fz) force components are indicated by the red, green, and black lines, respectively. The resultant force magnitude is displayed by the dark blue line. This step contains a single slip phase, indicated by the pink box. Objective kinematic timings are indicated by the vertical lines and include maximum nose elevation (yellow), minimum nose elevation (dark green), minimum abduction angle (light blue), and minimum abduction angular velocity (brown). The kinematic motions illustrated were observed at the midpoint between the timings of interest, and include the onset of loading to the end of the stance (B). The mean magnitudes of forward (Fx) (blue), lateral (Fy) (green), and vertical (Fz) (purple) forces are recorded in the tables.

Figure A6 Force trace (A) and illustrations depicting kinematic motion, force components, and predicted resultant force vector (B-D) of step 6 (Table 2.2). Step 6 belongs to the '*mid-slip*' subgroup of category *slip.* Stance duration is depicted as percent stance. Forward (Fx), lateral (Fy), and vertical (Fz) force components are indicated by the red, green, and black lines, respectively. The resultant force magnitude is displayed by the dark blue line. This step contains a single slip phase, indicated by the pink box. Objective kinematic timings are indicated by the vertical lines and include maximum nose elevation (yellow), minimum nose elevation (dark green), minimum abduction angle (light blue), and minimum abduction angular velocity (brown). The kinematic motions illustrated were observed at the midpoint between the timings of interest, and include the onset of loading to the onset of the slip phase (B); the onset of the slip phase to the end of the slip phase (C); the end of the slip phase to the end of the stance (D). The mean magnitudes of forward (Fx) (blue), lateral (Fy) (green), and vertical (Fz) (purple) forces are recorded in the tables.

Figure A7 Force trace (A) and illustrations depicting kinematic motion, force components, and predicted resultant force vector (B-D) of step 7 (Table 2.2). Step 7 belongs to the '*variable slip*' subgroup of category *slip.* Slip occurs prior to 50% stance. Stance duration is depicted as percent stance. Forward (Fx), lateral (Fy), and vertical (Fz) force components are indicated by the red, green, and black lines, respectively. The resultant force magnitude is displayed by the dark blue line. This step contains a single slip phase, indicated by the pink box. Objective kinematic timings are indicated by the vertical lines and include maximum nose elevation (yellow), minimum nose elevation (dark green), minimum abduction angle (light blue), and minimum abduction angular velocity (brown). The kinematic motions illustrated were observed at the midpoint between the timings of interest, and include the onset of loading to the onset of the slip phase (B); the onset of the slip phase to the end of the slip phase (C); the end of the slip phase to the end of the stance (D). The mean magnitudes of forward (Fx) (blue), lateral (Fy) (green), and vertical (Fz) (purple) forces are recorded in the tables.

Figure A8 Force trace (A) and illustrations depicting kinematic motion, force components, and predicted resultant force vector (B-D) of step 8 (Table 2.2). Step 8 belongs to the '*variable slip*' subgroup of category *slip.* Slip occurs prior to 50% stance. Stance duration is depicted as percent stance. Forward (Fx), lateral (Fy), and vertical (Fz) force components are indicated by the red, green, and black lines, respectively. The resultant force magnitude is displayed by the dark blue line. This step contains a single slip phase, indicated by the pink box. Objective kinematic timings are indicated by the vertical lines and include maximum nose elevation (yellow), minimum nose elevation (dark green), minimum abduction angle (light blue), and minimum abduction angular velocity (brown). The kinematic motions illustrated were observed at the midpoint between the timings of interest, and include the onset of loading to the onset of the slip phase (B); the onset of the slip phase to the end of the slip phase (C); the end of the slip phase to the end of the stance (D). The mean magnitudes of forward (Fx) (blue), lateral (Fy) (green), and vertical (Fz) (purple) forces are recorded in the tables.

Figure A9 Force trace (A) and illustrations depicting kinematic motion, force components, and predicted resultant force vector (B) of step 9 (Table 2.2). Step 9 belongs to the '*special slip*' subgroup of category *slip.* Stance duration is depicted as percent stance. Forward (Fx), lateral (Fy), and vertical (Fz) force components are indicated by the red, green, and black lines, respectively. The resultant force magnitude is displayed by the dark blue line. This step contains a single slip phase, indicated by the pink box. Objective kinematic timings are indicated by the vertical lines and include maximum nose elevation (yellow), minimum nose elevation (dark green), minimum abduction angle (light blue), and minimum abduction angular velocity (brown). The kinematic motions illustrated were observed at the midpoint between the timings of interest, and include the onset of loading to the end of the stance (B). The mean magnitudes of forward (Fx) (blue), lateral (Fy) (green), and vertical (Fz) (purple) forces are recorded in the tables.

Figure A10 Force trace (A) and illustrations depicting kinematic motion, force components, and predicted resultant force vector (B-D) of step 10 (Table 2.2). Step 10 belongs to the '*mid-slip*' subgroup of category *slip.* Stance duration is depicted as percent stance. Forward (Fx), lateral (Fy), and vertical (Fz) force components are indicated by the red, green, and black lines, respectively. The resultant force magnitude is displayed by the dark blue line. This step contains a single slip phase, indicated by the pink box. Objective kinematic timings are indicated by the vertical lines and include maximum nose elevation (yellow), minimum nose elevation (dark green), minimum abduction angle (light blue), and minimum abduction angular velocity (brown). The kinematic motions illustrated were observed at the midpoint between the timings of interest, and include the onset of loading to the onset of the slip phase (B); the onset of the slip phase to the end of the slip phase (C); the end of the slip phase to the end of the stance (D). The mean magnitudes of forward (Fx) (blue), lateral (Fy) (green), and vertical (Fz) (purple) forces are recorded in the tables.

LIST OF FORMULAS

$$F_b = (\rho_a - \rho_w) \cdot V \cdot g \quad \text{(eq.1)}$$

$$\Re = \frac{\rho D v}{\mu} \quad \text{(eq.2)}$$

$$F_g = m \cdot g \quad \text{(eq.3)}$$

$$LME_{whole\ group} = lme\ (dependent\ variable \sim fixed\ effect, random = \sim 1|Fish/step) \quad \text{(eq.4)}$$

$$LME_{subgroup} = lme\ (dependent\ variable \sim fixed\ effect * subgroup\ effect, random = \sim 1|Fish/step) \quad \text{(eq.5)}$$

$$F = m \cdot a \quad \text{(eq.6)}$$

$$\Sigma F_x = m \cdot a_x \quad \text{(eq.7)}$$

$$\Sigma F_y = m \cdot a_y \quad \text{(eq.8)}$$

$$M = I \cdot \alpha \quad \text{(eq.9)}$$

$$R_{xp} = m \cdot a_x \quad \text{(eq.10)}$$

$$R_{yp} = m \cdot a_y \quad \text{(eq.11)}$$

$$M_{medial\ radials} = (I_{medial\ radials} \cdot \alpha_{medial\ radials}) + \omega + F_{x_{medial\ radials}} \cdot L_{y_{medial\ radials}} - F_{y_{medial\ radials}} \cdot L_{x_{medial\ radials}} \quad \text{(eq.12)}$$

$$L_{x_{medial\ radials}} = (x_d - x_{CoM}) \quad \text{(eq.13)}$$

$$L_{y_{medial\ radials}} = (y_{CoM} - y_d) \quad \text{(eq.14)}$$

$$M_p = -M_d - r_p \cdot F_p - r_d \cdot F_d + (I \cdot \alpha) + \omega \cdot (I \cdot \omega) \quad \text{(eq.15)}$$

$$M_{shoulder\ joint} = I_{shoulder\ joint} \cdot \alpha_{shoulder\ joint} - M_{medial\ radials} - F_{x_{shoulder\ joint}} \cdot L_{y_{shoulder\ joint}} + F_{y_{shoulder\ joint}} \cdot L_{x_{shoulder\ joint}} + F_{x_{medial\ radials}} \cdot L_{y_{medial\ radials}} - F_{y_{medial\ radials}} \cdot L_{x_{medial\ radials}} \quad \text{(eq.16)}$$

$$L_{x_{shoulder\ joint}} = (x_{CoM} - x_p) \quad \text{(eq.17)}$$

$$L_{y_{shoulder\ joint}} = (y_p - y_{CoM}) \quad \text{(eq.18)}$$

LIST OF ABBREVIATIONS AND SYMBOLS

α	angular acceleration
ab. pro.	abductor profundus
ab. sup.	abductor superficialis
ad.	adductor
BoS	base of support
cmt. I	coracometapterygialis I
cmt. II	coracometapterygialis II
CoM	center of mass
CoP	center of pressure
d	distal joint
D	diameter
F_b	force of buoyancy
F_g	gravitational force
g	gravitational acceleration
GRF	Ground reaction force
I	moment of inertia
L	length
LME	Linear mixed effects model
M	joint moment
m	mass
μ	fluid viscosity
ω	angular velocity
p	proximal joint
$\Re$	Reynolds number
R	reaction force
ρ	density
ρ_a	density of air
ρ_w	density of water
V	volume
v	fluid velocity
x	horizontal coordinates
y	vertical coordinates
zp	zonopropterygialis

Chapter 1 Introduction

Evolution of tetrapods: using Polypterus senegalus to study the transition from fins to limbs

The Late Devonian period, occurring approximately 380 million years ago, marked the beginning of the evolutionary transition into fully terrestrial vertebrate animals (Clack, 2012). Throughout the next 350 million years, descendants of these aquatic species evolved limbs with digits and gradually gained the ability to walk across terrestrial environments (Clack, 2012). During this transitional period, new behaviours and morphological changes occurred (Clack, 2012). The exact changes that occurred during this period are still unknown due to the extinction of the transitionary animals (Clack, 2012) and absence of clear fossil records (McGee, 2013). One of the most interesting aspects of the vertebrate transition from water to land is how these animals managed to use aquatically adapted bodies to locomote on land. Looking to extant fishes that resemble fossil animals that are thought to have surrounded the fin to limb transition allows us to formulate hypotheses about how these first vertebrates may have used fins to locomote overland.

Polypterus senegalus, an extant member of the ray-finned fishes (actinopterygians), is the closest relative to the common ancestor of actinopterygians and sarcopterygians (fleshy-finned fishes, or lobed-finned fishes) (Clack, 2012; Standen et al., 2014), the latter of which gave rise to tetrapods (Clack & Ahlberg, 2016) (Fig. 1.1).

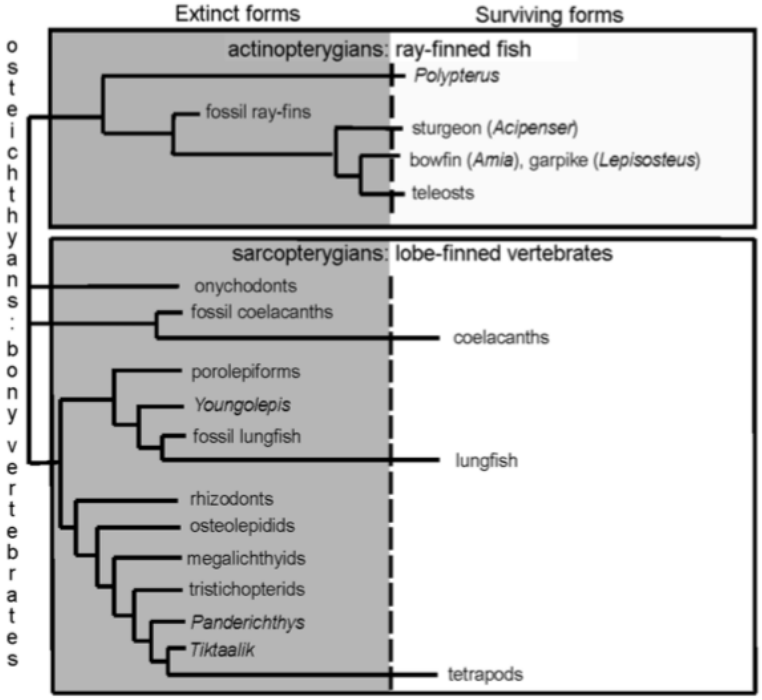

Figure 1.1 A cladogram depicting all species classified as Osteichthyans. Also known as *bony vertebrates*, members classified as Osteichthyans can be further subdivided into currently extinct and surviving Actinopterygians and Sarcopterygians (Clack, 2012).

Polypterus have morphologies similar to stem tetrapods, such as elongated bodies, rhomboid shaped scales, and ventrolaterally positioned pectoral fins. In addition, *Polypterus* have functional lungs, and are capable of surviving on land, and engaging in terrestrial locomotion (Standen et al., 2014). These morphological and behavioural features make *Polypterus* an excellent model to understand how a fin, evolved for aquatic locomotion can be used to propel terrestrial walking, and may provide insight into the evolutionary transition to life on land.

Polypterus Anatomy

In general, appendicular muscle morphology increases in complexity across the fish to tetrapod transition: limbs have more complex muscle morphology in comparison with fins (Wilhelm et al., 2015). The muscle anatomy of *Polypterus* appears to be intermediate in complexity between fishes and tetrapods (Wilhelm et al., 2015). In comparison with other bony-fishes, Wilhelm et al., (2015) noticed the presence of novel muscles in *Polypterus.* In contrast to the four muscles commonly seen in fishes, *Polypterus* have six independent muscles originating in the pectoral girdle and crossing into the pectoral fin (Fig. 1.2).

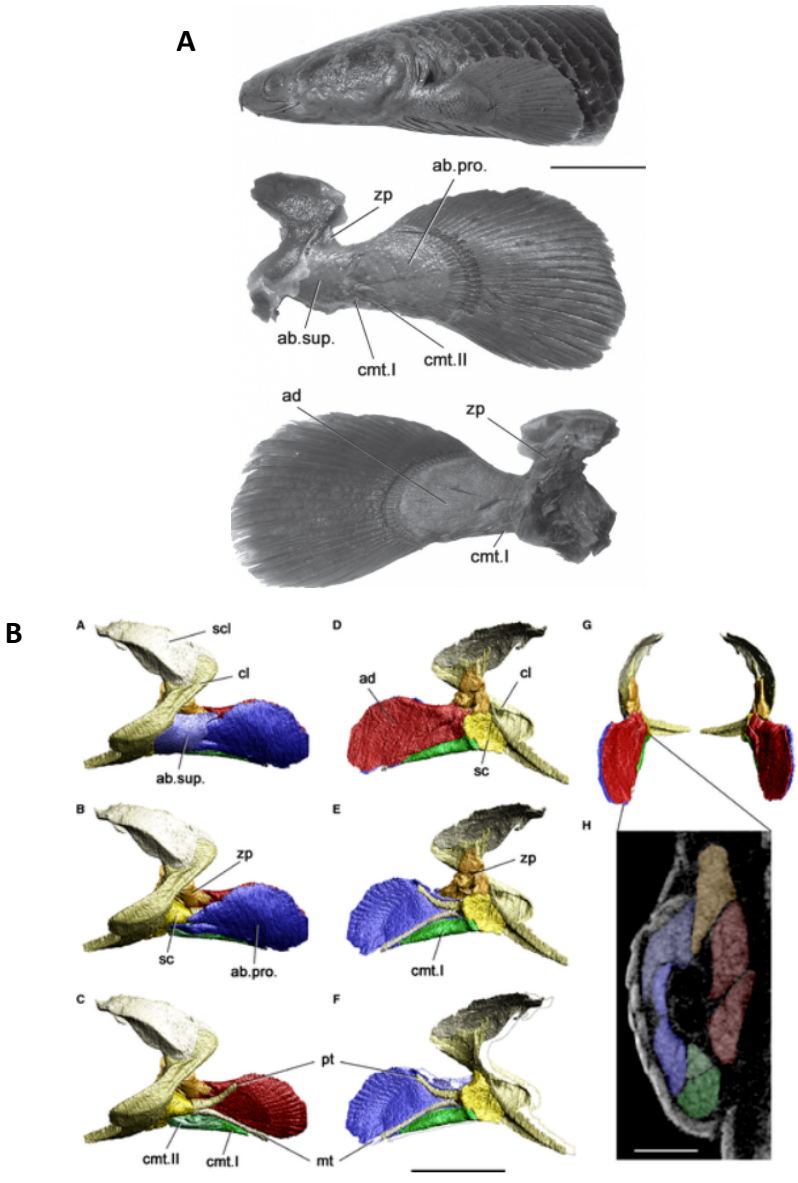

Figure 1.2 Pectoral anatomy of *Polypterus.* (A) lateral view of the left pectoral fin and anterior body (top), with partial component of left pectoral girdle and fin (center), and medial view (bottom). Pectoral anatomy reconstructed from microCT scan data (B), in lateral, medial and posterior views. Abductor profundus (ab. pro.); abductor superficialis (ad. sup.); adductor (ad); coracometapterygialis I (cmt. I); coracometapterygialis II (cmt. II); zonopropterygialis (zp) (Wilhelm et al., 2015).

Each muscle is responsible for a specific function that aids in fin motion. The abductor superficialis (ab. sup.) pronates and abducts the fin; abductor profundus (ab. pro.) is responsible for abducting the fin; and adductor (ad) is responsible for the adduction of the fin and pronation of the ventral portion of the scapulocoracoid (Wilhelm et al., 2015). The two novel muscles seen in *Polypterus* are the coracometapterygialis I+II (cmt. I and cmt.II) and zonopropterygialis medialis (zp). The coracometapterygialis I and II is responsible for supination and lowering of the fin while the zonopropterygialis (zp) aids in pronation and raising the fin. In addition, the morphology of the 'shoulder-joint' comprised of the scapulocoracoid, propterygium, and metapterygium of *Polypterus* allows for increased flexibility and wider range of motion in all directions within the pectoral fin. While the structure of the tetrapod 'shoulder-joint' differs from that seen in *Polypterus*, the joint functions in a similar manner (Wilhelm et al., 2015). This functional similarity between *Polypterus* and stem tetrapods is further incentive to use *Polypterus* as a model to study the evolution into tetrapods.

Differing forces experienced in aquatic versus terrestrial environments

The first vertebrates to foray onto land would have done so for short periods of time, initiating the rise of an amphibious lifestyle. Amphibious fishes must function in two dramatically different environments: land and water. From a physiological perspective there are many homeostatic challenges that must be overcome, including gas exchange, dehydration, ion balance, waste excretion and thermoregulation (Wright & Turko, 2016). From a mechanical perspective the forces an animal experiences change dramatically, impacting their musculoskeletal performance. In a terrestrial environment buoyancy – the most significant force experienced in aquatic environments – gives way to gravity, while frictional forces replace those of drag forces, as experienced in aquatic environments.

Forces in an aquatic environment

Buoyancy is directly proportional to the difference in total density between the body and the surrounding water (Ditsche & Summers, 2014). The force of buoyancy *(F_b)* can be calculated as

$$F_b = (\rho_a - \rho_w) \cdot V \cdot g \qquad \text{(eq. 1)}$$

where the overall density is determined by the difference between the density of the air (ρ_a) and water (ρ_w); *V* represents the volume; and *g* is the gravitational acceleration. As a fish's density in water *(ρ_w)* decreases, it begins to rise to the surface. The opposite occurs as fish submerge themselves into water (Watanabe et al. 2008). As fish descend into water, their density in water *(ρ_w)* increases, allowing them to further submerge. The force of gravity can be considered negligible in aquatic environments due to the density of water being much greater than that of air (Ditsche & Summers, 2014). The force of buoyancy acts in the direction opposite

to gravitational force. Other forces such as drag and lift also affect motion in aquatic environments. Drag force acts in the direction of the stream flow and consists of both friction and form (or pressure) drag. In aquatic environments, friction exists between the flowing water and body surface while form or pressure drag is caused by the shape of the animal and can be measured in the animals' wake (Ditsche & Summers, 2014). The size, shape and speed of an animal dictates the ratio of friction to form drag and is affected by the ratio of viscous to inertial forces in the fluid regime, which can be calculated using Reynolds number (*Re*) (LaNasa & Upp, 2014),

$$\Re = \frac{\rho D v}{\mu} \quad \text{(eq. 2)}$$

where ρ is the density of the fluid; *D* is the diameter; *v* is the fluid velocity; and μ is the fluid viscosity. With the exception of very small organisms, most adult fish operate at large Re numbers allowing them to locomote in fluid regimes dominated by inertial forces. Thus form or pressure drag is the dominant force, with minimal influence exerted from frictional drag. Drag force is directly influenced by the speed of motion, as well as the size and shape of the animal. Lift forces act perpendicular to the direction of flow and are dependent on the shape and surface area of the animal, as well as the density and velocity of the surrounding fluid (Ditsche & Summers, 2014).

Forces in a terrestrial environment

In contrast, terrestrial vertebrates lack the support of a buoyant environment and must counteract the force of gravity. Gravitational force is calculated as

$$F_g = m \cdot g \quad \text{(eq. 3)}$$

where the magnitude of gravitational force *(F_g)* is proportional to the mass *(m)* of the animal multiplied by gravitational acceleration *(g)* (Ditsche & Summers, 2014).

Since buoyancy no longer supports the animal's body, their musculoskeletal system must be able to withstand the load of their entire body weight on the ground. The forces produced by a terrestrially moving animal are called ground reaction forces (GRF). GRFs produced in the appropriate direction will generate forward propulsion (Pace & Gibb, 2009). The magnitude of a GRF varies with the mass, velocity and ground contact time of an animal and reflects the magnitude, direction, and duration of loading on the animal's bone and muscle tissues. Numerous studies have used GRF to assess gait in small animals, such as rodents, to estimate the effects of external loading on limbs (Zumwalt et al., 2006). Other studies have popularized the quantification of GRF in athletes and humans with lower limb injuries, to understand the impact of loading on lower limb bones (Ancillao et al., 2018). Similar to drag forces present in aquatic environments, friction also exists in terrestrial conditions, however, unlike in aquatic environments, frictional forces are much more influential on motion (Ditsche & Summers, 2014). In terrestrial environments, friction occurs as the resistance between a moving or stationary organism and the ground. The friction needed to begin moving is greater than the friction experienced during movement (Ditsche & Summers, 2014).

The significant differences between the forces experienced in aquatic and terrestrial environments greatly influences the motion required to navigate. *Polypterus*, as an amphibious fish, has adapted to both locomotion on land and in water, and therefore is an excellent model to study the effects locomoting in these differing force environments has on the pectoral fins.

Plasticity observed in *Polypterus senegalus*

Biological tissues can change their structure and function in response to changes in their force environment (Gatsey & Dial, 1996; Heisenberg & Ballaiche, 2013; Matijevich et al., 2019; Smit & Strong, 2020). The absence of buoyancy, coupled with the increase in gravitational force has profound effects on the body, suggesting that terrestrial and semi-terrestrial animals place different demands on their musculoskeletal systems when navigating over land versus in water (Ashley-Ross et al., 2013). Previous research has found that both short- and long-term exposure to walking on land causes observable plastic responses in the musculoskeletal tissues of *Polypterus* (Standen et al., 2014; Standen et al., 2016; Du & Standen, 2020).

Behavioural plasticity

The behavioural plasticity of *Polypterus* in response to a novel terrestrial environment was studied by Standen et al. (2014). Fish were divided into two groups: a control group in which fish were raised in water; and a treatment group in which fish were raised on land, over an eight (8) month period. *Polypterus* reared on land planted their pectoral fins on the ground for less time and had shorter stride durations. The duration and distance of the fin slip were also shorter in the fish raised on land. Land reared fish had smaller pectoral fin elevations, planted their fins closer to the body midline, and had higher nose elevations and smaller tail oscillations (Standen et al., 2014). These kinematic changes suggest that when reared on land *Polypterus* have a more effective walking gait than their aquatically-raised counterparts.

Skeletal plasticity

Mechanical loading also influences muscle and bone cellular structure and shape (Heisenberg & Ballaiche, 2013; Smit & Strong, 2020). *Polypterus* reared in terrestrial environments or exposed to terrestrial exercise regimes showed changes in pectoral fin and pectoral girdle musculoskeletal anatomy. After 8 months, Standen et al. (2014) observed that the clavicle and cleithrum, which are bones that support the pectoral fin, had significantly different shapes in land-raised compared with water-raised groups (Fig. 1.3). The group reared on land had narrower and more elongated clavicles as well as a narrower lateral surface on the cleithrum's horizontal arm. It has been proposed that the increased forces in the pectoral girdle from gravitational and postural changes may have induced a modelling response of the clavicle and cleithrum. In a second experiment, fish reared in a terrestrial environment were found to have longer bones, wider propterygia and metapterygia, more ossified metapterygia and medial radials, and showed changes in propterygial curvature compared to both aquatically reared groups (Du & Standen, 2020) (Fig. 1.4). Fish reared in an aquatic environment but exposed to periodic exercise on land had longer and more ossified medial radials than the group reared in a strictly aquatic environment. This suggests that long-term as well as periodic exposure to land has an observable effect on the skeletal structures of the pectoral fin. *It has been proposed that*

the gravitational forces experienced during exposure to terrestrial environments is the cause of these anatomical and behavioural changes, but the magnitude of these gravitational forces and how they differ from forces experienced in water remains unclear. Consequently, this thesis aims to quantify the forces experienced by fin bone and muscle during walking, in order to explain the observed skeletal changes in these amphibious fish due to exposure to land.

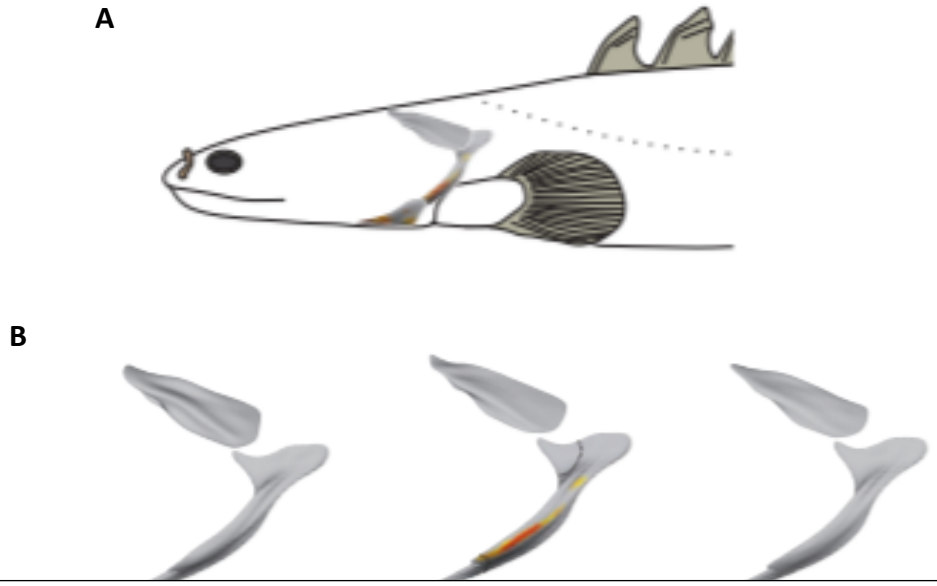

Figure 1.3 Skeletal plasticity observed in the supracleithrum, cleithrum, and clavicle of *Polypterus.* (A) illustrates the location of the skeletal groups within the anterior body. (B) lateral view of the pectoral girdle (Standen et al., 2014).

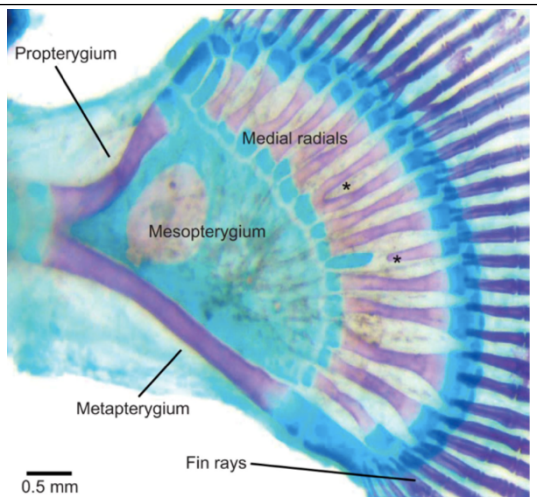

Figure 1.4 Left pectoral fin of *Polypterus* after staining. Blue staining represents cartilaginous tissue and red staining represents ossified tissue (Du & Standen, 2020).

Muscle plasticity

Du & Standen (2017) looked at the effects of terrestrial locomotion on fin tissues. The pectoral fin muscles of fishes are composed of three main fiber types: red fibers which have slow contractions, and are fatigue resistant; white muscle fibers which have fast contractions, higher muscle force production, and are easily fatigued; and pink fibers which have characteristics intermediate to red and white. Each muscle fiber type therefore has different functional performance and is used in different modes of locomotion. The slow-contracting red fibers are used at slower swimming velocities, and fast-contracting white fibers are used during periods of maximum speed (Jayne & Lauder, 1994). Du & Standen (2017) found that terrestrially-reared fish possessed more fast muscle fibers in their pectoral fins than their aquatic counterparts. There were also differences in the distribution of muscle fiber changes within the fin. The number of fast muscle fibers decreased towards the pectoral girdle in aquatically-reared fish, whereas there was an increase observed in terrestrial fish (Du & Standen, 2017). This increase in the proportion of white fibers and their position in the fin, suggest that the pectoral fin muscles of *Polypterus* during walking require faster and more powerful muscle force production. *The differences in forces experienced by the pectoral fins during swimming versus walking suggests that different muscle fibers types, as well as their respective proportions are best suited for different gaits. Using kinematic and ground reaction forces to hypothesize which muscle groups are experiencing peak forces, this thesis aims to provide a basis for future studies to better understand tissue plasticity within Polypterus.*

Studies that compare muscle activation patterns in swimming and walking *Polypterus*, show changes in muscle performance between gaits (Foster et al., 2018). In walking, most muscles were observed to have greater absolute duration of muscle activity (Foster et al., 2018). However, in the pectoral fin muscles, the magnitude of recruitment increased only during the secondary bursts of activity; and in the mid-body muscles, during the primary bursts (Foster et al., 2018). These localized bursts of intensity throughout the fin and mid-body muscles suggest an uneven distribution of force production during walking, further suggesting that walking may be powered by key areas in the fin and body. The exact tissues that are experiencing the greatest change in force distribution is not clear. A pilot study that used Evan's Blue Dye (EBD) to stain for myofiber permeability showed that walking induced the greatest damage in the adductor muscles of the pectoral fin (Dhuper, 2018). There was also a significant difference in the amount of EBD uptake across the proximal to distal areas within the zonopropterygialis, adductor, and abductor muscles. *Within these muscles, a greater difference in EBD uptake occurred in the medial sections than in the distal sections, suggesting that the majority of the force produced by the pectoral fins during walking may originate in the proximal to medial sections of these muscles (Dhuper, 2018). This thesis aims to describe the force profile experienced by fins during walking, which may aid in proposing hypotheses concerning at what stage in the stroke cycle this damage is being incurred in future studies.*

Modes of locomotion observed in *Polypterus senegalus*

Swimming behaviour

In aquatic environments, vertebrates make extensive use of their pectoral and caudal fins, which aid in balancing forces and maneuvering control during swimming (Fish, 2002; Wilga

and Lauder, 2000; Fish et al., 2018). The pectoral fins may aid in generating thrust, lift and drag forces during steady swimming (Drucker and Lauder, 2002; Fish and Lauder, 2017). Aquatic vertebrates that use asynchronous pectoral fin movement generate an imbalanced force production, resulting in body rotations about the horizontal axis (Drucker and Lauder, 2002). During escape responses, aquatic vertebrates may increase the drag forces during pectoral fin motion to create sharp turns (Kajiura et al., 2003*). Polypterus* are capable of this variety of fin motion, however, during routine slow steady swimming, they oscillate both pectoral fins synchronously allowing for symmetrical force generation, with overall minimal body undulation. Thrust is produced primarily through pectoral fin motion, with the tail and body acting as stabilizers (Standen et al., 2016). As speed increases, body undulations increase with the fins. *Polypterus* also move their fins and body at predictable timings through the gait cycle, with both pectoral fins abducting and adducting together, and the nose elevating maximally just after each fin adduction (Standen et al., 2016). These behaviours observed during swimming differ greatly from that seen during walking, which is characterized with asynchronous pectoral fin motion, and exaggerated body motion throughout locomotion.

Walking behaviour

Amphibious fishes use a wide array of strategies to locomote over land (Sayer, 2005), such as using short, propulsive bursts (Gibb et al., 2013) as seen in mudskippers, or through continuous and consistent movement, as seen in ropefish (Pace & Gibb, 2014). Amphibians attempt to limit contact with the ground to reduce overall friction and maximize their efficiency

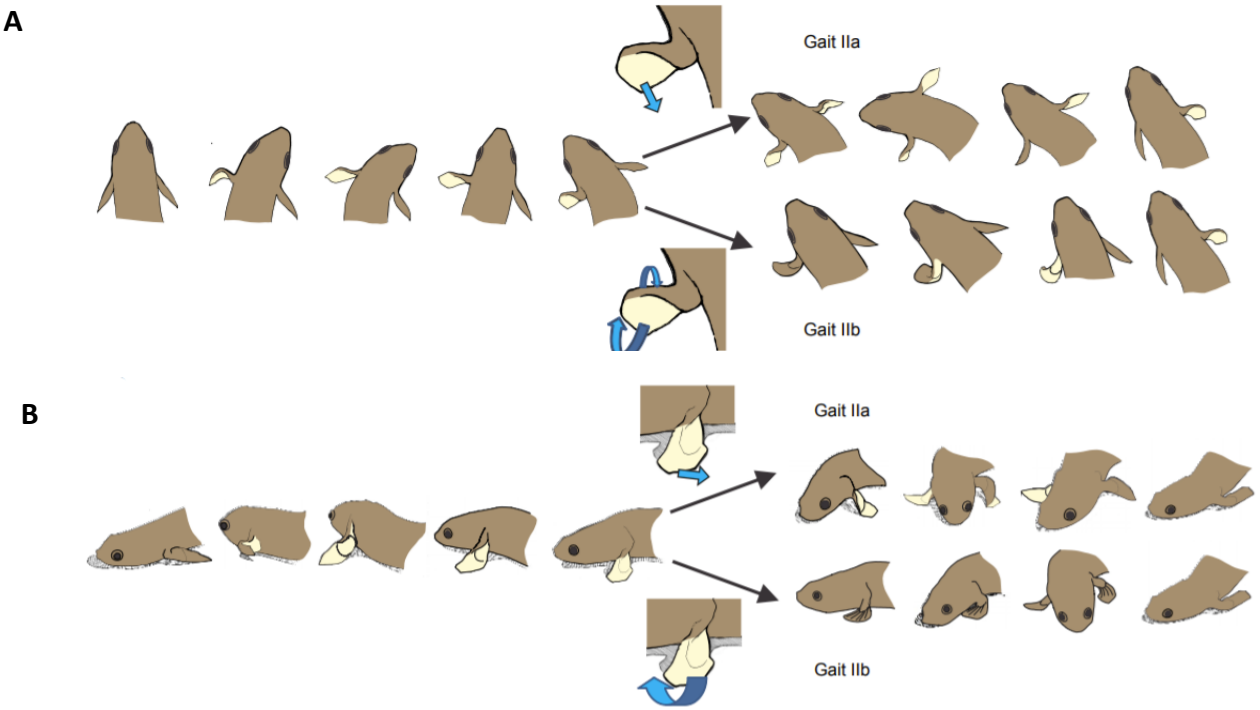

Figure 1.5 Walking gaits observed in *Polypterus.* (A) dorsal view and (B) lateral view. Both gaits begin similarly at the beginning of a step, however the motion changes once the fin is planted onto the ground (Standen et al., 2016).

during terrestrial locomotion (Kawano & Blob, 2013). Although *Polypterus* prefer to locomote in water, it has the ability to navigate across land (Standen et al., 2016). In contrast to swimming, during walking *Polypterus* increase their body oscillation amplitude and move their fins out of synch in a step-like contralateral oscillation. *Polypterus* walk by alternating their pectoral fins between a stance phase and a swing phase. During the stance phase, the fin is planted on the ground and supports weight generated by the lifting of the head and body off the ground. The swing phase consists of the fin moving in a forward motion and entering the next cycle of the stance phase (Standen et al., 2014). *Polypterus* are capable of multiple terrestrial gaits depending on the substrate they are moving over (Standen et al 2016). On uneven or rough terrain *Polypterus* will engage in a snake-like body undulation motion that pushes off the rough terrain. During this gait, pectoral fins are used not at all or opportunistically against the substrate, presumably for stabilization. Thrust was primarily produced by the body pushing against the rough terrain. Over mud, sand, or flat surfaces *Polypterus* use one of two similar axial-appendicular gaits (Fig. 1.5). These gaits demonstrate a contralateral fin plant pattern, with forward propulsion resulting from the head and anterior portion of the body being lifted and vaulted over the planted pectoral fin. Gait IIa occurs when the lateral side of the fin remains in contact with the ground for the entirety of a step. This differs from gait IIb, during which the fin flips from the lateral side to the medial side of the fin, midway through the step. It is unclear as to why there is a change in motion used over flat surfaces. However, it has been observed that individual fish consistently used either gait IIa or IIb for the entire trial, suggesting that the usage of either gait may be done purposefully. Compared to movement over gravel terrain, movement over relatively flat surfaces resulted in greater distance moved, and greater velocities seen over a single step cycle (Standen et al., 2014; 2016). *This suggests that a novel terrestrial environment greatly affects fin performance and requires larger force outputs from pectoral fin muscles to successfully locomote. The total force outputs generated during walking are currently unknown but would be highly informative to understanding how these forces are experienced by the tissues of the pectoral fins of Polypterus.*

Newton's laws of motion

Newton's laws of motion provide an important understanding to terrestrial locomotion. The first law states that objects at rest will remain at rest until acted upon by a large enough force. Without applied force, the object will not move. Newton's second law states that the applied force (*F*) is directly proportional to the object's mass (*m*) and acceleration (*a)*

$$F = m \cdot a \qquad \text{(eq. 4)}$$

Newton's third law states that for every action, there is an equal magnitude but opposite in direction reaction. The combining of Newton's second and third laws proposes that when a force is applied to the ground by a moving animal, the ground will apply an equal in magnitude but opposite in direction reactive force against the animal (Pace & Gibb, 2009; Beckham et al., 2014). This reactive force, also known as ground reaction force, is responsible for forward propulsion in terrestrial locomotion (Beckham et al., 2014) (Fig. 2.1). All motion done over a terrestrial environment must overcome these gravitational forces, and as a result, all horizontal, lateral, and vertical motion is affected by these GRFs (Beckham et al., 2014). The differences in the magnitudes and directions of GRFs will affect how a movement is performed (Beckham et al., 2014).

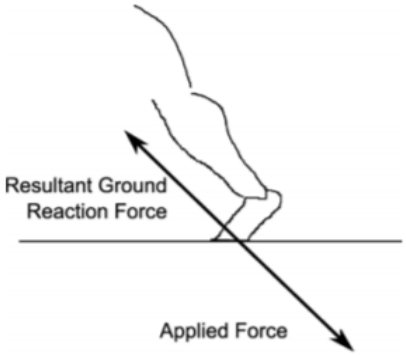

Figure. 2.1 An illustration depicting the combination of Newton's second and third laws of motion. When a force is applied to the ground during terrestrial locomotion, a reactive force of equal magnitude of opposite in direction is applied back to the moving animal. This is the fundamental basis of ground reaction forces and is critical to understanding terrestrial locomotion (Beckham et al., 2014).

Understanding key phases of a force-time curve during bipedal walking

In bipedal walking, the start of a step is defined from the initial impact of one foot with the ground, and ending at the moment when the foot lifts off. This lift off phase also corresponds to

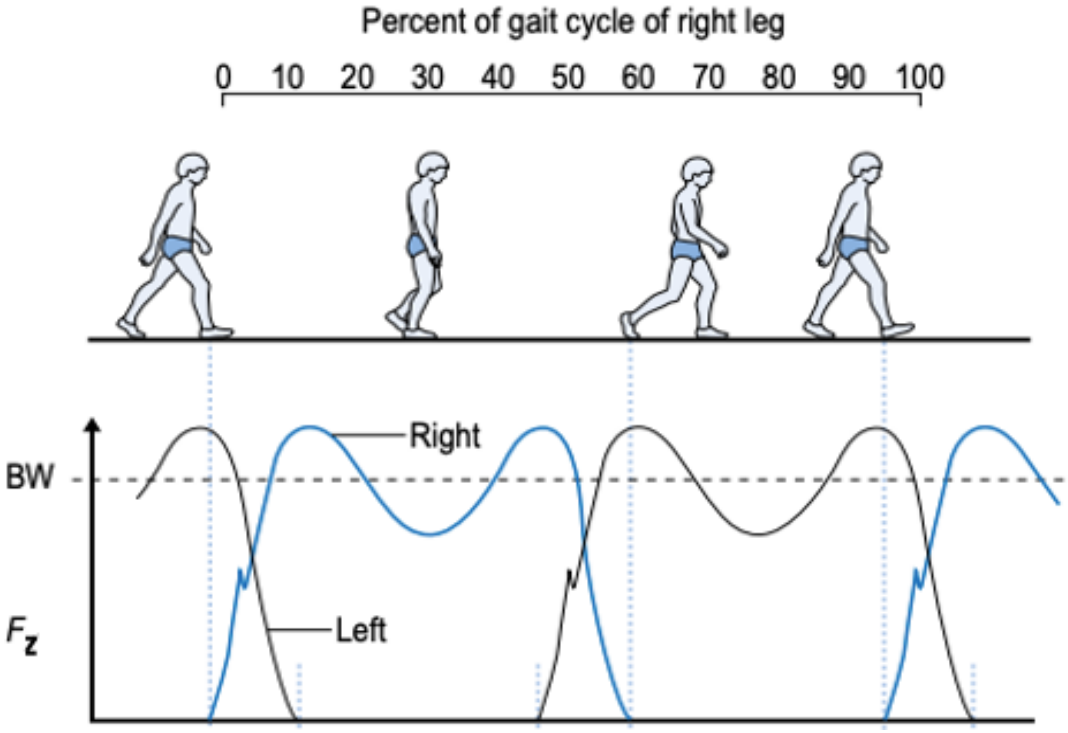

Figure 2.2 Vertical GRF component during bipedal walking (Fz), and body weight (BW) as a factor of percent of gait cycle (Watkins, 2009).

the initial impact of the other foot with the ground (Watkins, 2009), thereby exhibiting an asynchronous gait pattern. A stride encompasses two successive steps (Watkins, 2009). During walking, the musculoskeletal system extending from the feet upwards functions to counteract the effects of gravitational force exerted upon it, by creating the necessary GRFs to maintain standing and to propel forwards and backwards (Watkins, 2009). The foot acts as both a shock absorber, as well as a propulsor or thrust producer (Watkins, 2009). The vertical (Fz) GRF component is commonly the largest force component produced during bipedal walking (Toda et al., 2015). The vertical (Fz) GRF trace consists of a slight peak near the beginning of the stance phase, two prominent peaks, and a slight dip between the two prominent peaks (Tongen & Wunderlich, 2010) (Fig. 2.2).

The slight peak occurring at the beginning of the stance phase is a result of the initial impact as the foot hits the ground (Tongen & Wunderlich, 2010). The first of the two prominent peaks is a result of the heel hitting and loading or exerting an applied force onto the ground. The center of mass (CoM) de-elevates, and the resultant vertical GRF increases (Tongen & Wunderlich, 2010) as the weight is transferred from the heel to the toes (Cross, 1998). The second peak occurs as the toe pushes against the ground during the same stride, which increases the vertical GRF produced (Tongen & Wunderlich, 2010). The decrease between these two peaks occurs due to the CoM rising during mid-stance, thus decreasing the applied force exerted by the body onto the ground (Tongen & Wunderlich, 2010). The magnitude and timings of these prominent peaks exhibited by the vertical GRF has been proposed to not only influence the loading or applied force experienced by the bones and muscles within the foot, but also cautioning against potential injuries due to over loading (Toda et al., 2015). GRF magnitudes will increase as the speed of motion increases (Nigg et al., 1981; Voloshin, 2000). Subsequently, increases in GRF magnitudes result in an increased force experienced by the musculoskeletal system (Watkins, 2009).

The structure of a force trace recorded during bipedal locomotion provides an important foundation for understanding the relationship between GRFs and locomotion. During terrestrial walking, the mass of the subject must be supported against the force of gravity. Although *Polypterus* use both its body and pectoral fins together to produce supportive GRFs, understanding simple bipedal locomotion helps to clarify the force dynamics experienced in a more complex tripodal *Polypterus* system.

Thesis Objectives

Polypterus have been shown to undergo behavioural, anatomical, and physiological changes during both short- and long-term exposure to land. Differences in force environments and locomotor behaviour between aquatic and terrestrial environments are hypothesized to be the cause of these plastic changes observed in the musculoskeletal tissues of *Polypterus*. Despite these observable changes, it is unclear exactly how the pectoral fins are experiencing GRFs during terrestrial locomotion. By measuring and quantifying force production during walking in *Polypterus*, this thesis provides a first look at the relationship between GRFs produced and experienced during walking and the pectoral fins of the amphibious fish, *Polypterus.*

Chapter 2 Forces experienced by pectoral fins of *Polypterus senegalus* during terrestrial locomotion

Abstract

Previous studies have shown significant anatomical, behavioural, and physiological differences in the fins of *Polypterus* raised in terrestrial and aquatic environments. This study provides a first look into the kinematic and GRF data of terrestrial locomotion of the amphibious fish, *Polypterus*. We proposed that novel terrestrial force environments trigger the plastic changes seen in the fish. To understand how forces are experienced by the pectoral fins, *Polypterus* were filmed walking across a force platform synchronizing kinematic motion and ground reaction force data. We then described the kinematics and GRF of a step, using whole group analysis, and then categorizing the steps using two different criteria: 1. *slip;* and 2. *motion*. Within *whole group analysis*, we hypothesized that pectoral fins act primarily as stabilizers and support appendages rather than thrust producers. We predicted that stabilizing (or mediolateral) forces will be greater than thrust (or forward) forces. We also predicted that vertical forces will be greater than both forward and mediolateral forces. For category *slip*, we hypothesized that the duration of the slip phase within a step affects the effectiveness of the gait. We predicted that the slip phase duration is correlated with greater step distances, as well as greater GRF magnitudes. For category *motion*, we hypothesized that the motion of the fin affects the effectiveness of the step. *Polypterus* displays one of two fin motions during walking: *tucked fin* or *untucked fin* motion. We predicted that *untucked* fin steps are correlated with greater step distances, greater GRF magnitudes, and shorter stance durations. We found that there are kinematic and GRF patterns that appear to be a basic requirement of walking through whole group analysis. When analyzing magnitudes of each force component across all steps, we found that vertical (Fz) force magnitudes are consistently greater than both forward (Fx) and lateral (Fy) forces, thus supporting the idea that pectoral fins are used primarily to lift the fore body off the ground during walking. Subgroup analyses have shown that while the occurrence of slip does not have any significant effect on the kinematics or GRF patterns observed, fin motion, specifically *tucked fin* steps were found to have greater center of mass (CoM) distances, and greater mediolateral forces, but longer stance durations compared to *untucked fin* steps. The results from category *slip* suggest that the slip phase is not a requirement for effective walking, and may perhaps be an involuntary movement to simply regain balance during terrestrial locomotion. The change between fin motion also remains relatively stable within a step, but may differ across steps even within the same fish subject. More analysis is required to understand the significance between the fin motions and whether the change is a conscious maneuver during walking.

Introduction

Bipedal locomotion has been studied extensively in the literature and provides an understanding of GRFs produced during walking. Understanding bipedal locomotion can range in complexity, however, in its simplest experiments, researchers can use a single force platform to measure the GRFs produced through the asynchronous leg motion used. This also provides a simple framework that can then be extended to analyze GRFs produced in other quadruped animals, such as rodents or dogs and even hexapodal animals like the cockroach (Holmes et al., 2006; Dickenson et al., 2007). Although not bipedal themselves, *Polypterus* use their pectoral fins in a contralateral pattern, a motion that can be perceived similar to bipeds. Therefore, understanding the relationship between GRFs and bipedal locomotion serves as an excellent preliminary model.

In terrestrial environments, *Polypterus* must overcome gravitational and frictional forces to locomote. The contralateral gait employed by *Polypterus* consists of a single stance phase, during which one pectoral fin is in contact with the ground; and a double stance phase, during which both pectoral fins are in contact with the ground simultaneously (Soutas-Little, 1998). The end of the stance phase occurs as the fins lifts off the ground, entering its swing phase, similar to what is seen during bipedal walking. During terrestrial walking, the mass of the subject must be supported against the force of gravity. Although *Polypterus* use both its body and pectoral fins together to produce supportive GRFs, understanding simple bipedal locomotion helps to clarify the force dynamics experienced in a more complex tripodal *Polypterus* system.

Thesis Hypotheses and Predictions

The transition into fully terrestrial animals, beginning millions of years ago, required aquatic vertebrates to undergo drastic changes over time to overcome the vast differences between aquatic and terrestrial environments (Clack, 2012). One of the most influential differences between aquatic and terrestrial environments is the dominant acting force. Aquatic animals primarily experience the forces of buoyancy, drag and lift, while terrestrial animals must overcome gravitational and frictional forces in order to locomote (Ditsche & Summers, 2014). *Polypterus senegalus* is an amphibious fish that is able to both swim in water and walk overland, and is the closest relative to the common ancestor of actinopterygians and sarcopterygians, the latter of which contains stem tetrapods (Clack, 2012; Clack & Ahlberg, 2016; Standen et al., 2014), making *Polypterus* an excellent model to potentially understand the changes that occurred during this transitional period. Although *Polypterus* prefer to remain in water, when exposed to land they are able to locomote across various substrates using multiple gaits (Standen et al., 2016). Previous literature demonstrates that both periodic and long-term exposure to terrestrial environments produces plastic changes in *Polypterus* anatomy, physiology, and behaviour. It has been speculated that the forces encountered on land, specifically ground reaction forces (GRF), are the driving mechanism behind these observed plastic changes, however there is currently no data on the specific impacts of GRF on *Polypterus* limbs, and how this novel force environment may have influenced the evolutionary transition from water to land.

This thesis takes the shape of a primarily descriptive study. We begin by first describing the kinematics and GRF of a step, using whole group analysis, and then categorizing the steps using two different criteria: 1. when the slip phase occurs within the step; and 2. the motion of the fin during the step; Within group and between group comparisons will allow us to test for the following hypotheses and predictions. Hypothesis #1 states that the pectoral fins act primarily as stabilizers and support appendages rather than thrust producers. We predict that 1a. stabilizing force (Fy) will be greater than thrust (Fx) forces; and 1b. lifting (Fz) forces will be greater than both stabilizing (Fy) and thrust (Fx) forces.

Hypothesis #2 states that fin slip is detrimental to walking. We predict that ~~t~~longer slip durations will 2a. decrease the total distance during a step, and 2b. reduce the magnitudes of GRFs produced. Lastly, hypotheses #3 states that untucked fin motion is a more effective gait than tucked fin motion. We predict that steps in which the fin remains untucked are predicted to have 3a. greater step distances; 3b. greater GRF magnitudes; and 3c. shorter stance durations.

Materials and Methods

Subjects

Polypterus senegalus Cuvier 1829 were obtained from the pet trade (Mirdo Importations Canada, Montreal, QC, Canada). A total of five adults were used for data collection, however only data from two adults were used in the final data analysis. Each fish was held individually in identical aquatic environments and maintained in the University of Ottawa Aquatics Facility on a 12:12 h light cycle at a temperature of 25^{O}C ($\pm$1^{O}C). Fish received similar type and quantity of food and treatment. All experiments were conducted under the University of Ottawa animal care protocol BL-1926. The fish were taken directly from their tanks at the start of all experimental trials. Fish were not exercised prior to any experimental trials, nor was their diet or environment changed or manipulated in any way. The average mass (g) and length (cm) (measured from the tip of the nose to the tail) of each fish was taken across multiple trials obtained over a span of eight months (**Table 1**). All measurements were taken after the completion of data collection for the day.

Table 2.1 Average mass (g) and length taken for each subject. Mass and length measurements were taken after each day of data collection, which were then averaged for each fish. Data was collected from five (5) specimens, however data was analyzed from only two (2) fish.

Step number	Fish ID	Trial	Mass (g)	Length (cm)
1	Polyp2017-053	01	21.8	15.1
2	Polyp2017-053	03	21.8	15.1
3	Polyp2018-018	01	15.38	13.9
4	Polyp2018-018	02A	15.38	13.9
5	Polyp2018-018	02A	15.38	13.9
6	Polyp2018-018	02B	15.38	13.9
7	Polyp2018-018	03	14.49	13.4
8	Polyp2018-018	03	14.49	13.4
9	Polyp2018-018	04	14.49	13.4
10	Polyp2018-018	04	14.49	13.4

Kinematic set-up

Two synchronized, Fastec HS5 high-speed cameras (Fastec Imaging Corp., San Diego, CA, USA) were positioned directly above and in front of the force platform along with a 45^{O} mirror

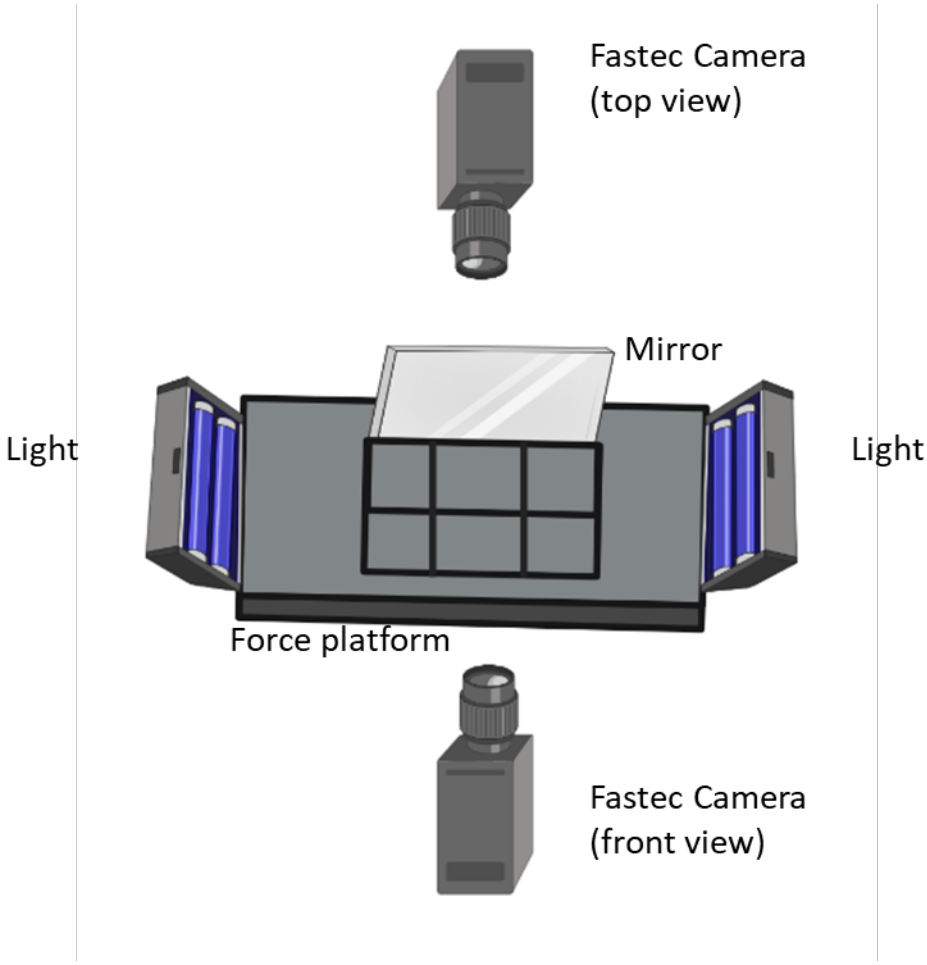

Figure 2.3 Experimental apparatus. Fish walked across an array of six 3D force transducers with two light sources placed on both ends. The lights provided extra illumination to allow for clear video capture. Two synchronized, high-speed cameras positioned dorsally and laterally captured kinematic performance.

to capture 3D motion from two side views and a top view (Fig. 2.3). Fish were taken out of their tanks in a random order and were allowed to walk for an average of two trials each, or until they displayed signs of fatigue or demotivation. Fish were then placed back into their respective tanks, where they remained until the end of all data collection, after which they were taken out again to obtain their mass and length measurements. The time spent walking during these experimental trials were the only form of terrestrial exercise experienced by each fish.

A custom Lego calibration device consisting of 84 known point locations (width=80mm; length=152mm) (Fig. 2.4) distributed about all sides of the Lego device, was used to calibrate the field of view for each camera. The calibration device filled the field of view of both cameras and using direct linear transformation (DLT), allowed us to calibrate camera positions relative to each other. A minimum of eleven points of known position were digitized in at least two camera views and residual values (a measure of point error) for these points were less than 0.5. Once the cameras were calibrated, the 3D position of any point digitized in at least two views could be calculated using DLTdv8 (Hedrick, 2008), through MatLab (version R2017a, The MathWorks, Natick, MA, USA).

A

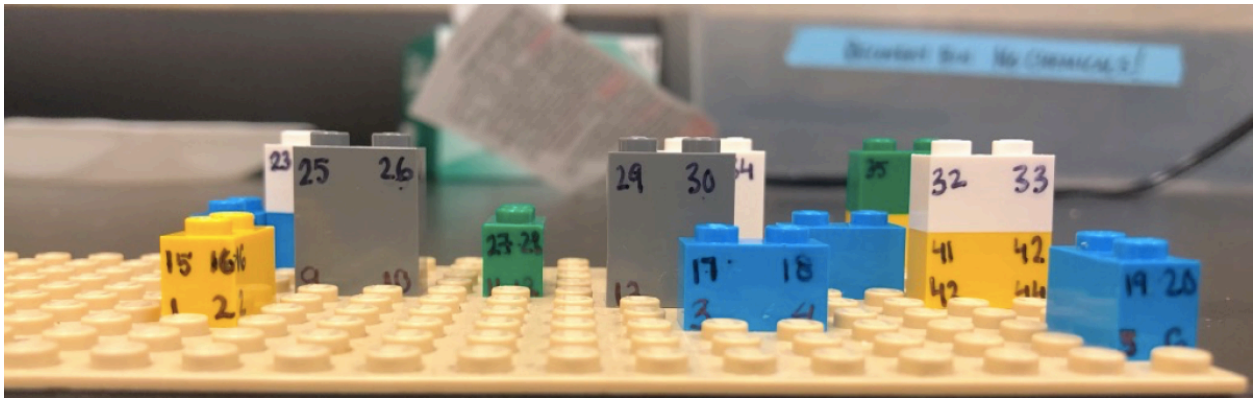

B

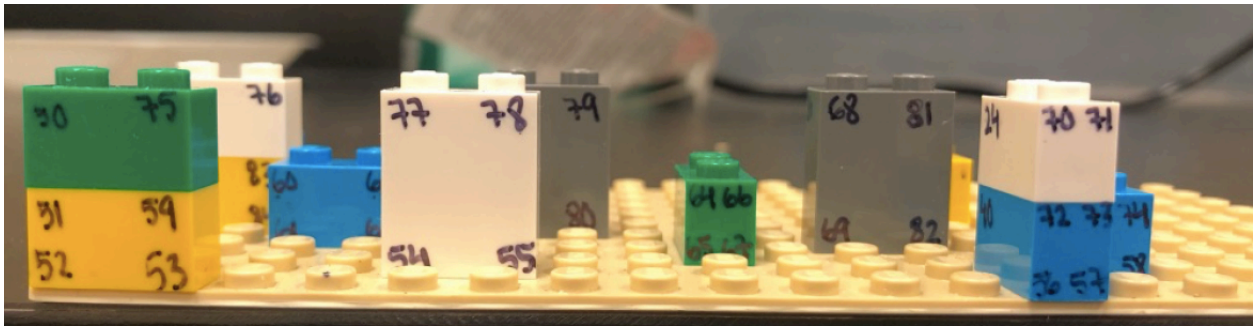

Figure 2.4 Custom Lego device. Images of this Lego device were taken from the front (A), top (not shown), and rear (B) view which were then used to calibrate the field of view for each camera.

Kinematic analysis

The points that were digitized on the body and fins of each fish are indicated in Fig. 2.5, and include the tip of the left fin (point 1), the tip of the right fin (point 2), the tip of the nose (point 3), and the center of the pectoral girdle placed on the top of the body (point 4). The stroke cycle was calculated in milliseconds (ms) from visual observation of the kinematic videos and was defined by the motion of the pectoral fin and anterior portion of the body. The stroke cycle consisted of both the stance phase and the swing phase. The start of stance phase corresponded to when the pectoral fin was visibly loaded, and was determined by visually assessing the moment in time the majority of the pectoral fin was placed directly parallell to the ground. At the same time, the anterior portion of the body slowed down noticeably, and began to either fold over the planted fin, or changes its direction of motion. The end of the stance phase represents the beginning of the swing phase, as well as the mid-cycle of the stroke and occurred when the pectoral fin ceased all contact with the ground. The stance phase consisted

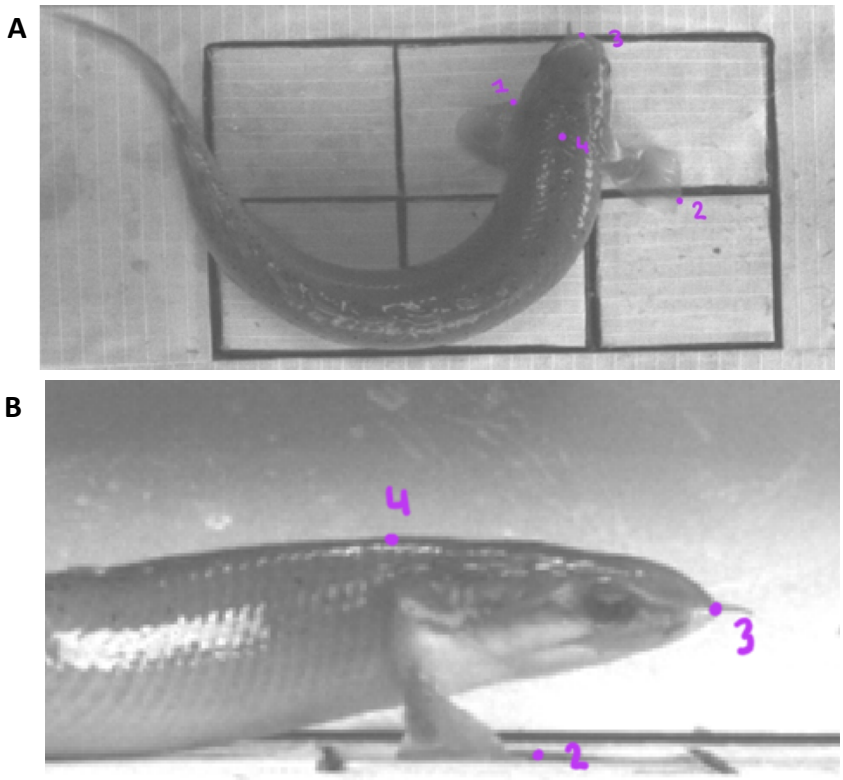

Figure 2.5 Digitized points on *Polypterus* (A) from top view and (B) side view (point 1 is not visible). Points 1 and 2 represent the tips of the left and right pectoral fins, respectively. Point 3 represents the tip of the nose. Point 4 is placed above the pectoral girdle, and represents the center of mass (CoM) of the fish.

of a subphase: fin slip phase. Stance and slip durations were calculated as percentage of stance duration. Duty factor was calculated as stance duration divided by total stroke duration. Fish body motion was quantified using the nose (point 3) and the midpoint of the pectoral girdle (CoM) (point 4) (Fig. 2.5) for each stroke cycle. Using custom Matlab software, kinematic data was translated and rotated about the x-axis, such that the path of the fish followed the x-axis in the increasing direction. This rotation allowed for comparisons between steps and force production to be made. This was done by taking the straightest path of motion over the duration of each stroke cycle. The kinematic variables analyzed for the stance phase included: nose distance, velocity and acceleration; CoM distance, velocity, and acceleration; maximum and minimum nose elevation (Fig. 2.6A); maximum and minimum CoM elevation (Fig. 2.6B); nose and CoM elevation amplitude, which was calculated as the difference between the maximum and minimum values of each respective body point; fin distance, velocity, and acceleration; fin to CoM distance; abduction angle, which was calculated as the angle formed between the nose, CoM, and fin tip (Fig. 2.7); and fin abduction angular velocity. The timings of when these variables occurred during the stance phase were analyzed and plotted using polar plots. Kinematic timings were reported in radians. The means, standard deviations, and standard error of means can be found in the Appendix. Variables calculated during the swing phase were assessed solely in their timings of occurrence and can be found in the Appendix.

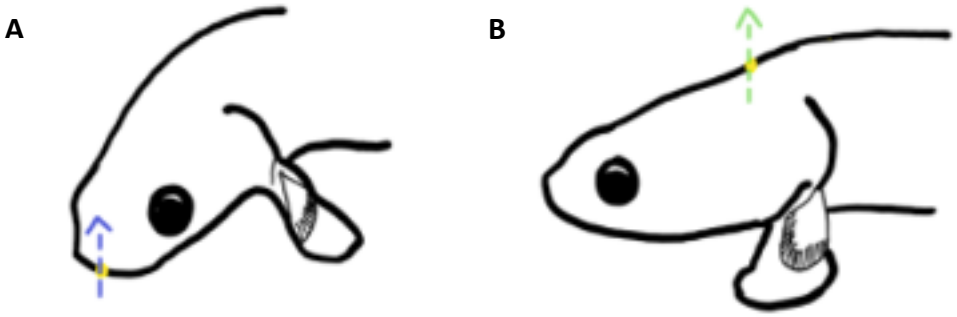

Figure 2.6 Kinematic variables. Body elevation during both the stance phase and the swing phase of the stroke cycle was calculated via (A) the nose, and (B) the CoM.

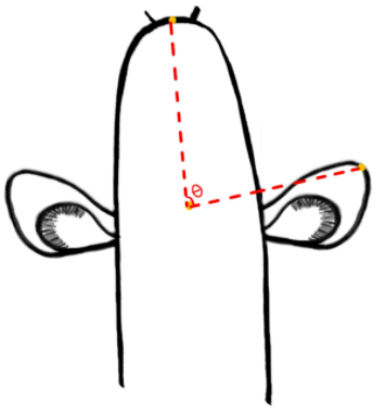

Figure 2.7 Kinematic variables. Fin abduction angle was calculated as the angle created between the nose, CoM, and the tip of the pectoral fin.

Force set-up

Force platforms are a common tool used in clinical studies assessing athletic performances, or locomotion amongst humans, rodents and dogs. Force platforms are useful for examining the kinetic characteristics (e.g. ground reaction forces) along with the kinematic performances (e.g. velocity and acceleration), together providing insight to the external forces involved in specific movements (Beckham et al., 2014).

A custom array of six force transducers were used to capture the raw ground reaction forces (GRFs) produced by each fish in the forward (Fx), lateral (Fy), and vertical (Fz) directions as they walked (Fig. 2.8). The kinematic data and force traces were synchronized using an external trigger. Force data was collected using National Instruments (NI) LabView NXG 5.0 LabView 2020 software. Force data was collected at a frequency of 5000 Hz. Force plate calibration was conducted each day prior to and after all experimental trials. Known weights (1, 3 and 4g) were placed sequentially onto each unloaded force transducer. The linear relationship between transducer output and weight was used to convert raw transducer signal into gF. In addition, for each walking trial, the period prior to loading (inactive portion) was selected as the baseline for each transducer and the average of the baseline was subtracted from the loaded force values to normalize the data. Steps were only considered for analysis if they occurred across transducers 1-5. Transducer 6 was not a reliable source for data as the signal for the vertical force component was extremely noisy, as seen in Fig. 2.8.

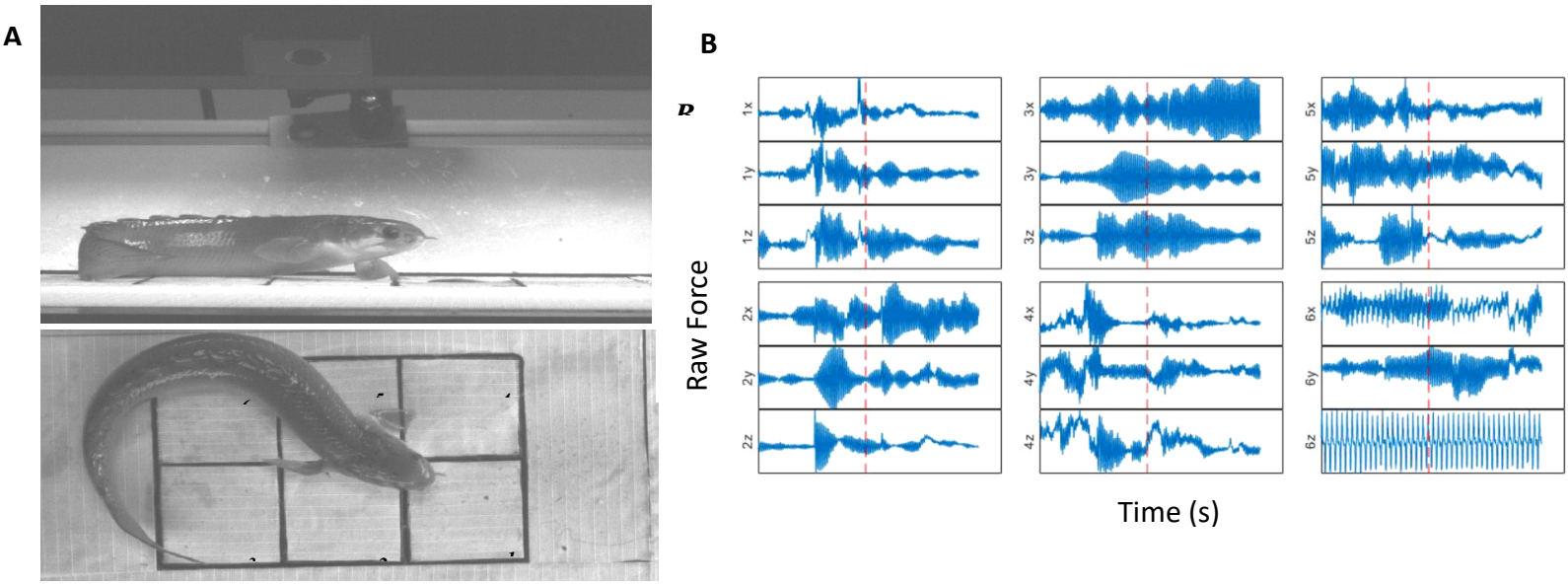

Figure 2.8 Kinematic motion and corresponding raw force signals obtained. *Polypterus* were allowed to freely walk across the force plate (A), which captured the raw force sigals across all six transducers in three axes (B). Force transducers were numbers 1-6 for identification.

Force analysis

All analysis was done using custom code in Matlab (Hedrick, 2008). External noise and unwanted signals were filtered with a 75 Hz Fourier Transform Lowpass filter. In order to align with the translated and rotated kinematic data, force data was similarly rotated. All steps were rotated such that the fish was moving from left to right. This was done by rotating all steps moving from right to left about the x-axis, aligning all steps to be parallel with the x-axis, and then further reflecting all right fin steps in the y-axis so they were measured on the same axis as left fins. Force data was normalized to body weight. In many cases a step occurred across multiple force transducers. The force transducers that were involved in a step were visually assessed from the kinematic videos. Force traces taken from each transducer involved were then summed to obtain a single trace in each direction (forward (Fx), lateral (Fy), and vertical (Fz)) (Fig. 2.9). Analysis was done for each force component in the forward (Fx), lateral (Fy), and vertical (Fz) directions. Force variables analyzed during the stance phase include peak force magnitude; minimum force magnitude; and force magnitude at the moment of impact. Timing variables include the duration between the onset of loading to the peak force produced for forward, lateral, and vertical propulsion. The mean, standard deviation, and standard error of means can be found in the Appendix. Resultant force vectors were calculated by taking the average force prior to the slip phase, during the slip phase, and after the slip phase for each

step. For steps with no slip phases, the resultant vector was calculated by taking the average force produced from onset to offset of the step.

Statistical analysis

All statistical tests were completed using custom R software (version 3.6.1, R Core Team, 2021). For *whole group* analysis, in which all steps were pooled together, paired T-test analyses

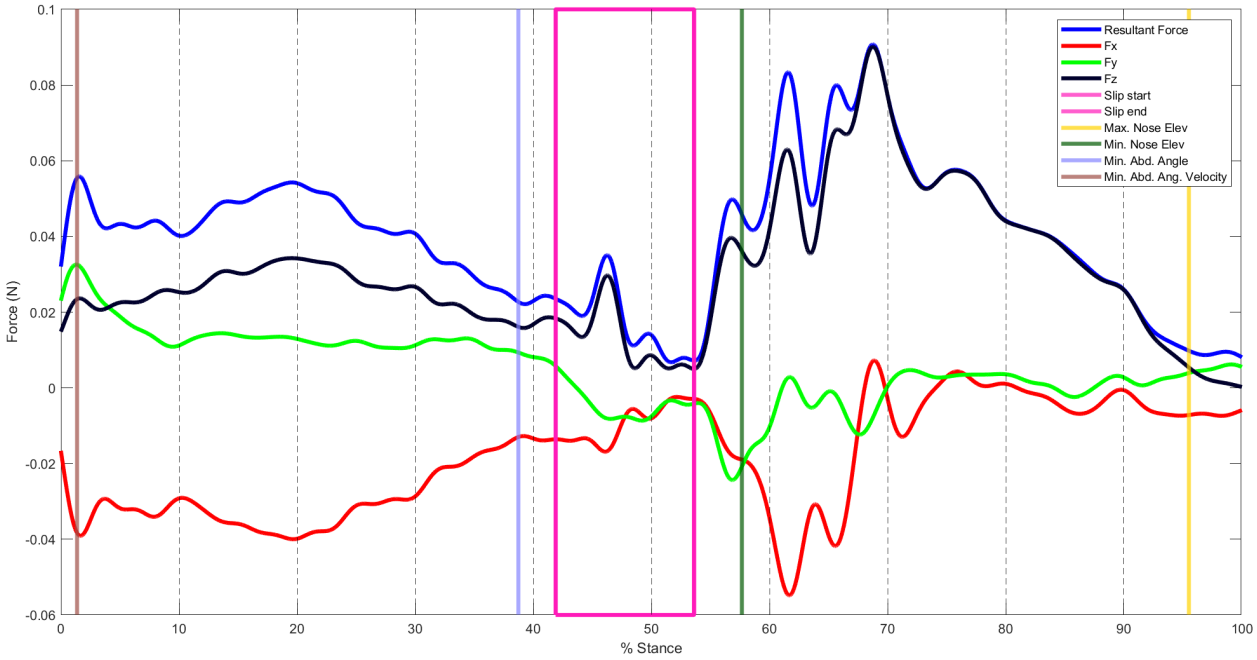

Figure 2.9 Representative force trace. The force trace represents each force component: anteroposterior (Fx) (red), mediolateral (Fy) (light green), vertical (Fz) (black) produced during a single stance phase, as well as the resultant GRF magnitude, depicted by the dark blue colour. Each coloured vertical line corresponds to a specific kinematic timepoint during the stance phase. The trace is composed of forces produced by both the pectoral fin and the anterior body as it was difficult to differentiate between the two and their contributions to the force production.

were conducted in order to determine for significant differences between maximum GRF magnitudes. Variables analyzed can be found in Table A9 listed in the Appendix. To assess the effects of the slip phase on the kinematic and force variables observed, a Linear Mixed Effects (LME) model was used (eq.6). Steps were numbered in the succession they occurred during each trial. Since multiple measurements were collected from each fish repeatedly, random effects were included as a nesting of a trial within the corresponding fish to account for non-independence. Fixed independent variables include stance duration and slip duration. Dependent variables include both kinematic and force variables and can be found in Table A10 listed in the Appendix. A sample of the code used to apply the LME model is given in equations. The significance level was set at $\alpha = 0.05$. For category *motion*, unpaired two sample T-Tests were conducted to assess for differences between *tucked* and *lateral* fin motions. Equality in the variances of the two fin motion groups was determined by conducting preliminary F-tests.

Variables analyzed can be found in Table A11 listed in the Appendix. The steps analyzed, as well as the category they were defined under can be found in Table 2.2.

Temporal variables were analyzed using circular statistics using custom Matlab software, and modified from Standen et al (2016) and Zar (1999). All angular data was recorded in radians, with a range of 0-2π. 0 radians represented the start of the stance phase, 2π radians represented the end of the stance phase. Rayleigh test was used to test for directionality or uniformity of all kinematic and force variables, by confirming the existence of von Mises distribution. Note: data was distributed about the entire polar plot prior to conducting the Rayleighs test. The polar plots provided throughout this thesis depict both the stance phase and swing phase of the stroke cycle on separate halves of the same plot, this was done for visual aesthetics.

$$LME = lme\ (dependent\ variable \sim fixed\ effect, random = \sim 1|Fish/step) \qquad \text{(eq.5)}$$

Table 2.2 Whole group and subgroup categories. Ten (n=10) individual steps (*column 1*) from two (n=2) fish (*column 2*) were recorded and analyzed, each with a unique force trace obtained from signals collected from the force platform. Force traces have been labeled numerically for simplicity and correspond to the number listed in the table. The specific trial (*column* 3) and fin of interest (*column 4*) have also been labeled to keep record of the steps analyzed. For fish with multiple steps within a single trial, steps have been ordered in the succession they occurred (*column 5*). Steps have been analyzed in a single whole study analysis (*'preliminary analysis', see below*), as well as three sub-analyses as indicated in *columns 6-8*. *Categorization by slip:* This group categorizes the steps depending on the time of occurrence of the slip phase within the stance phase. Subgroup *'mid-slip'* contains steps that have a slip phase around 50% stance; subgroup *'variable slip'* contains steps that have a slip phase either before or after 50% stance; and subgroup *'special slip'* contains steps that possess either no slip phase, or multiple (i.e. one or more) slip phases within a single stance. *Categorization by motion:* This group categorizes the steps depending on the motion of the fin during the stance phase. Subgroup *tucked fin'* contains steps in which the fin becomes 'tucked' underneath the anterior body at some point during stance; subgroup *'lateral fin'* contains steps in which the planted fin remains to the side of the anterior body at all times during the step. The number indicated beside each subgroup name corresponds to the number within the respective plots, which will be presented in both the *Results* section, as well as in the *Appendix* of this thesis.

Step number	Fish ID	Trial	Fin	Step order	Subgroup - Categorization by slip	Subgroup - Categorization by motion
1	Polyp2017-053	01	L	1	Special slip 3	Tucked fin 1
2	Polyp2017-053	03	L	1	Mid-slip 1	Untucked fin 2
3	Polyp2018-018	01	L	1	Mid-slip 1	Tucked fin 1
4	Polyp2018-018	02A	L	2	Variable slip 2	Untucked fin 2
5	Polyp2018-018	02A	R	1	Special slip 3	Untucked fin 2
6	Polyp2018-018	02B	L	1	Mid-slip 1	Tucked fin 1
7	Polyp2018-018	03	L	2	Variable slip 2	Untucked fin 2
8	Polyp2018-018	03	R	1	Variable slip 2	Untucked fin 2
9	Polyp2018-018	04	L	2	Special slip 3	Untucked fin 2
10	Polyp2018-018	04	R	1	Mid-slip 1	Untucked fin 2

Results

The role of the pectoral fins during walking

In this study, *whole group* analysis consisted of a total of ten (n=10) steps analyzed together in order to determine and describe general patterns observed in *Polypterus* during walking. Significant kinematic and force temporal variables analyzed using Rayleigh's test across whole group analysis are shown in Fig. 2.10. Rayleigh's test values, as well as the means of variables analyzed can be found in Appendix Table A2. Minimum abduction angular velocity occurred on average near the beginning of stance phase along with maximum lateral (Fy) force production (Fig. 2.10). In contrast, lateral forces reached its minimal magnitudes in the second half of stance (Fig. 2.10). Interestingly, the nose reaches its minimum and maximum elevations in the first half of the stance phase, with the maximum elevation occurring just after minimum elevation. Nose reaches its maximum elevation just prior to 50% stance (Fig. 2.10). Nose reaches its minimum velocity at the end of the swing phase, closer to the onset of the next stance phase (Fig. 2.10). This also coincides with visual observations in which the anterior body appears to decrease its velocity at the end of the swing phase as it enters into the next stance phase of the same fin.

GRFs were measured and defined as anteroposterior (Fx), mediolateral (Fy), and vertical (Fz). They can also be described as thrust, stabilizing, and lifting forces, respectively. Thrust forces aid in forward and backwards motion determined primarily by propulsion and braking movements during walking. Stabilizing forces refer to forces used to counteract external or internal perturbations in the mediolateral direction specifically. Lastly, lifting forces aid in the elevation of the anterior body during walking. Altogether, these forces allow for *Polypterus* to locomote across land. Statistical analyses between each force component revealed that there is no difference in the means of peak magnitudes of thrust (Fx) and stabilizing (Fy) forces during walking (Fig. 2.11A). There was also no difference in the distribution of peak magnitude values between thrust (Fx) and stabilizing (Fy) forces, suggesting that the peak magnitudes and range of values produced by the pectoral fins in the anteroposterior and mediolateral directions are comparable across all steps. The timings at which peak thrust (Fx) and stabilizing (Fy) forces during a single gait cycle differs however, with maximum and minimum stabilizing (Fy) force magnitudes occurring at predictable timings during the gait cycle (Fig. 2.10). Statistical analyses also revealed that across all steps, lifting (Fz) forces produced greater peak magnitudes

compared to both thrust (Fx) and stabilizing (Fy) forces (Fig. 2.11B & C). The range of individual values recorded for vertical (Fz) forces also occurred at greater values compared to both anteroposterior (Fx) and mediolateral (Fy) forces. The magnitudes of each force component generated at the beginning of a step were analyzed (Fig. 2.12). At the onset of the stance phase, the fin is being planted directly downward, producing greater vertical (Fz) forces relative to the amount of thrust (Fx) and stabilizing (Fy) forces being generated (Fig. 2.12B & C). Interestingly, there is no difference in the magnitude of forces being produced in the anteroposterior (Fx) and mediolateral (Fy) directions at the instantaneous moment of the beginning of the stance phase (Fig. 2.12A). These results, in combination with the predictability in the occurrence of peak mediolateral (Fy) forces during a step suggests that mediolateral (Fy) forces occur immediately after the onset of loading, when the fin begins to move laterally in an effort to stabilize itself against the incoming wave of propulsion generated by the posterior body.

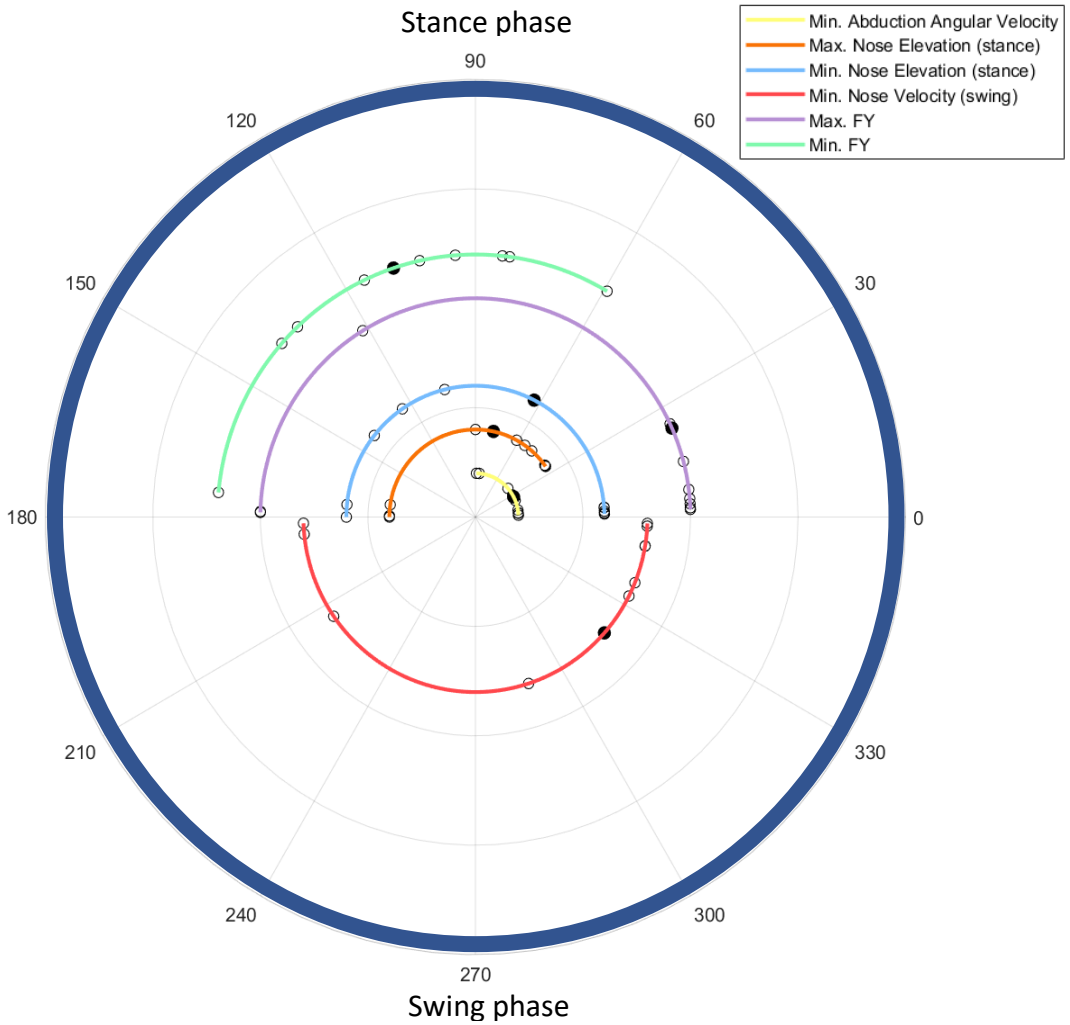

Figure 2.10 Significant kinematic and force temporal variables within whole group analysis. The entire stroke is represented from 0-360 °, with the stance phase beginning at 0° and ending at 180°, and swing phase beginning from 180° and ending at 0° or 360°. The variables that show directionality are minimum abduction angular velocity (yellow); maximum nose elevation during stance (orange); minimum nose elevation during stance (blue); minimum nose velocity during swing phase (red); maximum lateral (Fy) force (purple); and minimum lateral (Fy) force (green).

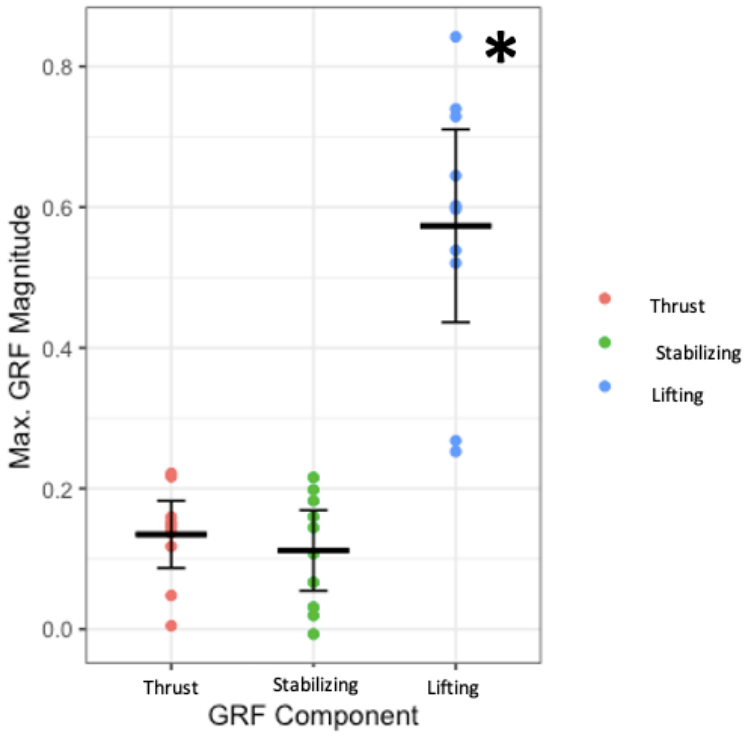

Figure 2.11 Differences in maximum GRF magnitudes measured during walking. Force components are differentiated by colour as indicated in the associated legend. Individual data points are represented by the respective coloured dots. Forces were measured in its component force directions: (A) Anteroposterior (Fx) versus mediolateral (Fy); (B) Anteroposterior (Fx) versus vertical (Fz); and (C) Mediolateral (Fy) versus vertical (Fz). Mean and 95% CI are indicated by the black bars. Asterisks indicate significant differences between the force components. P-values are reported in Table A9 in the Appendix.

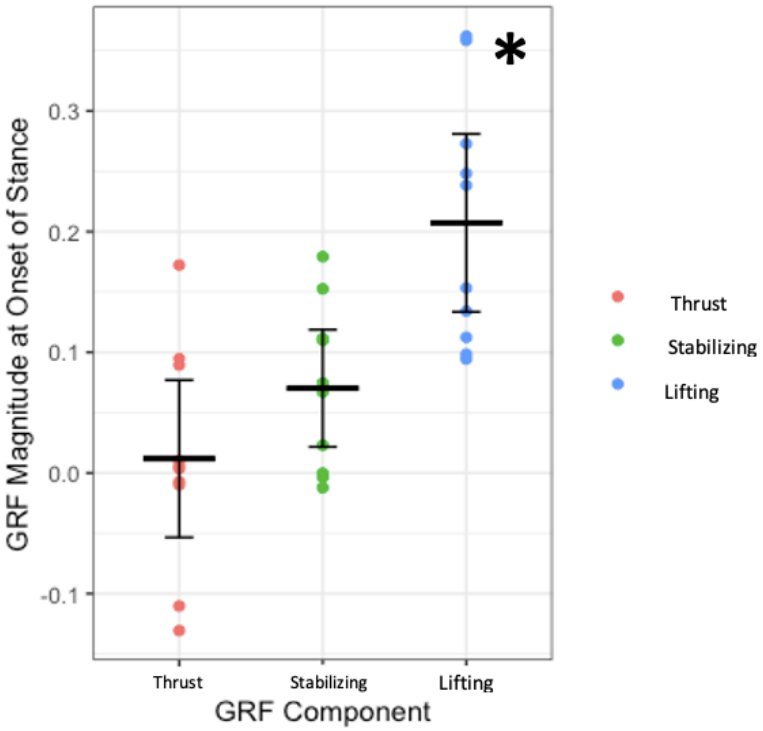

Figure 2.12 Differences in GRF magnitudes measured at the onset of the stance phase during walking. Force components are differentiated by colour as indicated in the associated legend. Individual data points are represented by the respective coloured dots. Forces were measured in its component force directions: (A) Anteroposterior (Fx) versus mediolateral (Fy); (B) Anteroposterior (Fx) versus vertical (Fz); and (C) Mediolateral (Fy) versus vertical (Fz). Mean and 95% CI are indicated by the black bars. Asterisks indicate significant differences between the force components. P-values are reported in Table A9 in the Appendix.

Category slip: The effects of the slip phase on walking

Slip durations had no significant correlation with the kinematic variables observed (Fig. 2.13). These variables included nose distance (Fig. 2.13A); CoM distance (Fig. 2.13B); and fin distance (Fig. 2.13C). This suggests that the occurrence and duration of the slip phase within a step provides neither enhances nor disrupts the distance moved during walking. With respect to the kinetic variables, slip duration was found to have no correlation to peak GRF magnitudes in the anteroposterior (Fx), mediolateral (Fy), or vertical (Fz) directions (Fig. 2.13D-F). The instantaneous GRF magnitudes at the onset of the stance phase were also analyzed. GRFs produced in the anteroposterior (Fx) and mediolateral (Fy) direction at the onset of the stance phase had no significant correlation to the duration of slip during a step (Fig. 2.13G & H). Interestingly, the only variable measured that was found to have a significant correlation to slip duration, was the magnitude of vertical (Fz) force at the onset of the stance phase (Fig. 2.13I). Since the slip phase occurs after the onset of the stance phase, this finding suggests that greater vertical (Fz) GRF magnitudes at the beginning of the step is correlated with longer slip durations.

The effects of stance duration were also analyzed. Statistical analyses found that stance duration had a positive correlation with nose distance (Fig. 2.14A), CoM distance (Fig. 2.14B), and fin distance (Fig. 2.14C). Stance duration had no significant correlation with peak force production in the anteroposterior (Fx), mediolateral (Fy), or vertical directions (Fz) (Fig. 2.14D-F). As the duration of the stance phase increased, fish were found to move their nose, CoM, and fins across greater distances. Although this suggests that longer stance durations may be more effective during walking, the inclusion of the slip phase within the stance phase suggests otherwise. Stance durations with shorter slip phases would provide the most effective walking gait. Although stance duration was not correlated to peak GRF magnitudes, there was a positive correlation to the time it takes to reach peak anteroposterior (Fx) and vertical (Fz) forces. This suggests as stance durations increase, peak anteroposterior (Fx) and vertical (Fz) forces will be reached later during the step.

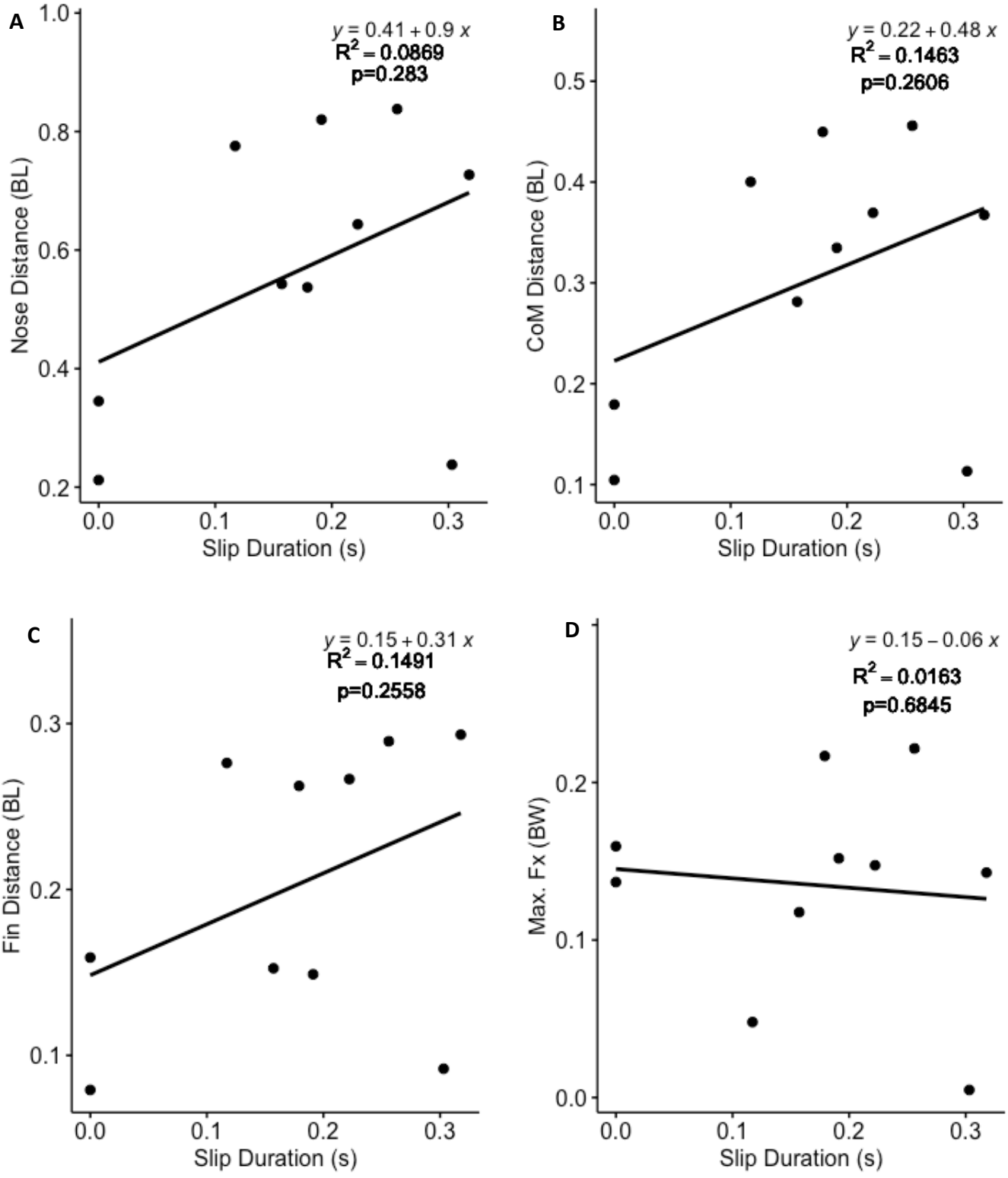
A
y = 0.41 + 0.9 x
R² = 0.0869
p=0.283
Nose Distance (BL)
Slip Duration (s)
B
y = 0.22 + 0.48 x
R² = 0.1463
p=0.2606
CoM Distance (BL)
Slip Duration (s)
C
y = 0.15 + 0.31 x
R² = 0.1491
p=0.2558
Fin Distance (BL)
Slip Duration (s)
D
y = 0.15 – 0.06 x
R² = 0.0163
p=0.6845
Max. Fx (BW)
Slip Duration (s)

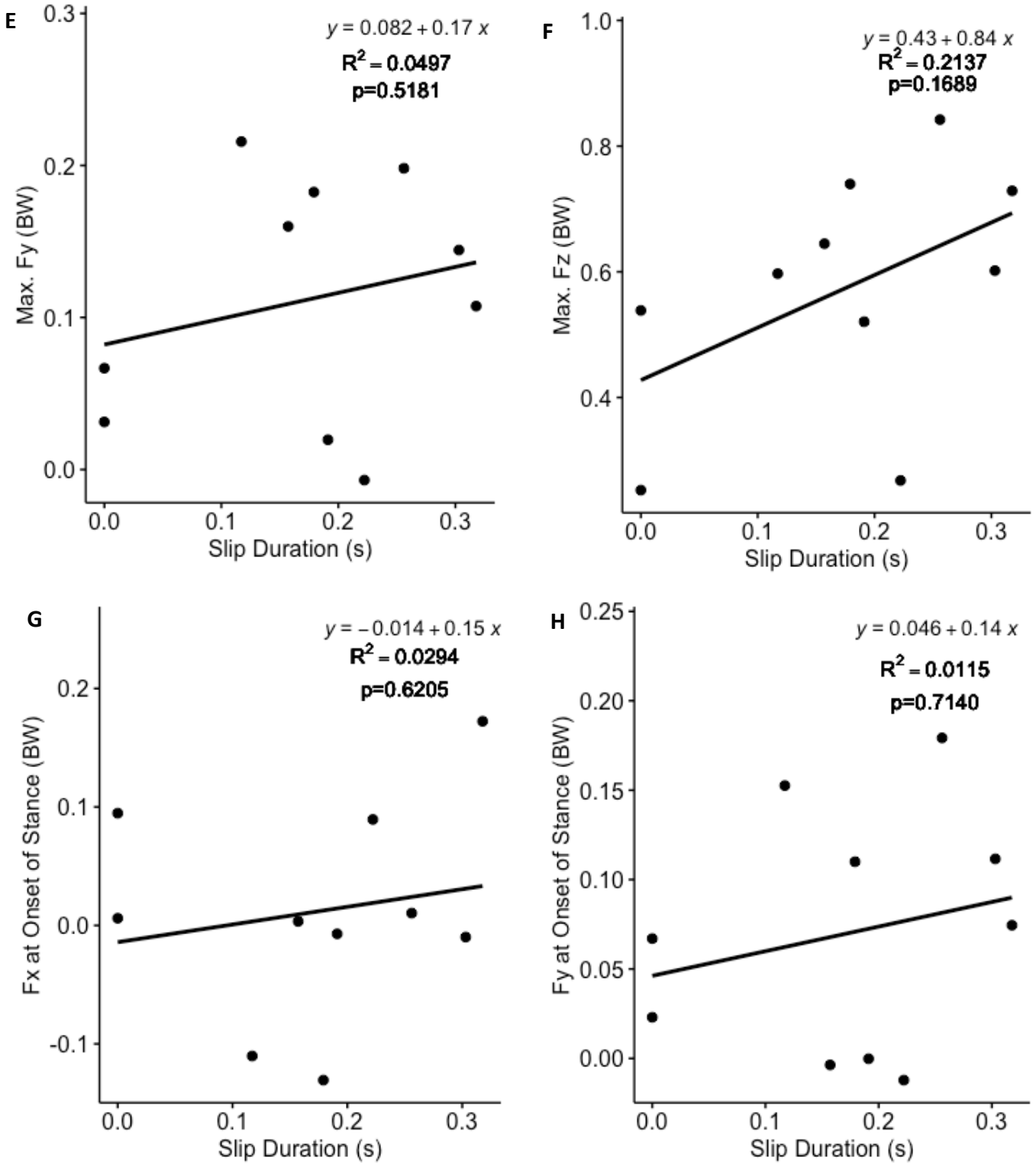
E
y = 0.082 + 0.17 x
R² = 0.0497
p=0.5181
Max. Fy (BW)
Slip Duration (s)
F
y = 0.43 + 0.84 x
R² = 0.2137
p=0.1689
Max. Fz (BW)
Slip Duration (s)
G
y = −0.014 + 0.15 x
R² = 0.0294
p=0.6205
Fx at Onset of Stance (BW)
Slip Duration (s)
H
y = 0.046 + 0.14 x
R² = 0.0115
p=0.7140
Fy at Onset of Stance (BW)
Slip Duration (s)

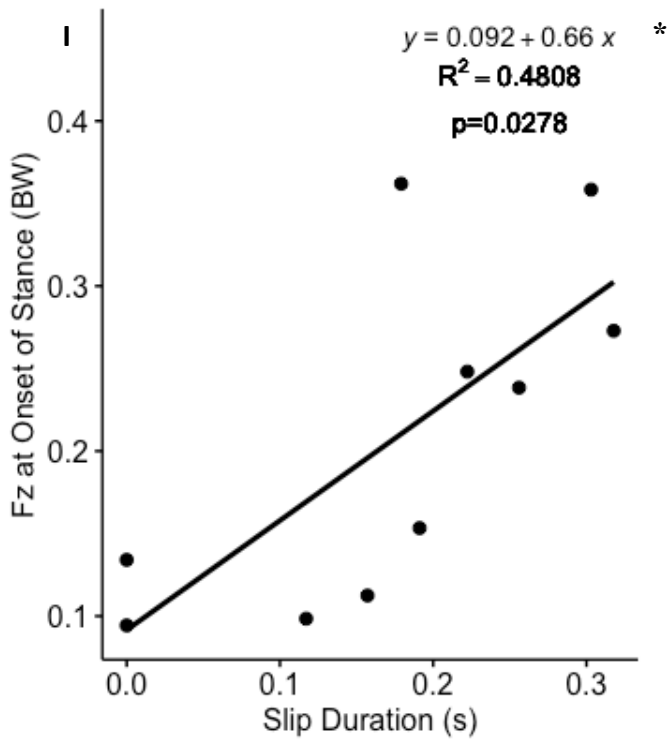

Figure 2.13 The effects of slip duration on kinematic and kinetic variables within whole group analysis (n=10). The duration of the slip phase within a step was found to have no significant correlation to (A) total nose distance; (B) total CoM distance; (C) total fin distance; (D) maximum anteroposterior (Fx) force production; (E) maximum mediolateral (Fy) force production; or (F) maximum vertical (Fz) force production. The linear relationship is indicated in the top right corner of each plot. The marginal R^2 value, along with the corresponding p-values are also indicated in the top right corner of each plot. Marginal and conditional R^2 values, as well as p-values are recorded in Table A10 in the Appendix.

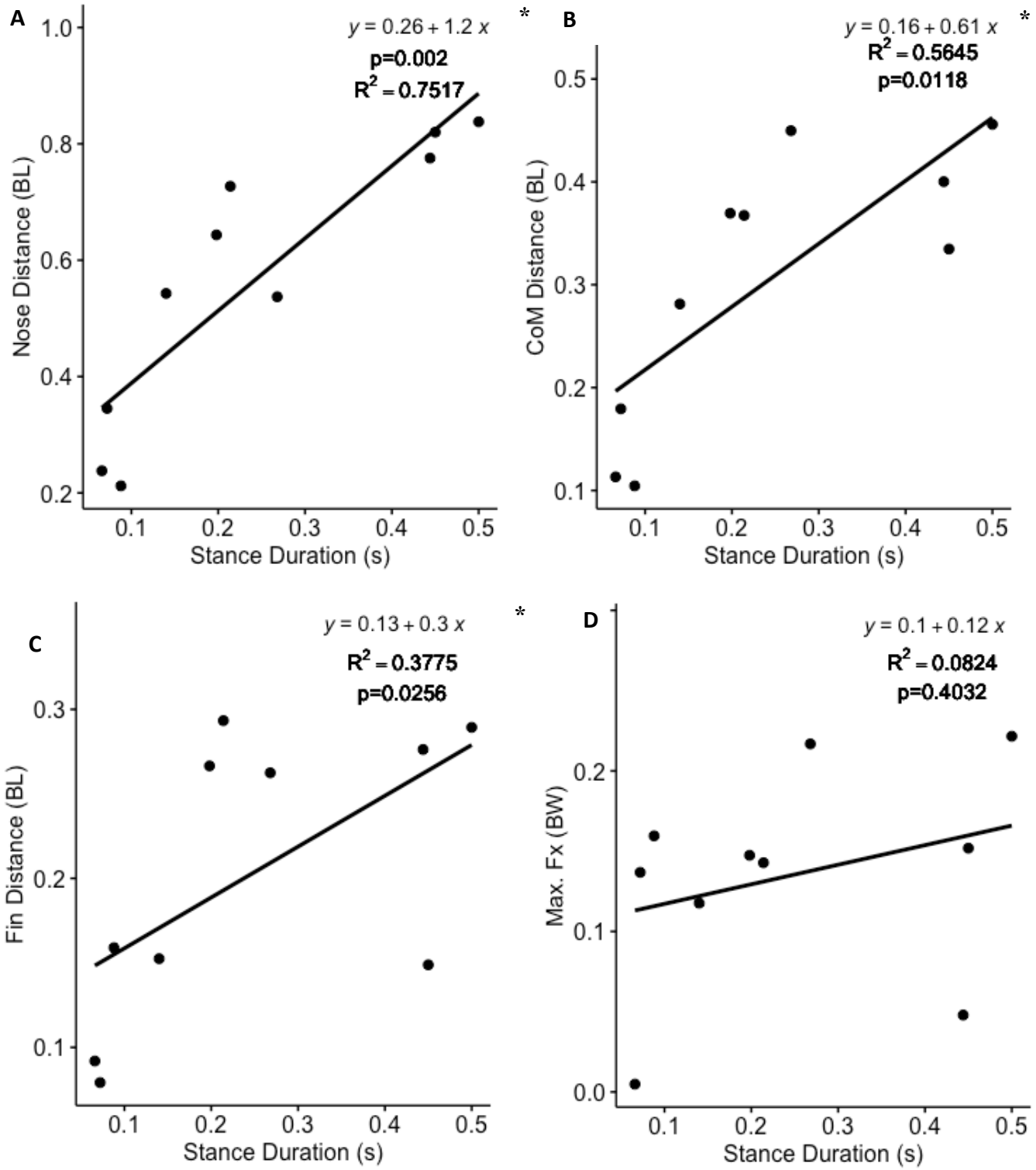
A
y = 0.26 + 1.2 x
p=0.002
R2 = 0.7517
Nose Distance (BL)
Stance Duration (s)
*
B
y = 0.16 + 0.61 x
R2 = 0.5645
p=0.0118
CoM Distance (BL)
Stance Duration (s)
*
C
y = 0.13 + 0.3 x
R2 = 0.3775
p=0.0256
Fin Distance (BL)
Stance Duration (s)
*
D
y = 0.1 + 0.12 x
R2 = 0.0824
p=0.4032
Max. Fx (BW)
Stance Duration (s)

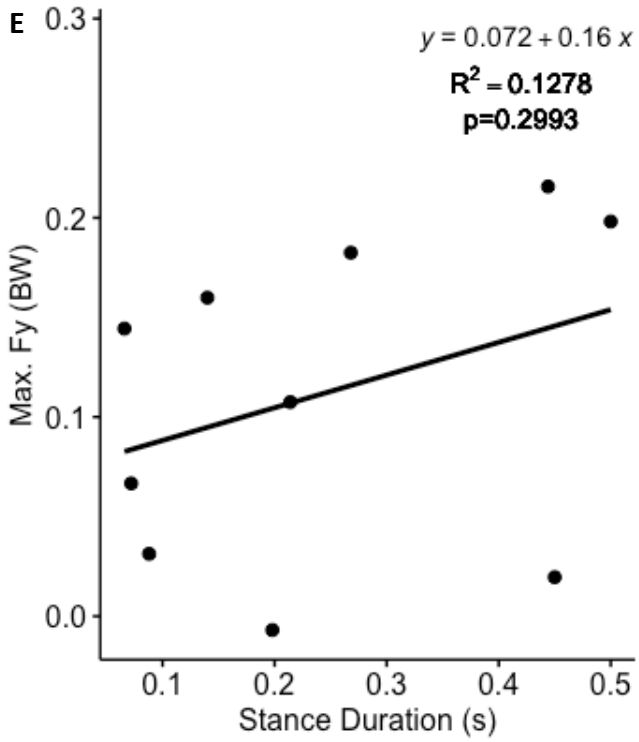
E
y = 0.072 + 0.16 x
R² = 0.1278
p=0.2993
Max. Fy (BW)
Stance Duration (s)

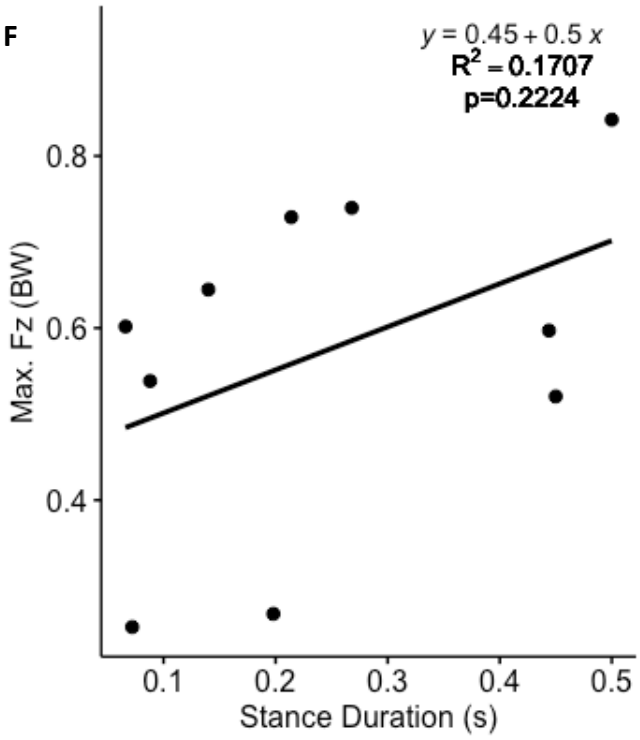
F
y = 0.45 + 0.5 x
R² = 0.1707
p=0.2224
Max. Fz (BW)
Stance Duration (s)

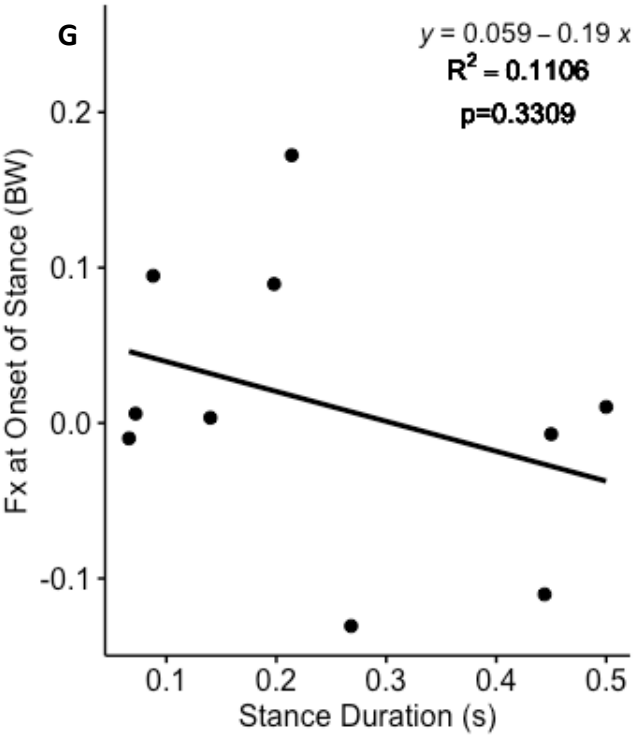
G
y = 0.059 – 0.19 x
R² = 0.1106
p=0.3309
Fx at Onset of Stance (BW)
Stance Duration (s)

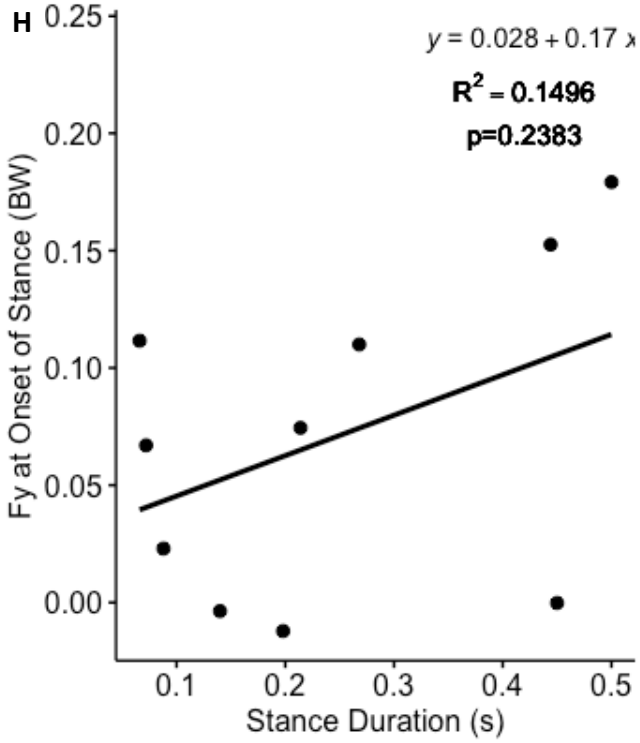
H
y = 0.028 + 0.17 x
R² = 0.1496
p=0.2383
Fy at Onset of Stance (BW)
Stance Duration (s)

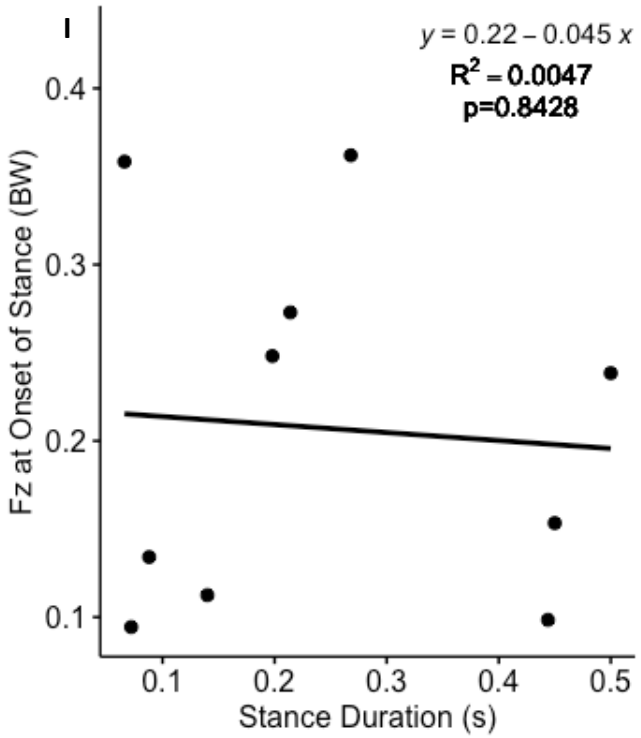

Figure 2.14 The effects of stance duration on kinematic and kinetic variables within whole group analysis (n=10). Significant correlations are indicated by the asterisks. Stance duration was found to have positive correlations with (A) nose distance, (B) CoM distance, and (C) fin distance. The duration of stance was found to have no correlation with peak GRF production (D-F). The linear relationship is indicated in the top right corner of each plot. The marginal R^2 value, along with the corresponding p-values are also indicated in the top right corner of each plot. Marginal and conditional R^2 values, as well as p-values are recorded in Table A10 in the Appendix.

Category motion: The effects of fin motion on walking

During swimming and walking, *Polypterus* use different motions of the fin and body to locomote. The pectoral fins switch roles from acting as propulsors in steady swimming to aiding in lifting and supporting the body during walking. Within walking, *Polypterus* have shown to use different gaits depending on the substrate they are walking over. In this present study, *Polypterus* were observed to use two different gaits during walking. The gait employed did not change within a single walking trial, however it may have switched between trials. Fin motion was categorized into two subgroups: subgroup *tucked fin* in which the fin would, at any point in a single step, get tucked underneath the anterior body. This motion would occur from approximately mid-stance until near end of the stance phase, as the fin would move out from underneath the body and enter the swing phase. Subgroup *untucked fin* contains steps in which the fin always remains visible and to the side of the body during a single step. Interestingly, despite the visible differences in motion, maximum lateral (Fy) force is predictable, occurring in the first half of stance within both subgroups (Fig. 2.15). Minimum lateral (Fy) force production is only predictable within subgroup *untuckedl fin* and occurs between 37-84% stance (Fig. 2.15). The only other predictable variable within subgroup *tucked fin* is minimum CoM velocity during the following swing phase, which occurs immediately at the start of the swing phase, just after

the end of the stance phase (Fig. 2.15). Within subgroup *untucked fin*, minimum abduction angular velocity occurs on average between 0-25% stance (Fig. 2.15). Both maximum and minimum nose elevation are also predictable, with minimum elevation occurring in the second half of stance, and maximum elevation occurring in the first half (Fig. 2.15). Nose velocity reaches its minimum between 75-100% swing (Fig. 2.15).

Statistical analyses conducted between the two fin motions revealed that on average, *tucked fins* were associated with greater CoM distances (Fig. 2.16B), higher peak mediolateral (Fy) force production (Fig. 2.16E), and longer stance durations (Fig. 2.16G) across steps compared to *untucked fin* steps. For maximum mediolateral (Fy) force magnitudes produced, *tucked fins* produced a significantly greater range of peak forces compared to *untucked fins.* Interestingly, for maximum anteroposterior (Fx) force magnitudes, *tucked fin* steps had a much larger range of recorded measurements compared to *untucked fin* steps (Fig. 2.16D). This suggests that thrust (Fx) production magnitudes were highly variable in *tucked fins*, while they appeared to be more concentrated in *untucked fin* steps. For stance duration*, tucked fin* steps also had a greater distribution of timings measured, whereas *untucked fin* steps appeared to have a more concentrated range. Despite the difference found in stance duration between the two fin motions, slip duration has no significant difference (Fig. 2.16H). The instantaneous GRF magnitudes produced at the onset of the stance phase were analyzed. GRF production in the anteroposterior (Fx) and mediolateral (Fy) directions were found to have significant differences between the two fin motions. Interestingly, *untucked fins* produced greater thrust (Fx) forces at the onset of the stance phase (Fig. 2.16I) compared to *tucked fin* steps, but smaller stabilizing (Fy) forces at the same time (Fig. 2.16J). There was no difference in vertical (Fz) force magnitudes at the onset of the stance phase between the fin motions (Fig. 2.16K). As mentioned before, *tucked fin* steps had longer stance durations (Fig. 2.16G). Interestingly, *tucked fins* also took longer to reach peak thrust (Fx) forces (Fig. 2.16L), although the timing of occurrence for peak thrust (Fx) forces were not found to be predictable (Fig. 2.15). The time to reach both stabilizing (Fy) and lifting (Fz) forces were not significantly different between *tucked* and *untucked* fin steps (Fig. 2.16M & N).

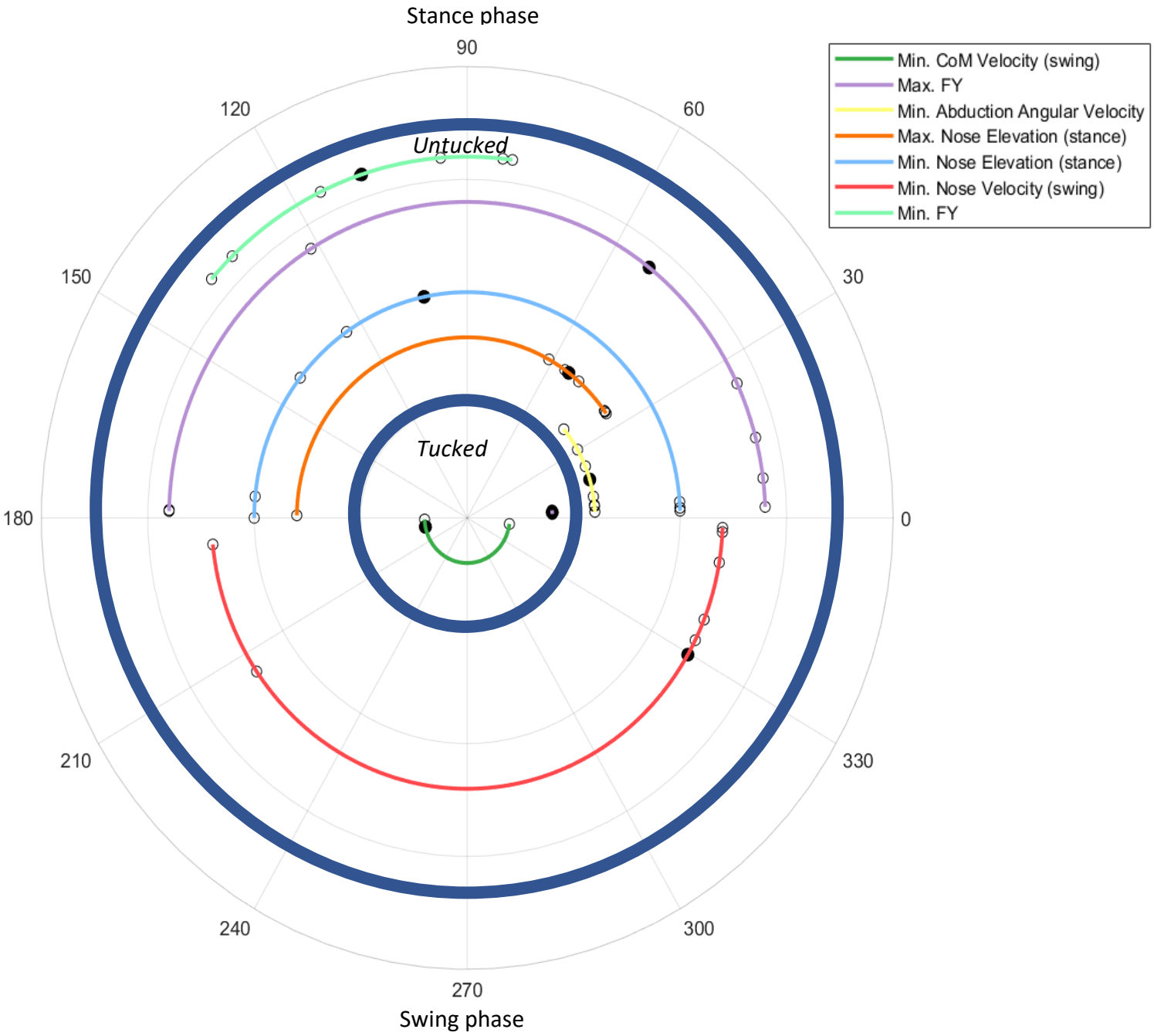

Figure 2.15 Significant kinematic and force temporal variables within the category *motion*. The entire stroke is represented from 0-360 °, with the stance phase beginning at 0° and ending at 180°, and swing phase beginning from 180° and ending at 0° or 360°. Thick dark blue lines are used to distinguish subgroups from each other. The variables that show directionality are minimum CoM velocity during swing phase (dark green), maximum lateral (Fy) force (purple), minimum abduction angular velocity (yellow), maximum nose elevation during stance (orange), minimum nose elevation during stance (light blue), minimum nose velocity during swing phase (red), and minimum lateral (Fy) force (green).

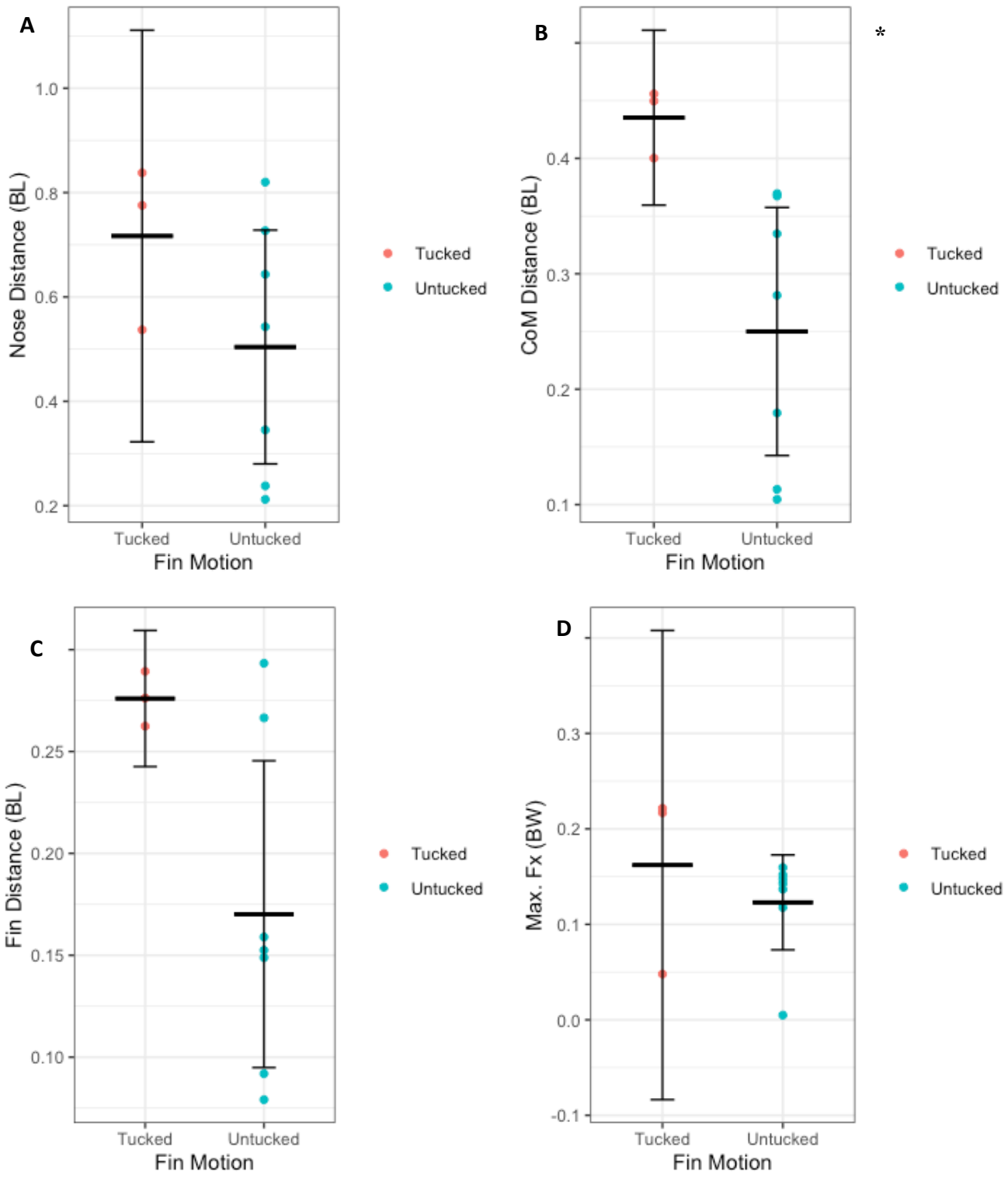
A
Nose Distance (BL)
1.0
0.8
0.6
0.4
0.2
Tucked
Untucked
Fin Motion
Tucked
Untucked
B
*
CoM Distance (BL)
0.4
0.3
0.2
0.1
Tucked
Untucked
Fin Motion
Tucked
Untucked
C
Fin Distance (BL)
0.25
0.20
0.15
0.10
Tucked
Untucked
Fin Motion
Tucked
Untucked
D
Max. Fx (BW)
0.3
0.2
0.1
0.0
-0.1
Tucked
Untucked
Fin Motion
Tucked
Untucked

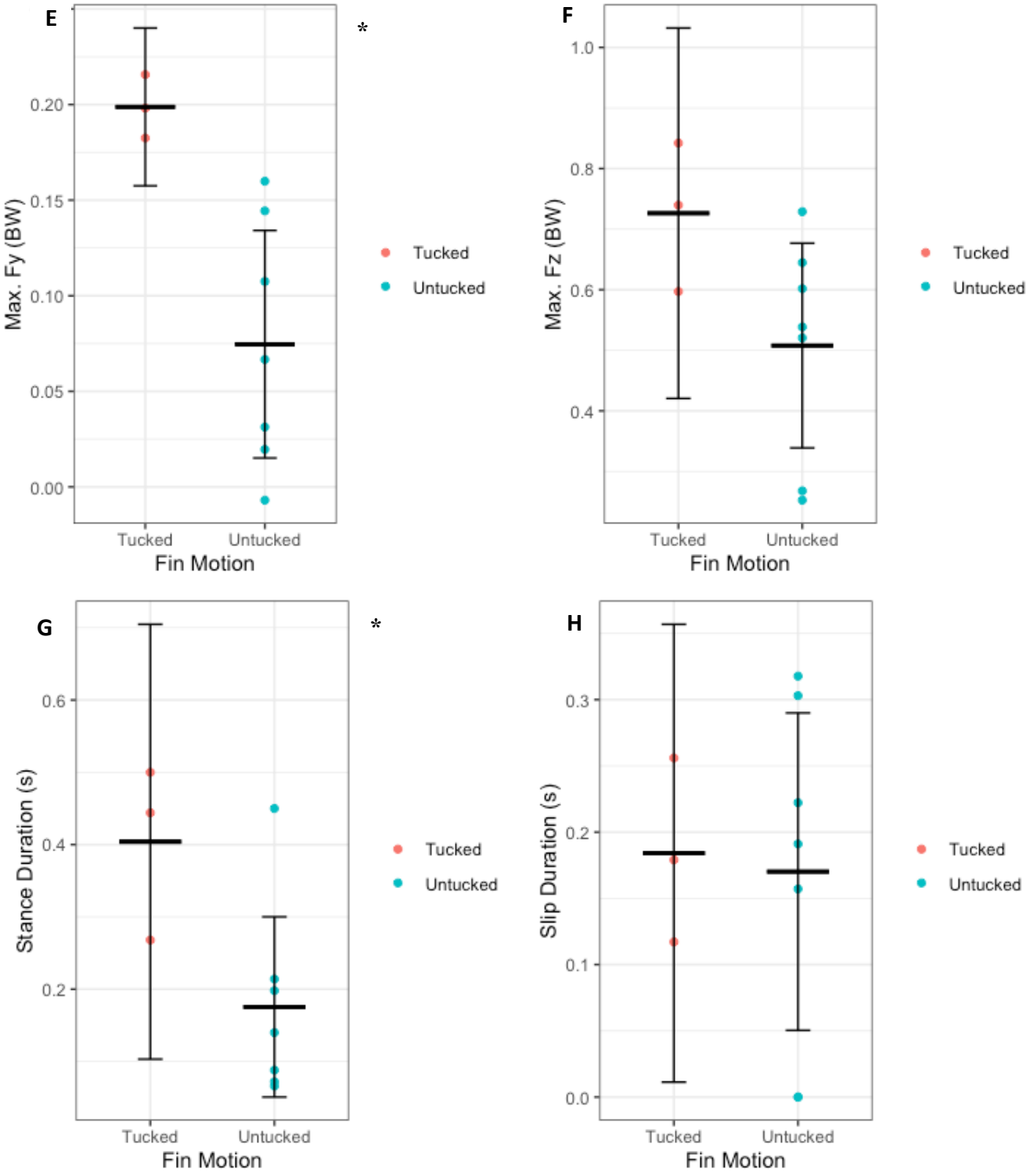
E
*
Max. Fy (BW)
0.20
0.15
0.10
0.05
0.00
Tucked
Untucked
Fin Motion
Tucked
Untucked
F
Max. Fz (BW)
1.0
0.8
0.6
0.4
Tucked
Untucked
Fin Motion
Tucked
Untucked
G
*
Stance Duration (s)
0.6
0.4
0.2
Tucked
Untucked
Fin Motion
Tucked
Untucked
H
Slip Duration (s)
0.3
0.2
0.1
0.0
Tucked
Untucked
Fin Motion
Tucked
Untucked

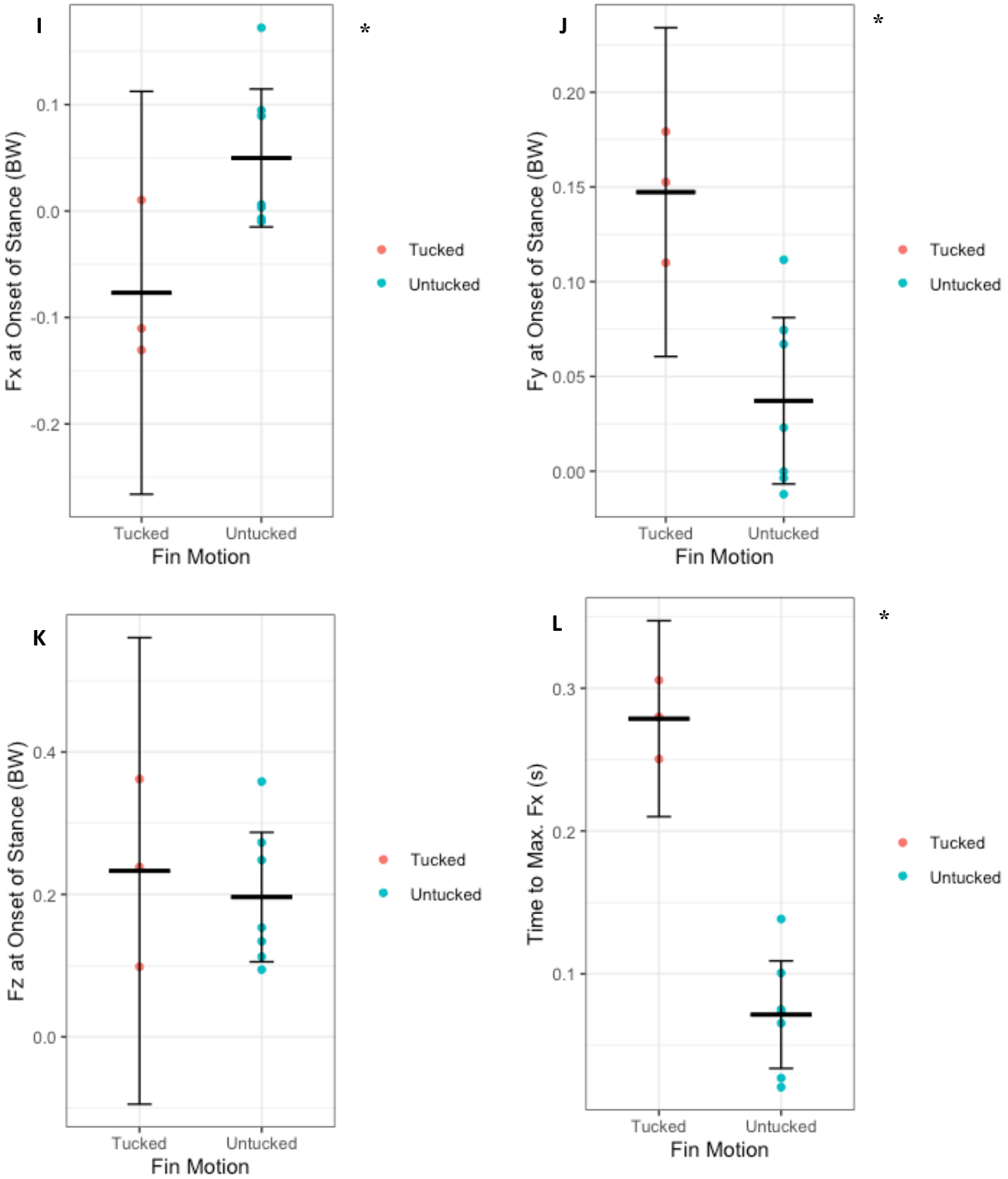
I
*
Fx at Onset of Stance (BW)
0.1
0.0
-0.1
-0.2
Tucked
Untucked
Fin Motion
Tucked
Untucked
J
*
Fy at Onset of Stance (BW)
0.20
0.15
0.10
0.05
0.00
Tucked
Untucked
Fin Motion
Tucked
Untucked
K
Fz at Onset of Stance (BW)
0.4
0.2
0.0
Tucked
Untucked
Fin Motion
Tucked
Untucked
L
*
Time to Max. Fx (s)
0.3
0.2
0.1
Tucked
Untucked
Fin Motion
Tucked
Untucked

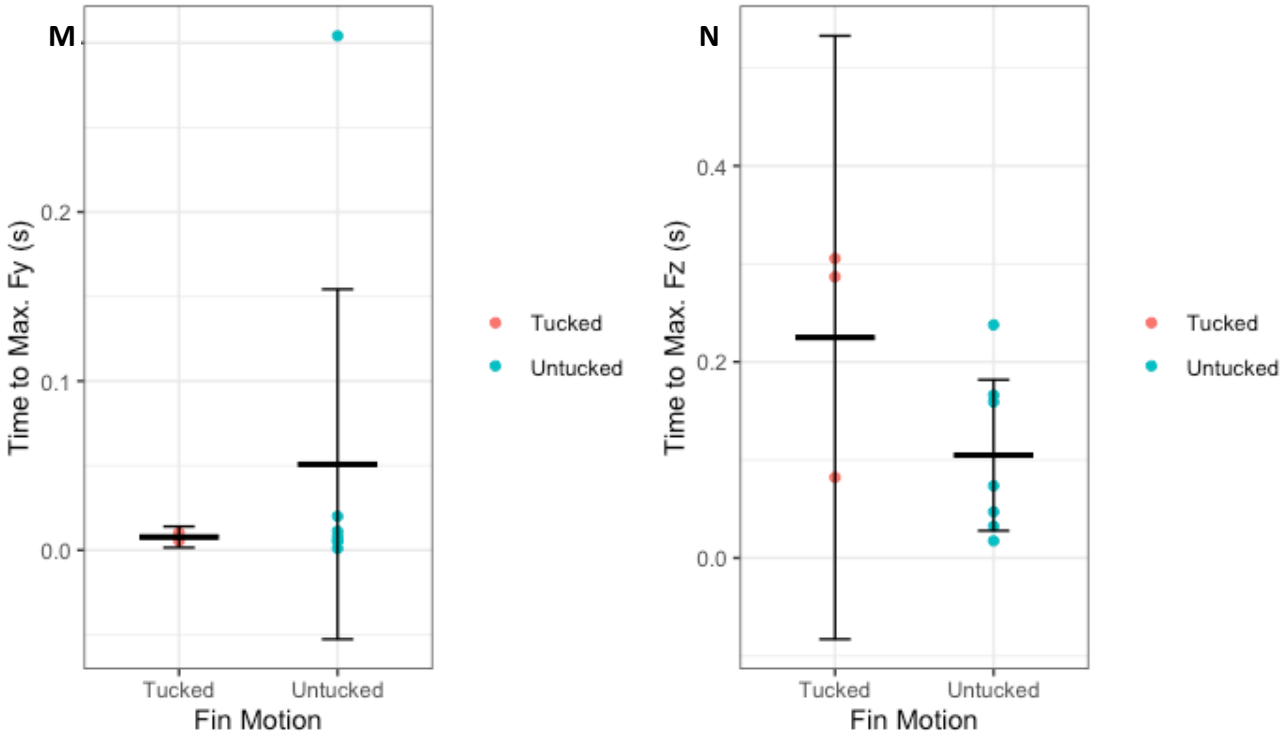

Figure 2.16 The effects of fin motion on kinematic and kinetic variables during walking. Two different motions of the pectoral fin were employed by *Polypterus* during walking. *Tucked* fin steps are indicated in red; *untucked* fin steps are indicated in blue. Individual data points are represented by the respective coloured dots. Asterisks indicate significant differences between the fin motions. Significant differences were found in (B) total CoM distance; (E) maximum mediolateral (Fy) force production; and (G) total stance duration. There were no differences found in (A) total nose distance; (C) total fin distance; (D) maximum anteroposterior (Fx) force production; (F) maximum vertical (Fz) force production; or (H) total slip duration. Mean and 95% CI are indicated by the black bars. P-values are reported in Table A11 in the Appendix.

Kinematic timings and GRF trace analysis

The mean magnitude and direction of GRFs produced were calculated for each step using objective timings: pre-slip phase, during slip phase, and post-slip phase. Steps that consisted of more or less than a single slip phase also possessed more or less objective timings to calculate the mean resultant force vectors. All force traces and resultant force vectors can be found in Figures A1-A10. Due to the distinction in occurrence of slip phase numbers and timings each step possesses, for simplicity, steps continued to follow category '*slip*' numbering system (Table 2.2).

General patterns can be seen when analyzing all steps pooled together as well. Interestingly, the slip phase did not occur past 75% stance for any of the steps. If slip phase occurred, it occurred at 10% stance for early slip, 50% for mid-slip, and 70% for late slip. The duration of the slip phase also varied across all steps. With respect to when abduction angle

and angular velocity occurred during walking, it was interesting to note that abduction angular velocity consistently reached its minimum during a step before minimum abduction angle occurred. Slight increases in GRF observed at the beginning of stance phase may be attributed to the impact force experienced.

Subgroup *mid-slip* contained steps 2 (Fig. 2.17 & A2), 3 (Fig. A3), 6 (Fig. A6), and 10 (Fig. 10). For step 2 (Fig. 2.17 & A2) slip phase occurred from 50% stance to just before reaching 70% stance. Minimum abduction angular velocity occurred just after 10% stance. Abduction angle reached its minimum angle just prior to 50% stance, which also corresponded to the onset of the slip phase. Within step 2, both maximum and minimum nose elevation occurred after 50% stance, with maximum nose elevation occurring near the end of the stance phase, just prior to the beginning of the swing phase. Peak vertical (Fz) forces occurred during the slip phase. Interestingly, the occurrence of peak vertical forces coincided with the decrease in both forward (Fx) and lateral (Fy) forces (Fig. 2.17 & A2). Step 3 (Fig. A3) contained a slip phase that occurred just after 40% stance to approximately 55% stance. Minimum abduction angular velocity occurred near the beginning of stance phase. Minimum abduction angle occurred just prior to 40% stance, and similar to step 2 (Fig. 2.17 & A2). just prior to the onset of the slip phase. Also similar to step 2, both maximum and minimum nose elevation occurred after 50% stance, with again maximum nose elevation occurring near the end of stance (Fig. A4). Peak vertical (Fz) forces occurred after the slip phase, but also coincided with a decrease in forward (Fx) forces (Fig. A3). For step 6 (Fig. A6), the slip phase occurred from approximately 42% stance to 61% stance. Minimum nose elevation occurred near the beginning of stance phase. Interestingly, there was a steep decrease in vertical (Fz) force during the slip phase (Fig. A6). This decrease also coincided with the occurrence of minimum abduction angular velocity, maximum nose elevation, and minimum abduction angle (Fig. A6). Lastly, for step 10 (Fig. A10), the slip phase occurred between approximately 32% stance to 62% stance. In contrast to the other steps within subgroup *mid-slip,* step 10 is the only step in which maximum and minimum nose elevation occur in different halves of the stance phase (Fig. A10). Minimum abduction angular velocity occurred near the beginning of stance phase. Minimum abduction angle occurred just prior to 40% stance, during the slip phase. Peak vertical (Fz) forces occurred during the slip phase (Fig. A10).

For subgroup *mid-slip*, during the pre-slip phase, the resultant vector pointed away from the CoM in two-thirds of the steps. For the steps in which the vector points away from the CoM, the vector also crosses the path of the fish at an angle occurring between approximately 45-90^{o}. In contrast, the step in which the resultant vector occurs towards the CoM, although it points in the opposite direction, the resultant vector is almost parallel to the path of the fish. During slip, the resultant vector points away from the CoM for all steps, and appears to occur opposite in direction but parallel to the path of the fish in one-third of the steps, and almost perpendicular to the path of the fish in the remaining two-thirds of the steps.

Subgroup *variable slip* contained steps 4 (Fig. A4), 7 (Fig. A7), and 8 (Fig. A8). Interestingly, this subgroup is the only one to show complete consistency to the occurrence of minimum nose elevation during walking. All steps within subgroup *variable slip* found that the nose reached its minimum elevation almost exactly at 20% stance. This is in despite of the fact that the slip phase occurred after 50% stance for step 4 (Fig. A4), while occurring prior to 50% stance for steps 7 (Fig. A7), and 8 (Fig. A8). For step 4 (Fig. A4), the slip phase occurred from

approximately 58% stance to 71% stance. Minimum abduction angular velocity occurred near the beginning of stance phase. Minimum abduction angle occurred just after 80% stance. For step 7 (Fig. A7), the slip phase occurred just prior to 10% stance, and ended at 30% stance. All kinematic timings (minimum abduction angular velocity, minimum abduction angle, and maximum and minimum nose elevations) occurred prior to 30% stance for step 7 (Fig. A7). Lastly, for step 8 (Fig. A8), the slip phase occurred very early in the step, from approximately 4% stance to 35% stance. Minimum nose elevation occurred just prior to 70% stance, and was the only kinematic variable that did not occur during the slip phase. Minimum abduction angular velocity, maximum nose elevation, and minimum abduction angle all occurred during the slip phase at around 20% stance (Fig. A8).

In subgroup *variable slip*, in which the slip phase occurred either prior to or after 50% stance, there appeared to be more similarities with respect to the direction of the resultant force vector. During the pre-slip phase, the resultant vector pointed towards the CoM for all steps, and away from the CoM during the slip phase. Similarly, during the post-slip phase, the resultant vector continued to point away from the CoM, and occurred at an angle approximately between 45-90^{o} from the path of the fish.

Subgroup *special slip* contained steps 1 (Fig. A1), 5 (Fig. A5), and 9 (Fig. A9). Step 1 contained two slip phases within its single step. The first slip phase occurred around 10% stance, and the second slip phase encompassed 50% stance. Interestingly, minimum and maximum nose elevations occurred at opposite ends of the stance phase, with minimum nose elevation occurring near the beginning of stance, and maximum nose elevation occurring at the very end, just prior to the swing phase. Both minimum abduction angle and minimum abduction angular velocity occurred during the second slip phase (Fig. A1). Peak vertical (Fz) force occurred after the second slip phase, and gradually decreased until the end of the step. Step 5 and 9 both occurred in the absence of a slip phase. For step 5 (Fig. A5), minimum abduction angular velocity occurred near the beginning of stance. Similar to step 1 (Fig. A1), maximum and minimum nose elevation occurred during opposite halves of the stance phase, however maximum nose elevation occurred prior to 50% stance, whereas minimum nose elevation occurred at the very end of stance, just prior to the swing phase. This again is in contrast to what is seen in step 9 (Fig. A9), where minimum and maximum nose elevation both occur prior to 50% stance. However, similar to step 1, step 9 also finds the nose reaches its minimal elevation near the beginning of stance phase. The differences in these findings pertaining to nose elevation suggests that it is highly variable to its timings of occurrence.

The force vector directions within subgroup *special slip* appeared to be highly variable. There were no consistencies with the direction of the resultant force vector between the steps without a single slip phase. Interestingly, vertical (Fz) force showed the greatest production of GRFs across all steps, although there does not appear to be a pattern in the direction of the resultant force vector within any of the subgroups. The magnitude and direction of the resultant force vector of the lateral (Fy) force appears to be highly variable across steps and within each subgroup.

A

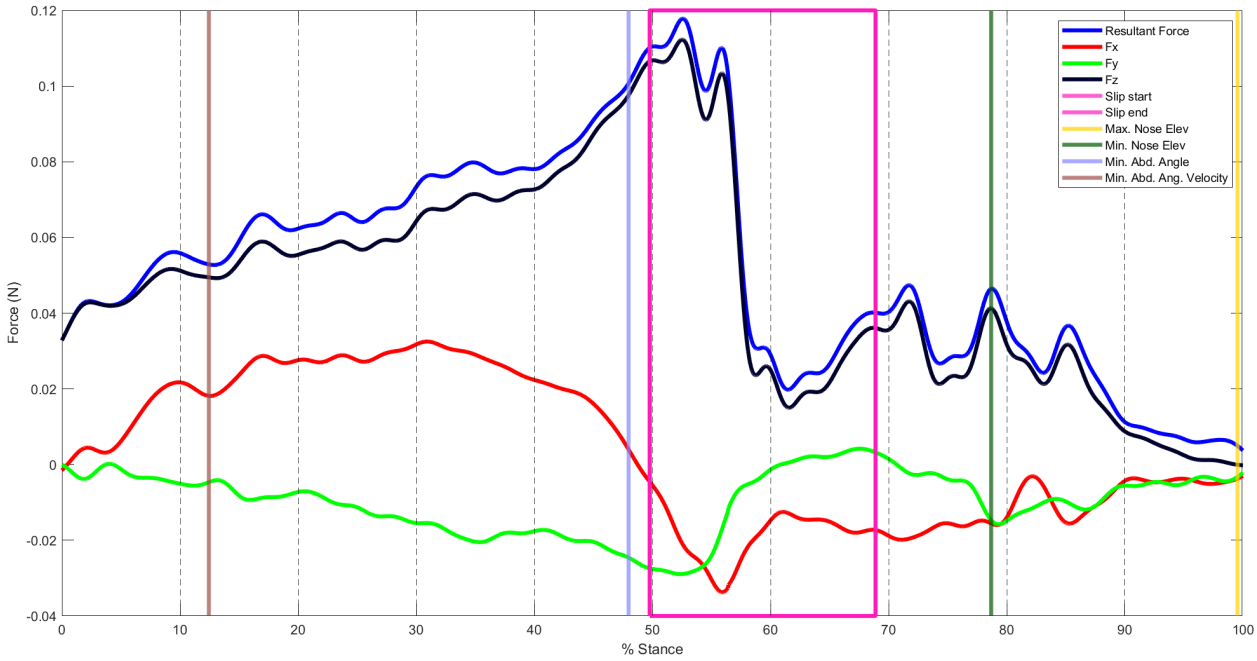

B

Mean Fx	Mean Fy	Mean Fz
0.017897	-0.01588	0.062525

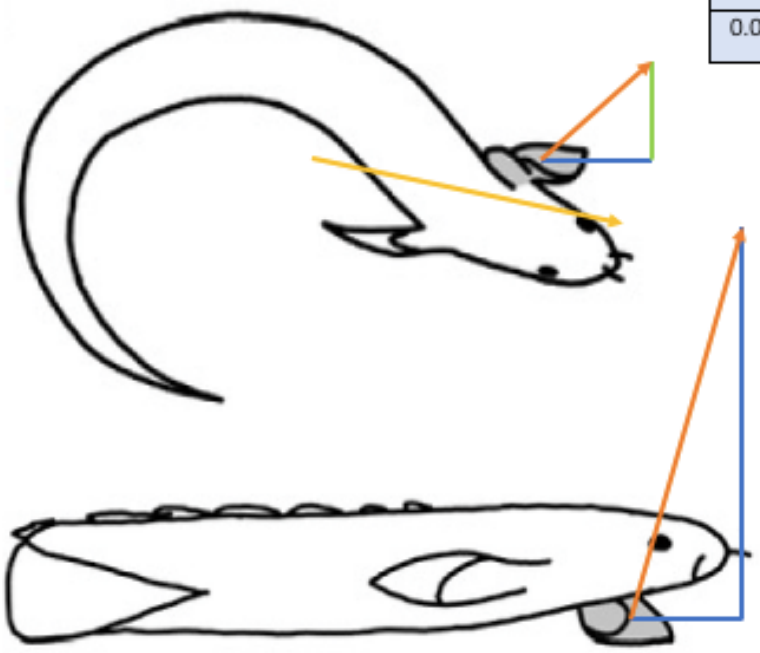

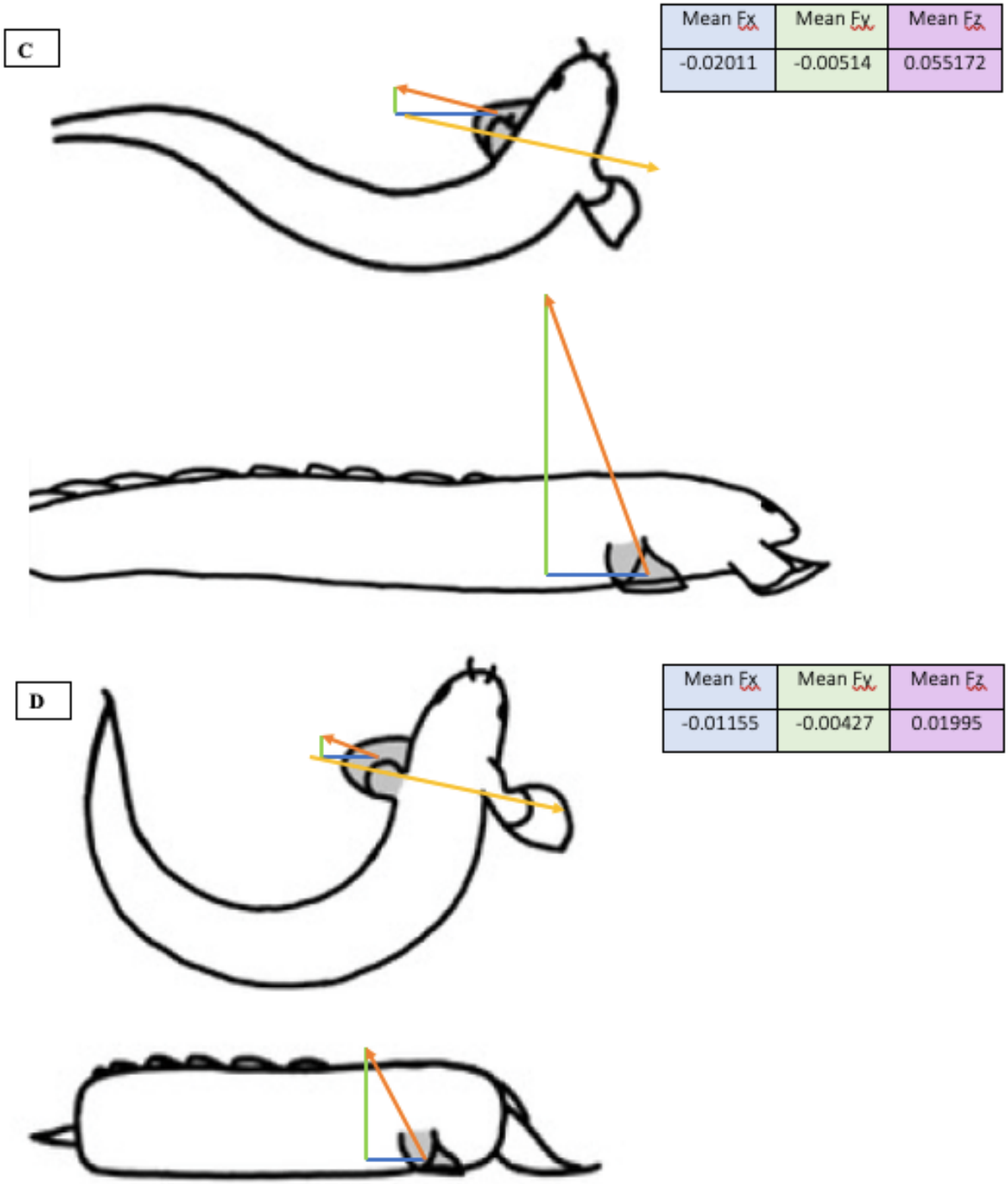

Figure 2.17 Representative force trace (A) and illustrations depicting kinematic motion, force components, and predicted resultant force vector (B-D) of step 2 (Table 2.2). Step 2 belongs to the '*mid-slip*' subgroup of category *slip.* (A) Stance duration is depicted as percent stance. Anteroposterior (Fx), mediolateral (Fy), and vertical (Fz) force components are indicated by the red, green, and black lines, respectively. The resultant force magnitude is displayed by the dark blue line. This step contains a single slip phase, indicated by the pink box. Objective kinematic timings are indicated by the vertical lines and include maximum nose elevation (yellow), minimum nose elevation (dark green), minimum abduction angle (light blue), and minimum abduction angular velocity (brown). (B-D) The kinematic motions illustrated were observed at the midpoint between the timings of interest, and include the onset of loading to the onset of the slip phase (B); the onset of the slip phase to the end of the slip phase (C); the end of the slip phase to the end of the stance (D). The mean magnitudes of forward (Fx) (blue), lateral (Fy) (green), and vertical (Fz) (purple) forces are recorded in the tables. Arrows in orange depict the resultant force vector, and arrows in yellow illustrate the straightest path of motion as determined by the kinematics measured from the CoM.

Discussion

The relationship between terrestrial locomotion and GRF production

The results presented in this study found that GRFs are predominately produced in the lifting(Fz) direction, thereby aiding in the lifting and supporting of the anterior body during walking. In addition, there was no significant difference found in peak thrust (Fx) and stabilizing (Fy) forces, supporting the hypothesis that the pectoral fins' primary role is to lift and support the anterior body during walking. This demonstrates a large shift in the role of the pectoral fins from steady swimming, during which they act primarily as thrust producers. *Whole group* analysis was conducted to determine kinematic and kinetic patterns amongst all steps. Irrespective of how the steps were organized and categorized into subgroups, there were similarities that provided an insight into potential fundamental basics of kinematic motion and force production required for effective walking.

Prior to the onset of the stance phase, the nose decreases velocity near the end of its swing (Fig. 2.10), allowing for the pectoral fin to become planted and subsequently loaded, thus initiating the stance phase. At the onset of the stance phase, fish produce greater vertical (Fz) forces. This initial peak in vertical (Fz) forces are generated by the impact of the fin striking the ground in a downward direction. Immediately after the initial touch-down, the fin progresses to full contact until the tip of the fin is in contact with the ground. As the planted fin becomes loaded (Fig. 2.19B), the anterior body begins to curve towards and over the planted fin. As the fin and body move laterally, peak mediolateral (Fy) forces occur (Fig. 2.10). As the anterior body curves towards the planted fin, the weight of the body, as indicated by the CoM, shifts laterally onto the planted fin, exerting large amounts of force, and pushing the planted fin laterally. In turn, the planted fin exerts peak mediolateral (Fy) forces to stabilize the CoM. The CoM is displaced laterally during each single stance phase, producing a shift in body weight towards the single planted fin. Mediolateral (Fy) forces decrease as abduction angle decreases (Fig. 2.19A), typically around mid-stance.

After mid-stance (Fig. 2.19D), the anterior body begins to curve away from the planted fin. This is due to the contralateral gait employed by *Polypterus*. The stance phase of one pectoral fin, corresponds to the swing phase of the other pectoral fin. As the nose begins to move away from the planted fin, fin loading decreases and mediolateral (Fy) forces reach its minimum magnitude. The nose continues moving away from the planted fin, decreasing its velocity as it enters the stance phase of the opposite fin. This initiates the double stance phase of the gait cycle. Soon after, the planted fin is enters its swing phase at the same time (Fig. 2.19E). When the opposite fin enters its stance phase, this represents the double stance phase. There is again a shift in body weight towards the newly planted fin. This shift in body weight continues as the initial planted fin lifts off and enters its swing phase. The newly planted fin now bears the load of the CoM, as it moves closer to the newly planted fin. This reinitiates the gait cycle.

As previously stated, the results presented in this study found that GRFs are predominately generated in the vertical (Fz) direction, with no significant difference found in peak thrust (Fx) and stabilizing (Fy) forces. The pectoral fins support the lifting of the head and anterior body off the ground, while the posterior body generates the propulsive burst needed to vault the head and anterior body over the planted fin, thus enabling forward locomotion.

This study did not measure GRFs produced by the posterior body. Future studies interested in the relationship between GRF and terrestrial locomotion in *Polypterus* may be interested in analyzing the force contribution of the posterior body as it may provide a deeper insight into how propulsion is generated, and forward locomotion occurs.

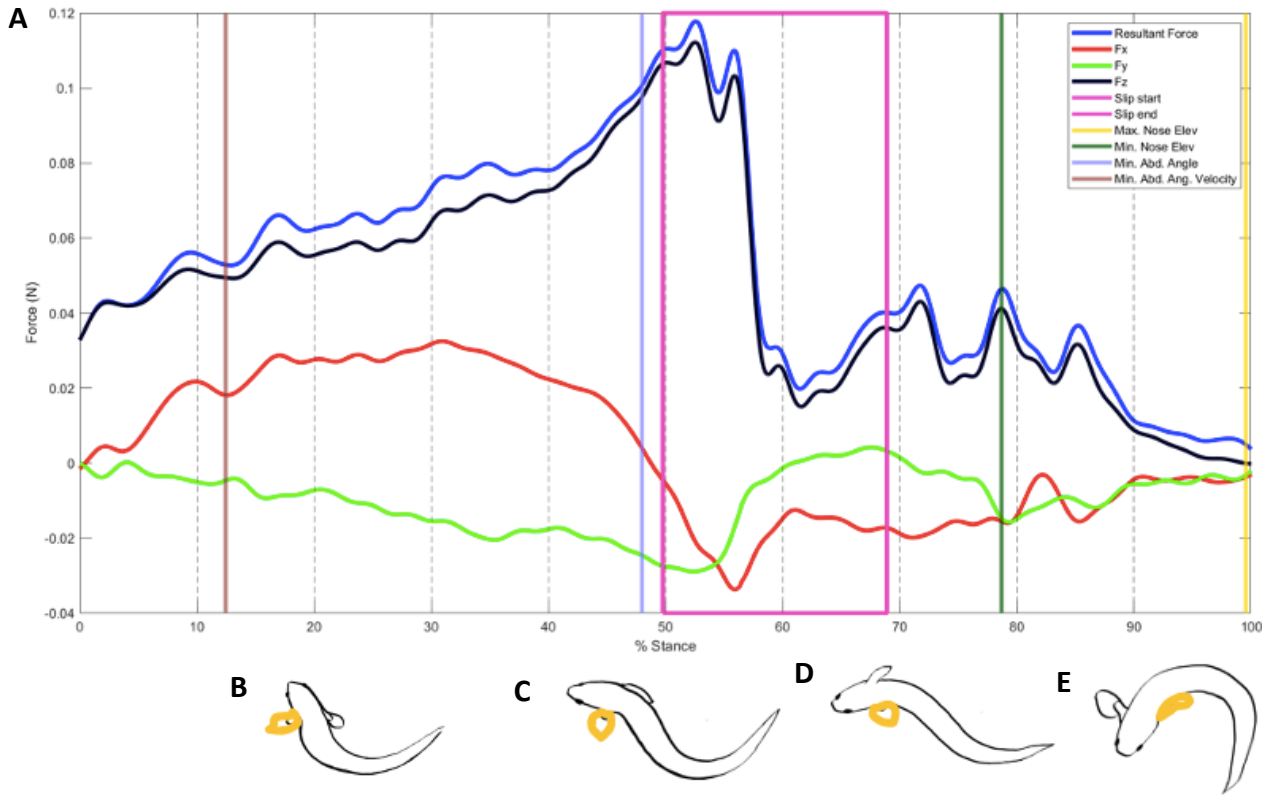

Figure 2.18 A representative force trace (A) and kinematic images (B-E) used to illustrate common kinematic and force patterns observed during walking. Stance duration is depicted as percent stance. Forward (Fx), lateral (Fy), and vertical (Fz) force components are indicated by the red, green, and black lines, respectively. The resultant force magnitude is displayed by the dark blue line. This step contains a single slip phase, indicated by the pink box. Objective kinematic timings are indicated by the vertical lines and include maximum nose elevation (yellow), minimum nose elevation (dark green), minimum abduction angle (light blue), and minimum abduction angular velocity (brown). The kinematic images (B-E) illustrate the motion of the pectoral fin (yellow) across a single step. (B) represents the fin at the onset of loading; (C) and (D) represent the start and end of the slip phase, respectively; and (E) represents the end of the stance phase.

The effect of fin 'slip' on terrestrial locomotion

Retaining balance is crucial for successful locomotion for any species and across many gait types (Reimann, 2018). GRFs and friction work in combination to retain balance and

support during terrestrial locomotion. Slipping during walking occurs when stability is compromised (Reimann, 2018). Complete loss of stability may result in larger slips and even falls.

In this study, the duration of slip was hypothesized to be detrimental to walking by decreasing step distances and producing smaller GRF magnitudes. However, it appears that the slip phase and its occurrence has no statistical benefits nor disadvantages towards walking. In fact, the occurrence of slip may be due to the newly exposed terrestrial environment, and not a conscious maneuver employed by *Polypterus.*

The duration of slip was analyzed across all steps. The timing of the slip phase was highly unpredictable, as it occurred at random times across a step, as well as with different frequencies and did not have a strong correlation with many kinematic or kinetic variables. The sole variable that had a positive correlation with slip duration was the magnitude of vertical (Fz) forces at the onset of the stance phase. The impact of the applied vertical (Fz) forces at the onset of the stance phase affects the slip duration during the step. This suggests that the kinematics of the pre-swing phase affect the magnitude of impact at the onset of stance.

The findings of this study suggest that the slip phase is not associated with effective locomotion. During the step, the duration of the slip phase does not aid in the fish moving greater distances, or producing greater magnitudes of GRFs. Despite this, the slip phase is present in nearly all steps, and is correlated with vertical (Fz) forces produced at impact. One hypothesis for the presence of slip may be that slipping acts as a protection against potential falls during walking, by allowing for the CoM to regain stability, rather than entering into a complete fall. Slipping may be a reactive action, rather than a purposeful motion, as it appears to be reduced in terrestrially-reared fish (Standen et al., 2014).

One way to compensate for slip is foot placement, as it aids in restoration of balance during walking (Wang & Srinivasan, 2014). Repeated exposure to walking decreased the slip phase (Standen et al., 2014), suggesting that terrestrially reared fish are able to maintain stability of the shoulder joint and CoM better. It appears that the results of this study present what happens in sudden, unpracticed exposure to land. More exposure, along with practice of walking, appear to provide more effective gait motions. In aquatically reared fish, the slip phase may act as an involuntary way to keep the CoM centered. The placement of the foot in aquatically reared fish on land does not support the CoM effectively compared to terrestrially reared fish. The behavioural changes seen in terrestrially reared fish support this as they plant their fins closer to body midline, and reducing the duration of slip (Standen et al., 2014). Polypterus not accustomed to walking on land placed fins father away from midline, and had longer slip durations, further suggesting that slip is ineffective for walking (Standen et al., 2014).

The role of pectoral fin motion on terrestrial locomotion

During walking, *Polypterus* employ one of two gaits: gait IIa or gait IIb, which correspond to subgroups *untucked fin* and *tucked fin,* respectively. Both gaits undergo different motions during stance. Tucked fin steps were correlated with greater CoM distances, peak stabilizing (Fy), and longer stance durations. There was no difference in slip duration, once again suggesting that slip duration is not required for effective locomotion. During stance, tucked fin motion appears to focus primarily on stabilization, while untucked fin steps appear to focus on thrust production. Tucked fins produced greater stabilizing (Fy) forces at impact, while

untucked fins produced greater thrust (Fx) forces at impact. There was no difference in vertical (Fz) forces at impact. Tucked fins also took longer to reach peak thrust (Fx) forces during walking, suggesting that tucked fins are used when greater stability is needed, or perhaps during steps that anticipate greater external perturbations. There was no difference in the time to reach peak mediolateral (Fy) or vertical (Fz) forces between the two fin motions, however, tucked fins had a much more concentrated range of peak stabilizing (Fy) force magnitudes, which again highlight the potential for a greater focus on stabilization. The potential difference in the role of the fin motions during walking may also be supported by the velocities observed at the end of stance. Tucked fins have the minimum CoM velocity at the end of the stance phase and beginning of the swing phase. Tucked fins work to stabilize the CoM across the entire step, thus controlling the velocity of the CoM into the swing phase. In contrast, the untucked fins may focus more on thrust during stance, thereby propelling the nose faster during swing, only slowing down at the end of the swing phase, as it gets ready to enter the next stance phase.

In human gait analysis, the forces produced immediately after heel contact are hypothesized to act as precursors to slip and falls (Redfern et al., 2001). The motion of the fin is correlated with either an increase in forward (Fx) forces or vertical (Fz) forces. These initial spikes may represent the impact of the fin as it initially hits the ground. The fin exits the swing phase, and transfers the momentum of the swing onto the planted fin thus resulting in initial spikes of forward (Fx) or vertical (Fz) forces. Interestingly, the momentum of the swinging fin may be the cause of the different motions observed during walking. The velocity of the swinging fin, as well as the angle at which the fin hits the ground initially may induce an adaptive response that causes the fish to either use a tucked fin or untucked fin motion during the subsequent stance phase. The switch between fin motions may be an active action to counteract the external perturbations, since the kinematics of the swing phase affects the subsequent stance phase.

In conclusion, fin motion also appears to determine the duration of stance. Furthermore, untucked fins produced greater thrust (Fx) forces at impact compared to tucked fins, which produced greater stabilizing (Fy) forces at impact. In this way, untucked fins are predisposed to focus on thrust and propulsion, while tucked fins anticipate a greater need for stabilization even prior to stance.

Conclusion

The kinematic and force data collected during terrestrial locomotion provided a first look into the how the GRFs produced during walking affect the pectoral fins in *Polypterus.* The present study found that lifting (Fz) forces were consistently greater than both thrust (Fx) forces, and stabilizing (Fy) forces. This supports the findings of previous studies, in which the pectoral fins were proposed to aid primarily in lifting and supporting the body during walking. This allows for the anterior body to elevate, thereby reducing the friction experienced against the ground, and vaulting over the planted fin. The posterior body is hypothesized to produce thrust forces required for forward propulsion. Together, the pectoral fins and the body work together to locomote across land. It was also determined that the duration of the slip phase during a step neither enhanced or deterred locomotion. Long-term exposure to walking has

determined that the slip phase is reduced, which also supports the idea that the slip phase is not required for effective locomotion. Finally, the motion of the fin observed during walking appears to be a significant determinant of the kinematics and GRF production. *Polypterus* were found to use two different gaits during walking. Interestingly, the fin motion did not change within a trial, but both fish were shown to use both fin motion types, suggesting that there may a need to change between the fin motions. The results of this study suggest that a tucked fin motion may be employed during needs for greater stabilization. In contrast, untucked fin steps appear to focus on thrust production more than stabilizing. Future studies analyzing the relationship between GRF and the pectoral musculature of *Polypterus* may also benefit from whole body analysis, particularly the tail as it appears to be the primary propulsor during walking.

Chapter 3 Inverse dynamics

Polypterus is an amphibious fish and is able to both swim in water and walk overland. The motion described during walking greatly differs from that seen during steady swimming, and each mode of locomotion experiences very different environmental forces. *Polypterus* has demonstrated the ability to adapt to novel force environments through behavioural, anatomical, and physiological plastic changes (Standen et al., 2014, 2016; Du & Standen, 2017; Foster et al., 2018; Dhuper, 2018; Du & Standen, 2020), suggesting that the GRFs experienced during walking are the driving mechanisms behind these plastic changes. From the findings in Chapter 2, we have an understanding of the magnitude and direction of forces that exist on fin tissues during walking. By using these forces results, and in combination with the known kinematics of each step, we can estimate the forces acting on different tissues in the fin. The pectoral anatomy is composed of six independent muscles originating in the pectoral girdle and crossing into the pectoral fin (Fig. 1.2). These musculoskeletal elements are responsible for transferring forces through the fin and into the pectoral girdle, to lift the anterior body. During walking, *Polypterus* employ one of two gaits: gait IIa or gait IIb, which correspond to subgroups un*tucked fin* and *tucked fin,* respectively, throughout Chapter 2. Both gaits undergo different motions during stance, in addition, the musculoskeletal system of the pectoral fin may also undergo different alterations in activity. Although it is postulated that the fin is loaded in different ways in these two step styles, we have chosen to define an untucked fin step as the average step cycle to attempt our first inverse dynamics model.

Forward dynamics versus Inverse dynamics

The need to understand the relationship between body movement, muscle activity, and force production has been observed in countless studies analyzing gaits across humans, and other animals. Two mathematical models are commonly used: forward dynamic and inverse dynamic analysis (Pamies-Vila et al., 2012; Buchanan et al., 2004). In forward dynamics, body kinematics are predicted from known muscle forces and joint torques, with the goal to understand the energetic costs associated with locomotion (Pamies-Vila et al., 2012). In contrast, inverse dynamics attempts to estimate net joint torques, given known kinematic data and measured force production, shedding light on how muscles produce forces during locomotion (Pamies-Vila et al., 2012). Inverse dynamics is more commonly, however the combination of both provide a deeper understanding into locomotion, and allow for greater accuracy in the mathematical models.

Inverse dynamics

During walking, the musculoskeletal system functions to counteract the effects of gravitational forces by producing and transmitting GRFs (Watkins, 2009). Previous literature as well as our findings indicate that the pectoral fins aid in lifting and supporting the fins and anterior body during terrestrial locomotion. This contrasts with their role in steady swimming, in which the pectoral fins aid primarily in thrust production. During walking, the anterior body is elevated which concentrates force through the fin. As the fin remains planted, the CoM shifts upwards and backward, producing greater vertical (Fz) or lifting forces. The center of pressure

(CoP) is located in the center of the base of support (BoS). The CoP represents the focus point for generated GRFs. Realistically, both the BoS, and subsequently the CoP, continuously change as fin position changes. Changes in the center of pressure point can significantly alter how the internal forces about the joints are applied, and how the muscles experience loading (Watkins, 2009). As the muscles experience loading, they will transmit the force through the tendons to the surrounding bones and cause movement around the joint, or a joint reaction force (Chockalingam et al., 2018). Movement that involves both force and displacement is called a moment, calculated as the product of the magnitude of the applied force and the distance of the line of action acting perpendicular to the applied force (Chockalingam et al., 2018). In order to calculate the magnitude of forces experienced about the bones, muscles and joints within a musculoskeletal system, a non-invasive, mathematical technique known as inverse dynamics can be used. Inverse dynamics uses measured kinematic data, in combination with quantified force data, to calculate net joint torques within a model (Faber et al., 2018, Mayo & Ojeda, 2020), and can be used to quantify the forces experienced by the musculoskeletal system of the pectoral fins of *Polypterus*. The musculoskeletal system of a living organism can be very complex. The inverse dynamics approach attempts to reduce a complex living body to its anatomical structures, which is then further simplified into a set of solvable equations to calculate the internal forces and moments acting about each joint (Robertson et al., 2004). Total moment of the fin can be determined by the sum of all individual moments about each joint. Joint moments are determined through the interaction between GRFs, joint reaction forces, and muscle forces, and provide an understanding into joint power. Understanding joint power will provide an insight into the positive or negative energy produced by the muscles, which correspond to the type of contraction occurring. Terrestrial locomotion involves coordination and activation of fin and body muscles. The focus of this study was predominately on pectoral fins. The muscle activity of pectoral fins is caused by contractions in muscle segments that produce the forces necessary for locomotion. Wilhelm et al., provided a detailed account of the pectoral fin musculature. Wilhelm et al., stated that the pectoral fin is composed of six independent muscles crossing into the pectoral girdle. Each of these muscles have unique activation patterns, posing the first challenge: how to propose an inverse dynamics model that takes into account each individual muscle and its contribution to force production. One way to get around this is to reduce all of the pectoral fin components, such as all muscle, bones, etc. into a single resultant joint force and torque. This method allows for the inverse dynamics approach to then focus on the single resultant vector to estimate joint torques (Vaughan, 1996).

Assumptions and limitations

Each structure or segment is assumed as a rigid body with fixed mass and inertial properties. Each segment cannot be deformed, or if deformations do occur, can be considered negligible (Vaughan et al., 1982). Each segment is linked together in a chain, and each joint is assumed to undergo pure rotation about its axis. Oversimplification of a musculoskeletal system can cause errors in joint force calculations, as the tendons and ligaments within the system affect how the transmitted force is distributed about each joint (Kawcak, 2016). Known variables generally include the mass moment of inertia, masses of each segment, and position coordinates of the CoM, and joints. If coordinates were not used, then the length of each

segment would also be required prior to analysis. Known anatomical measurements from measured CT scans can also apply to general fin motion. The mass and inertial properties of each segment is assumed to be fixed in inverse dynamics, however the method used to calculate mass and inertial properties may vary between studies using techniques such as regression equations, different scanning methods, and modelling techniques. Force platforms provide crucial information in understanding the relationship between the kinematics and GRFs produced during locomotion. Despite their advantages, there are also limitations in recording, analyzing, and reporting data obtained from these force platforms. The methods used in Chapter 2 provided a significant insight to two limitations – force transducer size and sensitivity. Despite using the smallest transducer size available to us at the time of data collection, the transducers were still larger than ideal. Both body and pectoral fins were consistently recorded on the same transducer, making it difficult to distinguish GRF production between the anterior body specifically and the pectoral fins. It is possible that with smaller transducers, the pectoral fins may have had a better opportunity to land on a single transducer, allowing for a clearer differentiation in the body and fin force contributions. This would be an ideal solution if not for the issue with transducer sensitivity. The force transducers used were also highly sensitive, so much so that they were able to pick up signals from motion occurring near the edge of the platform. Because of the high sensitivity, filtering out noisy signals from the data may have resulted in a loss of crucial information. Figure A1 in the Appendix presents an excellent example of the difficulties in filtering force signals, especially across multiple force transducers. The transmission of a signal across multiple transducer face both calibration and filtering issues.

The sample size used this study also presents challenges with data interpretation. Due to the small sample size, any existing outliers may significantly affect data analysis, thereby affecting subsequent calculations. A larger sample size or post-hoc analyses accounting for the existing outliers may provide additional accuracies in the data collected. The assumptions made in this model are greatly simplified and not realistic. The kinematics of the slip phase and its effect on stance kinematics and GRF production needs to be quantified and accounted for, as it will affect muscle activity, joint kinematics, and joint moments. Additionally, the model also needs to account for the differences in fin motion observed. This can be done by creating a separate model accounting for the increased rotation in fin musculature during tucked fins. Despite its usefulness as a non-invasive technique, inverse dynamics is not without its limitations. This approach is susceptible to measurement errors in the kinematic data, due to external noise or other factors which can then affect the resulting calculations in net joint torques (Faber et al., 2018). Nevertheless, inverse dynamics continues to be a useful technique in further understanding motion and the necessary internal forces and moments required to achieve that motion.

Objectives

We aim to formulate a simple two-dimensional model of the pectoral musculature of *Polypterus* for the basis of an inverse dynamics analysis. Using inverse dynamics, along with the GRF data and kinematic data recorded, analyzed, and reported in Chapter 2, we aim to quantify the moments (or torque) about each joint within the musculoskeletal system. The joint moments can then be used to quantify the net sum of all internal moments about that joint. Overall, we hope to gain a deeper understanding into the effects of GRFs on the

musculoskeletal system of the pectoral fin and girdle during terrestrial locomotion in *Polypterus*.

Methods

The center of pressure (CoP) is assumed to be located at the midpoint between the two joints: the shoulder joint and the medial radials. Software such as Matlab contain applications that allow for digitization of specific points during kinematic motion. This technique was used in Chapter 2, and digitized points used in Chapter 2 analysis can be found in Fig. 2.5. Together, the GRF data and kinematic motion will allow for the quantification of the forces experienced by the CoP across the stance. For simplification, the slip phase and duration is largely ignored in the model presented. Additionally, the differences in fin motion are also ignored. Untucked fin motion will be used in the model presented. Left and right pectoral fins can be assumed to be symmetrical. Although we did not measure a center of pressure for our fin steps, from visual observations of motion during walking, we assume that the CoP point occurs at the midpoint of the distal most edge of the medial radials, where they attach to the fin rays. Equipment used and calibration methods can be found in the methods section in Chapter 2.

Inverse dynamics calculation

The pectoral fin and girdle anatomy consists of two joints. The first is the 'shoulder-joint', comprised of the scapulocoracoid, propterygium, and metapterygium. The shoulder joint allows for increased flexibility and a wider range of motion of the pectoral fin during walking. The second joint is located at the midpoint of the distal-most edge of the medial radials, where it meets the fin rays. In order to simplify the model down in its entirety, we chose to focus on the pectoral fin solely. This allows for the model to be broken down to a single joint system, without the influence of the shoulder joint. Figure 2.34 provides an illustration depicting a simple model that can be used as a basis for inverse dynamics. From kinematic and kinetic observations made in Chapter 2, it appears that the initial force loading occurs when the medial radials make contact with the ground. Center of pressure point (CoP) is then assumed to occur at the contact point between the medial radials and the fin rays. The CoP is assumed to be a fixed point. The transfer of the GRFs produce can act in two directions through the

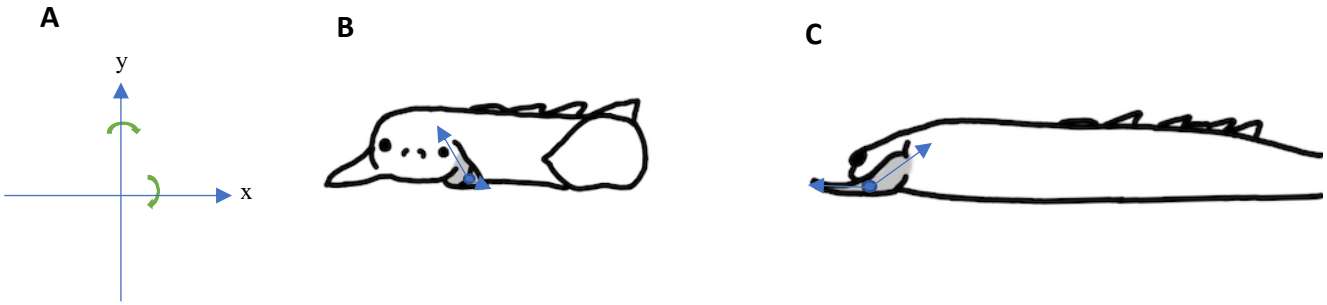

Figure 3.1 Axis of reference (A); front view (B) and rear view (C). In this single segmented model, the contact point between the medial radials and fin rays act as the sole joint, and CoP point. (A) Motion can occur linearly and angularly in two directions along and about the horizontal (x) and vertical (y) axes. Force transfer originates at the CoP point and can travel in two directions, as depicted by the direction of the arrows (B & C).

musculoskeletal anatomy of the pectoral fin. The single joint can undergo two possible motions: linear and angular. Each motion can occur in three directions corresponding to the axes of an orthogonal plane (Watkins, 2009) (Fig. 3.1A). The number of directions a joint can move about represent the number of degrees of freedom of that particular joint (Watkins, 2009). Therefore, the joint will contain six degrees of freedom. However, for further simplification, the model proposed will be a two-dimensional model, occurring in the horizontal (x) and vertical (y) directions.

A diagram of a two-dimensional model corresponding to angular and linear motion is illustrated in Fig. 3.2. Two fundamental ideas are required to calculate the moments and forces about a joint. Newton's second law of motion can be used to determine the sum of forces, *F*, given the mass moment of inertia, *m*, and linear accelerations, *a*:

$$F = m \cdot a \qquad \text{(eq.6)}$$

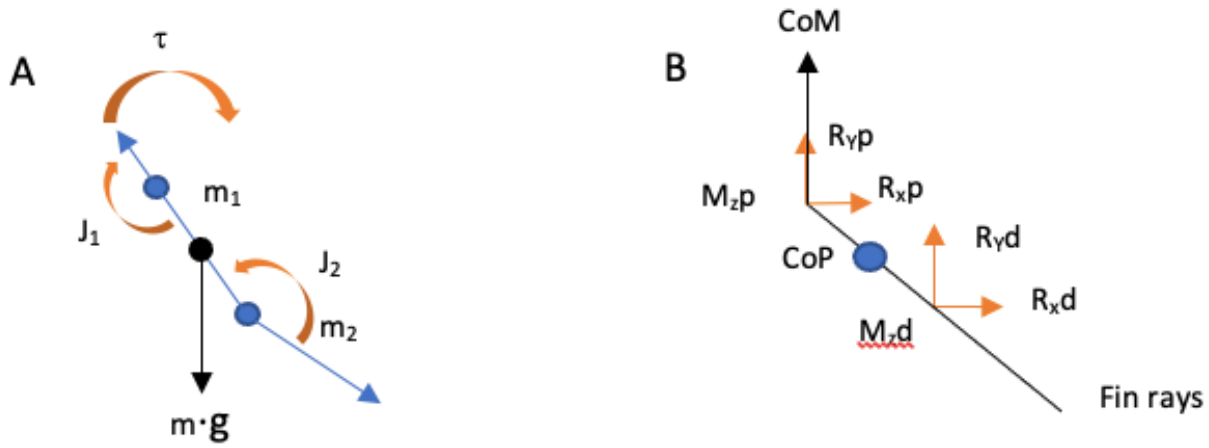

Figure 3.2 Free body diagrams taken from Fig. 3.1(B). (A) A diagram illustrating angular motion about each joint. J_1 is located at the shoulder joint of the pectoral fin and is the proximal-most joint; J_2 is located where the medial radials meet the fin rays, and represents the distal-most joint. The net joint torque is represented by τ. The mass of each segment is indicated by m_1 and m_2. (B) A diagram illustrating the reaction forces and moments about each joint within the musculoskeletal system.

This can be further simplified into the components of the applied force:

$$\Sigma F_x = m \cdot a_x \qquad \text{(eq.7)}$$
$$\Sigma F_y = m \cdot a_y \qquad \text{(eq.8)}$$

The second fundamental idea belongs to Euler (eq. 11), where *M* represents a joint moment, *I* represents the mass moment of inertia, and α represents the angular acceleration.

$$M = I \cdot \alpha \qquad \text{(eq.9)}$$

These equations in combination provide derivations known as the Newton-Euler equations (eq. 9-12), used to calculate joint reaction forces and joint moments for each segment in the model in both linear and angular directions. The joint reaction forces are given by equations 10 and 11:

$$R_{xp} = m \cdot a_x \quad \text{(eq.10)}$$
$$R_{yp} = m \cdot a_y \quad \text{(eq.11)}$$

where *R* is the reaction force for each joint, and *p* is a proximal joint. Equation 12 was modified from Holden & Stanhope (1998)

$$M_{medial\ radials} = (I_{medial\ radials} \cdot \alpha_{medial\ radials}) + \omega + F_{x_{medial\ radials}} \cdot L_{y_{medial\ radials}} - F_{y_{medial\ radials}} \cdot L_{x_{medial\ radials}} \quad \text{(eq.12)}$$

The moment about the medial radial joint ($M_{medial\ radials}$) can be calculated by the mass inertial properties of the segment ($I_{medial\ radials}$), the angular acceleration ($\alpha_{medial\ radials}$), the reaction force in the horizontal and vertical components ($F_{x_{medial\ radials}}$, $F_{y_{medial\ radials}}$), and the length of the segment in the horizontal and vertical axes ($L_{x_{medial\ radials}}$, $L_{y_{medial\ radials}}$).

$$L_{x_{medial\ radials}} = (x_d - x_{CoM}) \quad \text{(eq.13)}$$

$$L_{y_{medial\ radials}} = (y_{CoM} - y_d) \quad \text{(eq.14)}$$

Equation 12 can be altered with respect to the distance between the proximal and distal joints to the CoM, depending on the location of the joints relative to the CoM. X coordinates are assumed to be positive towards the right and negative towards the left relative to the CoM point; and Y coordinates are positive above and negative below the CoP point. Using these assumptions, we can find the length of each segment in the horiztonal (x) and vertical (y) axes relative the the CoP. The distance between the CoM and the proximal joint is given by equations 13-14.

Future Directions

Simplifying the pectoral anatomy solely to the pectoral fin is not realistic. The shoulder joint is responsible for the wide range of motion in the pectoral fin during terrestrial locomotion. The formulas proposed in the previous section can be applied to the shoulder joint, or the proximal joint in what would then become a multisegmented model. Contribution to muscle activity provided by EMG analysis would provide an insight into muscle activation patterns that can then be analyzed with the proposed inverse dynamics model and power calculations. This holistic approach would allow us to understand the extent to which the musculoskeletal system of the pectoral fins undergo plasticity changes caused by terrestrial locomotion.

Holden & Stanhope (1998) proposed the following equations (eq. 15,16) to determine the net moment of the multisegmented model:

$$M_p = -M_d - r_p \cdot F_p - r_d \cdot F_d + (I \cdot \alpha) + \omega \cdot (I \cdot \omega) \quad \text{(eq.15)}$$

The net moment of the proximal end of the segment is given by (M_p); (M_d) is the moment of the distal end of the segment; (r_p) and (r_d) represent the vector from the CoP to the proximal and distal segment, respectively; (F_p) and (F_d) represent the proximal and distal joint reaction forces, respectively; *I* is inertia; and finally, α and ω represent the segmental angular acceleration and velocity relative to the coordinate system. Inverse dynamic analysis involving the human leg commonly divides the entire leg into three segments. Eq. 12 is used to calculate the moments about the distal most joint in the system, working upwards towards the most proximal joint. For our 2D model of the pectoral musculature of *Polypterus,* we propose a model (eq. 13) that can be used to calculate the moment about the distal most joint, which we indicated as the distal most edge of the medial radials. Because the model proposed occurs in a two-dimensional plane, only the horizontal (x) and vertical (y) axis are considered in the following equations.

$$M_{shoulder\ joint} = I_{shoulder\ joint} \cdot \alpha_{shoulder\ joint} - M_{medial\ radials} - F_{x_{shoulder\ joint}} \cdot L_{y_{shoulder\ joint}} + F_{y_{shoulder\ joint}} \cdot L_{x_{shoulder\ joint}} + F_{x_{medial\ radials}} \cdot L_{y_{medial\ radials}} - F_{y_{medial\ radials}} \cdot L_{x_{medial\ radials}} \quad \text{(eq.16)}$$

Once the net joint moment about the medial radials has been calculated, the subsequent proximal joint can then be inferred (eq. 17). For the proximal joint, which corresponds to the shoulder joint, the moments and forces produced by the distal joint need to be taken into consideration. Using position coordinates of both the proximal and distal segments, as well as the CoM, the length of each segment can be approximated by calculating the distance between the corresponding coordinate values.

$$L_{x_{shoulder\ joint}} = (x_{CoM} - x_p) \quad \text{(eq.17)}$$

$$L_{y_{shoulder\ joint}} = (y_p - y_{CoM}) \quad \text{(eq.18)}$$

Equation 14 can be altered with respect to the distance between the proximal and distal joints to the CoM, depending on the location of the joints relative to the CoM. X coordinates are assumed to be positive towards the right and negative towards the left relative to the CoM point; and Y coordinates are positive above and negative below the CoP point. Using these assumptions, we can find the length of each segment in the horiztonal (x) and vertical (y) axes relative the the CoP. The distance between the CoM and the proximal joint is given by equations 18-19.

Conclusion

The inverse dynamics model presented in this study is a highly simplified model. Numerous parameters were not accounted for, and key kinematic variables were not available to carry out the calculations. Despite these limitations, the model presented provides a strong foundation in both a simple single segment body, and a simple multisegmented model. Future studies would require greater analysis into the kinematics and GRF produced during both the swing and stance phases, measurements into body segments, and CoP displacement during walking.

Chapter 4 Future Directions

This study provided a first look into the kinematic and GRF produced by aquatically reared, non-exercised fish. We proposed that novel terrestrial force environments trigger the plastic changes seen in the fish. Ten steps were analyzed together (*whole group analysis*) and categorized into subgroups (*slip* and *motion*). We found that there are kinematic and GRF patterns that appear to be a basic requirement of walking through whole group analysis. When analyzing magnitudes of each force component across all steps, we found that vertical (Fz) force magnitudes are consistently greater than both forward (Fx) and lateral (Fy) forces, supporting the hypothesis that pectoral fins aid primarily in lifting the anterior body off the ground during walking. This contrasts with their role in steady swimming, in which pectoral fins act as the primary thrust producers. Subgroup analyses have shown that while the occurrence of slip does not have any significant effect on the kinematics or GRF patterns observed, fin motion, specifically *tucked fin* steps were found to have greater center of mass (CoM) distances, and greater mediolateral forces, but longer stance durations compared to *untucked fin* steps. The results from category *slip* suggest that the slip phase is not a requirement for effective walking, and may perhaps be an involuntary movement to simply regain balance during terrestrial locomotion. The change in fin motion also remains relatively stable within a step, but may differ across steps even within the same fish subject. Further analysis is required to understand the significance between the fin motions and whether the change is a conscious maneuver during walking. Future studies may be interested in analyzing the kinematics of the pre- and post-swing phases as it appears that the swing phase may be the trigger for the instability experienced during stance.

Inverse dynamics was used as a dynamic model to predict the effects of GRFs on the joint moments. Analysis of joint moments is important for understanding how plastic changes occur within the bones, joints, and muscles of the pectoral fin musculoskeletal system. Joint moments correspond to resultant force magnitudes and are an indicator of the magnitude of loading experienced by different joints and associated tissues. Forward dynamics, in combination with the inverse dynamics model, may provide a complete description into the effects of GRFs on the musculoskeletal system of the pectoral fins, including muscle activation patterns; the total magnitude of GRFs produced; the moments of force about each joint; and the effects of muscle contraction. The quantification of muscle activation patterns would also provide an even deeper insight into the effects of GRFs on the pectoral fin musculoskeletal anatomy. This may be done used strategically placed electrodes into the fin musculature and

analyzing signals produced during active and passive states. This would also provide a better understanding of individual muscle contribution, as well as the effects of antagonistic muscle activity during walking. The addition of EMG analysis may also provide a better understanding into tissue loading at the joints (Buchanan et al., 2004). With the aid of EMG analysis, a forward dynamics model may be presented and calculated. The results can then be compared with those obtained from the inverse dynamics model to measure the accuracy between results. Together, inverse dynamics and forward dynamics may provide a wholistic view into terrestrial locomotion.

Future studies may look at differences in force production during swimming and walking, as well as in differences in force production between aquatically reared and terrestrially reared fish, to understand how the transition from land-to-water may have occurred. Previous literature looking at both short- and long-term studies have found significant changes in the behavioural, anatomy, and physiology of fully aquatic, semi-terrestrial and fully terrestrial reared *Polypterus*. To this extent, it would be interesting to use the methods provided in this study on semi-terrestrial and fully terrestrial fish in order to truly understand the effects of the force profile on a predominantly aquatic, amphibious fish, like *Polypterus.* The anatomical, behavioural, and physiological plasticity observed in *Polypterus* make it an excellent model to study the effects of terrestrial locomotion on a predominately aquatic animal and may provide a deeper insight into the changes that occurred during the evolutionary fin to limb transition during the Devonian period.

References

Ancillao, A., Tedesco, S., Barton, J., & O'Flynn, B. (2018). Indirect Measurement of Ground Reaction Forces and Moments by Means of Wearable Inertial Sensors: A Systematic Review. *Sensors (Basel, Switzerland)*, *18*(8), 2564. https://doi.org/10.3390/s18082564

Bauer J., Fuchs R., Smith G., Snow C. (2001) Quantifying force magnitude and loading rate from drop landings that induce osteogenesis. *Journal of Applied Biomechanics* 17, 142-152

Bennett, M. B. (2001). Tetrapod walking and running. *Encyclopedia of Life Sciences*. doi: 10.1038/npg.els.0001867

Binder, M. D., Hirokawa, N., & Windhorst, U. (2009). Inverse dynamics approach. *Encyclopedia of neuroscience.* Berlin: Springer. doi: 10.1007/978-3-540-29678-2

Blob, R. W. & Biewener, A. A. (2001) Mechanics of limb bone loading during terrestrial locomotion in the green iguana (*Iguana iguana*) and American alligator (*Alligator mississippiensis*). *The Journal of Experimental Biology*, *204*, 1099-1122

Budsberg SC, Chambers JN, Lue SL, Foutz TL, Reece L. Prospective evaluation of ground reaction forces in dogs undergoing unilateral total hip replacement. Am J Vet Res. 1996 Dec;57(12):1781-5. PMID: 8950435.

Budsberg SC, Verstraete MC, Soutas-Little RW. Force plate analysis of the walking gait in healthy dogs. Am J Vet Res. 1987 Jun;48(6):915-8. PMID: 3605807.

Clack, J. A. (2012). Gaining ground second edition: The origin and evolution of tetrapods. Indiana University Press, Bloomington, IN.

Clack, J. A., & Ahlberg, P. E. (2016). Sarcopterygians: From lobe-finned fishes to the tetrapod stem group. In *Evolution of the Vertebrate Ear* (Vol. 59). SPRINGER. Retrieved from https://doi.org/10.1007/978-3-319-46661-3_3

Cleather, D. J., & Bull, A. M. (2010). Influence of inverse dynamics methods on the calculation of inter-segmental moments in vertical jumping and weightlifting. *BioMedical Engineering OnLine, 9*(1), 74. doi:10.1186/1475-925x-9-74

Coates, M. I., Ruta, M. & Friedman, M. (2008). Ever since Owen: changing perspectives on the early evolution of tetrapods. *Annu. Rev. Ecol. Evol. Syst.* **39**, 571-592

Conte, S., Bergeron, R., Gonyou, H., Brown, J., Rioja-Lang, F. C., Connor, L., Devillers. N. (2014). Measure and characterization of lameness in gestating sows using force plate, kinematic, and accelerometer methods, *Journal of Animal Science*, *92*(12), 5693 5703, https://doi.org/10.2527/jas.2014-7865

Crossley K., Bennell K.L., Wrigley T., Oakes B.W. (1999) Ground reaction forces, bone characteristics, and tibial stress fracture in male runners. *Medicine and Science in Sports and Exercise* 31(8), 1088-1093

Dhuper, M. (2018). Understanding the functional morphology of the pectoral fin in *Polypterus senegalus*. (dissertation).

Delp, S. L., Anderson, F. C., Arnold, A. S., Loan, P., Habib, A., John, C. T., Guendelman, E., & Thelen, D. G. (2007). OpenSim: open-source software to create and analyze dynamic simulations of movement. *IEEE Trans Biomed Eng.*

De Groote, F., De Laet, T., Jonkers, I., De Shutter, J. (2008). Kalman smoothing improves the estimation of joint kinematics and kinetics in marker-based human gait analysis. *J. Biomech*. 41, 3390-3398.

Dickenson, M. H., Farley, C., Full, R. J., & Koehl, M. A. R. (2007). How animals move: an integrative view. *Science*. *288*(5463), 100-106. DOI: 10.1126/science.288.5463.100

Ditsche, P., & Summers, A. P. (2014). Aquatic versus terrestrial attachment: Water makes a difference. *Beilstein journal of nanotechnology*, *5*, 2424–2439. https://doi.org/10.3762/bjnano.5.252

Du, T. Y., & Standen, E. M. (2017). Phenotypic plasticity of muscle fiber type in the pectoral fins of *Polypterus senegalus* reared in a terrestrial environment. *The Journal of Experimental Biology*, *220*(19), 3406-3410. Doi: 10.1242/jeb.162909

Du, T. Y., & Standen, E. M. (2020). Terrestrial acclimation and exercise lead to bone functional response in *Polypterus senegalus* pectoral fins. *The Journal of Experimental Biology, 223.* doi: 10.1242/jeb.217554

Faber, H., van Soest, A. J., & Kistemaker, D. A. (2018). Inverse dynamics of mechanical multibody systems: an improved algorithm that ensures consistency between kinematics and external forces. *PloS one*, *13*(9), e0204575. https:doi.org/10.1371/journal.pone.0204575

Foster, K. L., Dhuper, M., & Standen, E. M. (2018). Fin and body neuromuscular coordination changes during walking and swimming in *Polypterus senegalus*. *The Journal of Experimental Biology, 221*(17). doi: 10.1242/jeb.168716

Full, R., Yamauchi, A., & Jindrich, D. (1995). Maximum single leg force production: Cockroaches righting on Photoelastic Gelatin. *Journal of Experimental Biology*, *198*(12), 2441–2452. https://doi.org/10.1242/jeb.198.12.2441

Gatesy, S. M., & Dial, K. P. (1996). Locomotor modules and the evolution of avian flight. *Evolution*. 50, 331-340.

Graham, J. B., Wegner, N. C., Miller, L. A., et al. (2014). Spiracular air breathing in polypterid fishes and its implications for aerial respiration in stem tetrapods. *Nat Comm*, **5**, e3022.

Hedrick, T. L. (2008). Software techniques for two- and three-dimensional kinematic measurements of biological and biomimetic systems. *Bioinspiration & Biomimetics, 3*(3).

Hoffmann, S. L., Donatelli, C. M., Leigh, S. C., Brainerd, E. L., & Porter, M. E. (2019). Three dimensional movements of the pectoral fin during yaw turns in the Pacific spiny dogfish, *Squalus suckleyi*. *Biol Open, 8*(1). doi: https://doi.org/10.1242/bio.037291

Holden, J. P., & Stanhope, S. J. (1998). The effect of variation in knee center location estimates on net knee joint moments. *Gait & Posture*, *7*(1), 1–6. https://doi.org/10.1016/s0966-6362(97)00026-x

Holmes, P., Full, R. J., Koditschek, D., and Guckenheimer, J. (2006). Dynamics of legged locomotion: Models, analyses, and challenges. *SIAM Review (SIREV)*, 48(2), 207-304.

LaNasa, P. J., & Upp, E. L. (2014). Basic Flow Measurement Laws. In *Fluid Flow Measurement: a Practical Guide to Accurate Flow Measurement* (pp. 19–30). essay, Elsevier Science.

Lechleuthner, A., Schumacher, U., Negele, R. D., Welsch, U. (1989). Lungs of *Polypterus* and Erpetiochthys. *The Journal of Morphology,* **201,** 161-178.

Jayne, B. C. and Lauder, G. V. (1994) How swimming fish use slow and fast muscle fibers: implications for models of vertebrate muscle recruitment. *J. Comp. Physiol. A* **175**, 123-131.

Kawano, S. M., & Blob, R. W. (2013). Propulsive forces of mudskipper fins and salamander limbs during terrestrial locomotion: implications for the invasion of land. *Integr. Comp. Biol.* 53, 283-294.

Matijevich, E. S., Branscombe, L. M., Scott, L. R., & Zelik, K. E. (2019). Ground reaction force metrics are not strongly correlated with tibial bone load when running across speeds and slopes: implications for science, sport and wearable tech. *Plos One, 14*(1). doi: 10.1371/journal.pone.0210000

Mayo, J., Ojeda, J. (2020). Influence of the kinematic constraints on dynamic residuals in inverse dynamic analysis during human gait without using force plates. *Multibody Syst Dyn* **50,** 305-321. https://doi.org/10.1007/s11044-020-09739-9

McGee, G. R. (2013). When the invasion of land failed: the legacy of the devonian extinctions. Columbia University Press, New York, NY.

McLaughlin RM Jr, Gaughan EM, Roush JK, Skaggs CL. Effects of subject velocity on ground reaction force measurements and stance times in clinically normal horses at the walk and trot. Am J Vet Res. 1996 Jan;57(1):7-11. PMID: 8720231.

Metscher, B. D., Takahashi, K., Crow, K., Amemiya, C., Nonaka, D. F., Wagner, G. P. (2005). Expression of *Hoxa-11* and *Hoxa-13* in the pectoral fin of a basal ray-finned fish, *Polyodon spathula*: implications for the origin of tetrapod limbs. *Evolution & Development, 7*(3), 186-195.

Nordquist, R. E., Meijer, E., Staay, F. J. V. D., & Arndt, S. S. (2017). Pigs as model species to investigate effects of early life events on later behavioural and neurological functions. *Animal Models for the Study of Human Disease*, 1003-1030. doi: 10.1016/b978-0-12-809468-6.00039-5

Pace, C. M., & Gibb, A. C. (2014). Sustained periodic terrestrial locomotion in air-breathing fishes: terrestrial locomotion in fishes. *Journal of Fish Biology.* 84, 639-660.

Pierce, S. E., Clack, J. A. & Hutchinson, J. R. Three-dimensional limb joint mobility in the early tetrapod *Ichthyostega*. *Nature* **486**, 523-527 (2012).

R Core Team (2021). R: A language and environment for statistical computing. R foundation for statistical computing, Vienna, Austria. https://www.R-project.org/.

Roberts, T. J., & Scales, J. A. (2004). Adjusting muscle function to demand: Joint work during acceleration in wild turkeys. *Journal of Experimental Biology*, *207*(23), 4165–4174. https://doi.org/10.1242/jeb.01253

Robertson, D. G., Caldwell, G. E., Hamill, J., Kamen, G., Whittlesey, S. N. (2004). Research methods in biomechanics. *Human Kinetics.*

Roush JK, McLaughlin RM Jr. Effects of subject stance time and velocity on ground reaction forces in clinically normal greyhounds at the walk. Am J Vet Res. 1994 Dec;55(12):1672-6. PMID: 7887509.

Rumph PF, Lander JE, Kincaid SA, Baird DK, Kammermann JR, Visco DM. Ground reaction force profiles from force platform gait analyses of clinically normal mesomorphic dogs at the trot. Am J Vet Res. 1994 Jun;55(6):756-61. PMID: 7944010.

Sayer, M. D. (2005). Adaptations of amphibious fish for surviving life out of water. *Fish Fish*. 6, 186-211.

Standen, E. M., Du, T. Y., & Larsson, H. C. E. (2014). Developmental plasticity and the origin of tetrapods. *Nature, 513*(7516), 54-58. doi: 10.1038/nature13708

Standen, E. M., Du, T. Y., Laroche, P., & Larsson, H. C. E. (2016). Locomotor flexibility of *Polypterus senegalus* across various aquatic and terrestrial substrates. *Zoology.* 119(5), 447-454.

Strasser, T., Peham, C. & Bockstahler, B.A. A comparison of ground reaction forces during level and cross-slope walking in Labrador Retrievers. *BMC Vet Res* **10,** 241 (2014). https://doi.org/10.1186/s12917-014-0241-4

Vaughan, C. L., Hay, J. G., Andrews, J. G. (1982). Closed loop problems in biomechanics. Part I- a classification system. *J. Biomech*. 15, 197-200.

Wilhelm, B. C., Du, T. Y., Standen, E. M., & Larsson, H. C. (2015). *Polypterus* and the evolution of fish pectoral musculature. *Journal of Anatomy*, 226(6), 511-522. doi: 10.1111/joa.12302

Wright, P. A., & Turko, A. J. (2016). Amphibious fishes: evolution and phenotypic plasticity. *Journal of Experimental Biology,* 219, 2245-2259. doi: 10.1242/jeb.126649

Zatsiorsky, V. M. (2002). Kinetics of human motion. *Human Kinetics*.
Zumwalt, A. C., Hamrick, M., & Schmitt, D. (2006). Force plate for measuring the ground reaction forces in small animal locomotion. *Journal of Biomechanics,* 39(15), 2877-2881.

Appendix

Table A1 Mass (g) and length taken for each step. Mass and length measurements were taken after each day of data collection. Each row corresponds to the experimental trial taken on the same day by each fish. The number of steps used by that fish on that particular date is indicated under the column labeled *'steps'*. Data was obtained over two days of filming. Trials that are reported to have the same mass and length for a particular fish were collected on the same day.

Fish ID	Mean Mass (g)	Mean Length (cm)
Polyp2017-053	21.58	15.15
Polyp2017-054	13.9	12.33
Polyp2017-055	14.21	14.03
Polyp2018-017	14.34	14.15
Polyp2018-018	14.94	13.65

Table A2 Significant temporal variables have been plotted along a circular plot, also known as a polar plot. Each colour corresponds to a specific variables, as indicated in the table. Variables were analyzed for directionality using Rayleigh's test.

Variables – all steps (n=10)	Rayleigh's test value	Mean
AbdVelMin (yellow)	0.038924	0.7056
NoseElevMaxPlant (orange)	0.037701	1.2320
NoseElevMinPlant (blue)	0.015319	-0.3350
NoseVelMinSwing (red)	0.005336	-0.2504
ForceMaxY (purple)	0.000538	0.1206
ForceMinY (green)	0.04721	-2.6059

Table A3.1 Statistically significant variables, as indicated using Rayleigh's test for directionality for category *slip,* subgroup *mid-slip.* This group categorizes the steps depending on the time of occurrence of the slip phase within the stance phase. Subgroup *mid-slip* contains steps that have a slip phase around 50% stance. Significant temporal variables have been plotted along a circular plot, also known as a polar plot. Variables were found to have directionality if their Rayleigh's test value was less than 0.05. Each colour corresponds to a specific variable, as indicated in the table.

Variables – group 1.1 (slip at 50%)	Rayleigh's test value	Mean
AbdAngMin (blue)	0.017057	2.7891
NoseVelMaxSwing (very light blue)	0.015277	0.1789

Table A3.2 Statistically significant variables, as indicated using Rayleigh's test for directionality for category *slip,* subgroup *variable slip.* This group categorizes the steps

depending on the time of occurrence of the slip phase within the stance phase. Subgroup *variable slip* contains steps that have a slip phase either before or after 50% stance. Significant temporal variables have been plotted along a circular plot, also known as a polar plot. Variables were found to have directionality if their Rayleigh's test value was less than 0.05. Each colour corresponds to a specific variable, as indicated in the table.

Variables – group 1.2 (slip before or after 50%)	Rayleigh's test value	Mean
NoseElevMaxPlant (orange)	0.033597	1.2530
NoseVelMinSwing (red)	0.035805	-0.1693

Table A3.3 Statistically significant variables, as indicated using Rayleigh's test for directionality for category *slip,* subgroup *special slip.* This group categorizes the steps depending on the time of occurrence of the slip phase within the stance phase. Subgroup *special slip* contains steps that possess either no slip phase, or multiple (i.e. one or more) slip phases within a single stance. Significant temporal variables have been plotted along a circular plot, also known as a polar plot. Variables were found to have directionality if their Rayleigh's test value was less than 0.05. Each colour corresponds to a specific variable, as indicated in the table.

Variables – group 1.3 (no slip or multiple slips)	Rayleigh's test value	Mean
NoseElevMinPlant (blue)	0.034369	0.0979
ForceMaxY (purple)	0.034346	0.0492

Table A4.1 Statistically significant variables, as indicated using Rayleigh's test for directionality for category *motion,* subgroup *tucked fin.* This group categorizes the steps depending on the motion of the fin during the stance phase. Subgroup *tucked fin* contains steps in which the fin becomes 'tucked' underneath the anterior body at some point during stance. Significant temporal variables have been plotted along a circular plot, also known as a polar plot. Variables were found to have directionality if their Rayleigh's test value was less than 0.05. Each colour corresponds to a specific variable, as indicated in the table.

Variables – group 2.1 (tucked fins)	Rayleigh's test value	Mean
COMVelMinSwing (medium green)	0.037979	-0.0432
ForceMaxY (purple)	0.033757	0.1248

Table A4.2 Statistically significant variables, as indicated using Rayleigh's test for directionality for category *motion,* subgroup *lateral fin.* This group categorizes the steps depending on the motion of the fin during the stance phase. Subgroup *lateral fin* contains steps in which the planted fin remains to the side of the anterior body at all times during the step. Significant temporal variables have been plotted along a circular plot, also known as a polar

plot. Variables were found to have directionality if their Rayleigh's test value was less than 0.05. Each colour corresponds to a specific variable, as indicated in the table.

Variables – group 2.2 (lateral fins)	Rayleigh's test value	Mean
AbdVelMin (yellow)	0.001327	0.5647
NoseElevMaxPlant (orange)	0.00567	1.4092
NoseElevMinPlant (blue)	0.016346	-0.3565
NoseVelMinSwing (red)	0.005828	-0.1552
ForceMaxY (purple)	0.019819	0.1181
ForceMinY (green)	0.01345	-2.5227

Table A5 Means, standard deviation, and s.e.m. of all variables analyzed within whole group analysis for stance duration and slip duration.

All steps (n=10)	Mean	Standard Deviation	s.e.m
Plant duration	0.244	0.165993	0.052492
Slip duration	0.174349	0.110932	0.03508

Table A6 Means, standard deviation, and s.e.m. of all variables analyzed within whole group analysis. A total of twelve (12) kinematic and force variables were analyzed during the stance phase. Variable names can be found in **column 1**.

Whole group analysis	Mean	Standard deviation	s.e.m
Nose distance during stance	0.567915	0.235076	0.074338
CoM distance during stance	0.305585	0.13122	0.041495
Fin distance during stance	0.201928	0.084096	0.026594
Max. magnitude Fx	0.134721	0.066754	0.02111
Max. magnitude Fy	0.111868	0.080105	0.025331
Max. magnitude Fz	0.573397	0.191706	0.060623
Fx magnitude at loading	0.011848	0.09115	0.028824

Fy magnitude at loading	0.070182	0.06784	0.021453
Fz magnitude at loading	0.207254	0.103057	0.03259
Time to max. Fx	0.13358	0.106294	0.033613
Time to max. Fy	0.03786	0.093718	0.029636
Time to max. Fz	0.14082	0.106768	0.033763

Table A7 Means and s.e.m. of all variables analyzed within category *slip*. A total of thirty-three (33) kinematic and force variables were analyzed during the stance phase. Variable names can be found in **column 1**. **Columns 2-4** represent each subgroup, and their respective means and s.e.m. of each variable analyzed.

Category *slip*	Mid-slip Mean±sem	Variable slip Mean±sem	Special slip Mean±sem
Nose distance during stance	0.592662076 ±0.133567	0.637787 ±0.053236401	0.465047± 0.190359
CoM distance during stance	0.324478021 ±0.074237	0.339381 ±0.029045235	0.246598± 0.106833
Fin distance during stance	0.194867041 ±0.044638	0.237449 ±0.043188528	0.175823± 0.061263
Max. magnitude Fx	0.105370337 ±0.048288	0.135955 ±0.009245752	0.17262± 0.025337
Max. magnitude Fy	0.140535406 ±0.042863	0.086812 ±0.049258538	0.098702± 0.050752
Max. magnitude Fz	0.614802027 ±0.045607	0.547185 ±0.141727662	0.544401± 0.170215
Fx magnitude at loading	-0.064460143 ±0.032583	0.088388 ±0.048757531	0.037053± 0.028864
Fy magnitude at loading	0.093484681 ±0.032747	0.019549 ±0.027563473	0.089744± 0.046516
Fz magnitude at loading	0.243058828 ±0.068571	0.211152 ±0.049863655	0.155617± 0.042959
Time to max. Fx	0.18035 ±0.061827	0.0828 ±0.00892263	0.122± 0.080052
Time to max. Fy	0.08055 ±0.074552	0.011267 ±0.004430701	0.007533± 0.003275
Time to max. Fz	0.1645 ±0.06423	0.114267 ±0.048475469	0.1358± 0.075889

Table A8 Means and s.e.m. of all variables analyzed within category *motion*. A total of thirty-three (33) kinematic and force variables were analyzed during the stance phase. Variable names can be found in **column 1**. **Columns 2-3** represent each subgroup, and their respective means and s.e.m. of each variable analyzed.

Category *motion*	Tucked fins Mean±sem	Untucked fins Mean±sem
Nose distance during stance	0.716854± 0.091663	0.504084± 0.09153
CoM distance during stance	0.435256± 0.017614	0.250011± 0.043927
Fin distance during stance	0.276021± 0.007764	0.170175± 0.030768
Max. magnitude Fx	0.162106± 0.057106	0.122984± 0.02031
Max. magnitude Fy	0.198766± 0.009589	0.074626± 0.024318
Max. magnitude Fz	0.726313± 0.071054	0.507861± 0.06905
Fx magnitude at	-0.07682±	0.049851±
Fy magnitude at loading	0.147266± 0.020165	0.037146± 0.017938
Fz magnitude at loading	0.232959± 0.076132	0.196238± 0.037154
Time to max. Fx	0.278667± 0.015949	0.0714± 0.015388
Time to max. Fy	0.007733± 0.001453	0.050771± 0.042299
Time to max. Fz	0.224867± 0.071539	0.1048± 0.031477

Table A9 Results from paired T-tests used to compare differences between GRF components. Maximum GRFs were measured in three planes: anteroposterior (Fx), mediolateral (Fy), and vertical (Fz). The magnitudes of GRFs produced at the onset of the stance phase were also measured. The corresponding p-values are listed in column 2. Asterisks indicate the that significant difference exists between the two force components.

Force Components	P-value
Max. anteroposterior (Fx) versus Max. mediolateral (Fy)	0.5293
Max. anteroposterior (Fx) versus Max. vertical (Fz)	4.345e-05*

Max. mediolateral (Fy) versus Max. vertical (Fz)	3.405e-06*
Anteroposterior (Fx) at onset versus Mediolateral (Fy) at onset	0.2063
Anteroposterior (Fx) at onset versus Vertical (Fz) at onset	0.001623*
Mediolateral (Fy) at onset versus Vertical (Fz) at onset	0.00265*

Table A10 Results from a Linear Mixed Effects (LME) model. Dependent variables are listed in column 1. Fixed variables include slip duration and stance duration. P values, as well as marginal (*m*) and conditional (*c*) R^2 values are reported. Asterisks indicate the existence of significant correlations between the corresponding dependent variable and the fixed effect.

Dependent variables	Slip duration P-value	R^2m [R^2c]	Stance duration P-value	R^2m [R^2c]
Nose distance	0.283	0.0869 [0.4580]	0.002*	0.7517 [0.7518]
CoM distance	0.2606	0.1463 [0.1463]	0.0118*	0.5645 [0.7542]
Fin distance	0.2558	0.1491 [0.1491]	0.0256*	0.3775 [0.7910]
Max. magnitude Fx	0.6845	0.0163 [0.2137]	0.4032	0.0824 [0.0824]
Max. magnitude Fy	0.5181	0.0497 [0.0497]	0.2993	0.1278 [0.2874]
Max. magnitude Fz	0.1689	0.2137 [0.2137]	0.2224	0.1707 [0.1707]
Fx at onset of stance	0.6205	0.0294 [0.0294]	0.3309	0.1106 [0.1106]
Fy at onset of stance	0.7140	0.0115 [0.3445]	0.2383	0.1496 [0.4892]
Fz at onset of stance	0.0278*	0.4808 [0.4808]	0.8428	0.0047 [0.0047]
Time to max. Fx	0.8126	0.0066 [0.0306]	0.0026	0.6087 [0.8813]
Time to max. Fy	0.7909	0.0034 [0.6226]	0.9172	0.0009 [0.6239]
Time to max. Fz	0.6914	0.0109 [0.4587]	0.0007	0.8204 [0.8204]

Table A11 Results from unpaired T-tests used to compare differences between fin motions. Two fin motions were observed during walking and were defined at *tucked* and *untucked* fin steps. The corresponding p-values are listed in column 2. Asterisks indicate the that significant difference exists between the two force components.

Dependent variables	P-value of unpaired T-test
Nose distance	0.2064
CoM distance	0.02985*
Fin distance	0.06222
Max. Fx	0.428
Max. Fy	0.01274*
Max. Fz	0.0992
Stance duration	0.03584*
Slip duration	0.8681
Fx at onset of stance	0.03355*
Fy at onset of stance	0.007258*
Fz at onset of stance	0.6345
Time to max. Fx	4.643e-05*
Time to max. Fy	0.3484
Time to max. Fz	0.1046

A

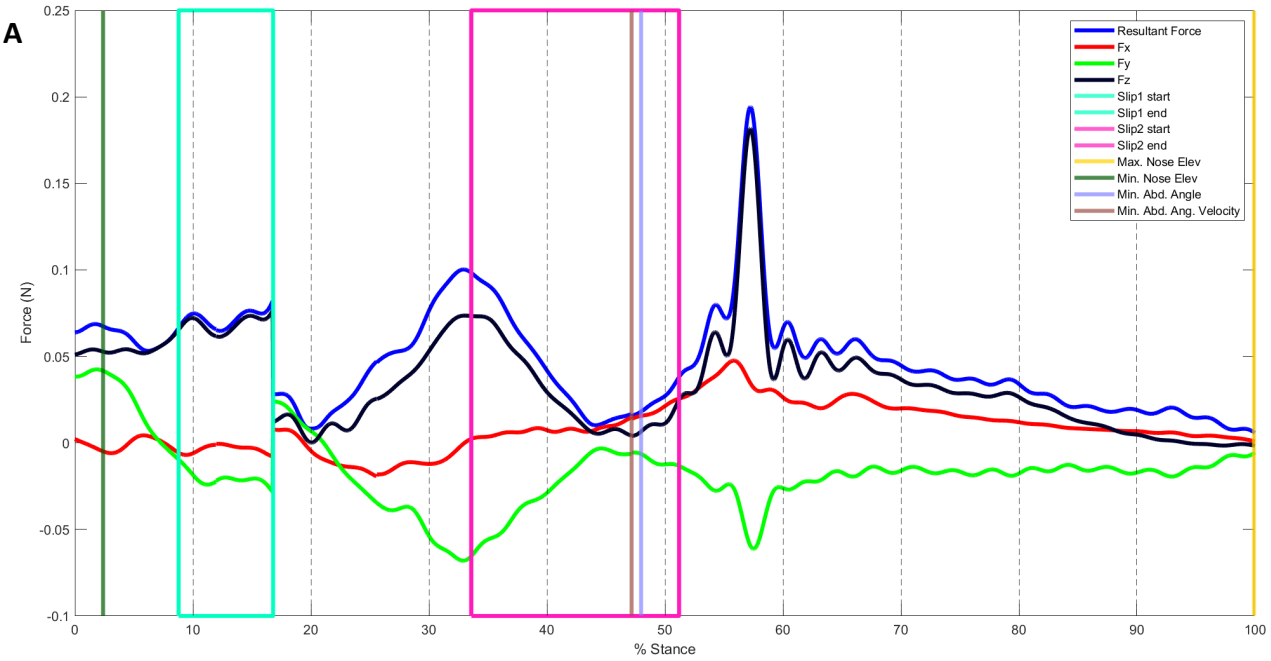

B

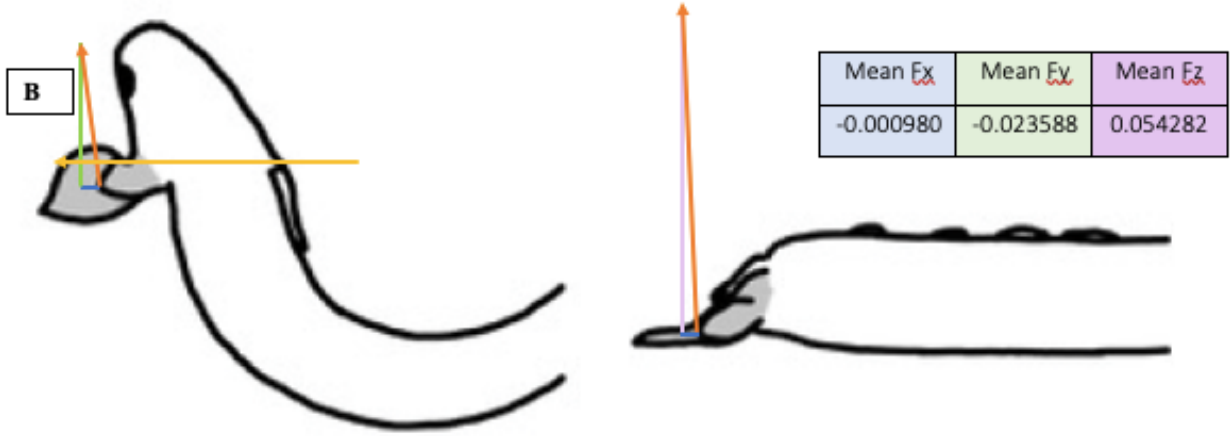

Mean Fx	Mean Fy	Mean Fz
-0.000980	-0.023588	0.054282

C

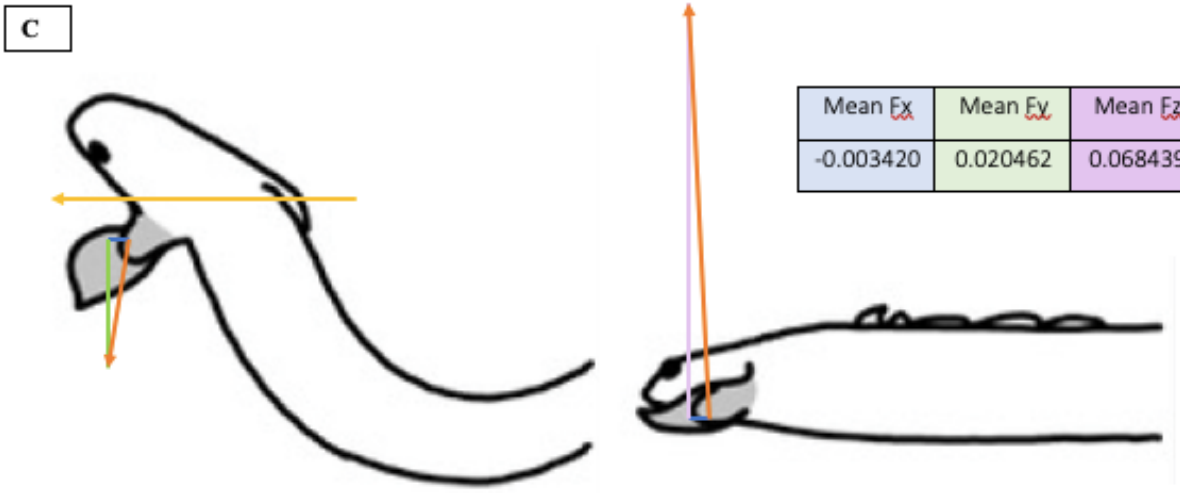

Mean Fx	Mean Fy	Mean Fz
-0.003420	0.020462	0.068439

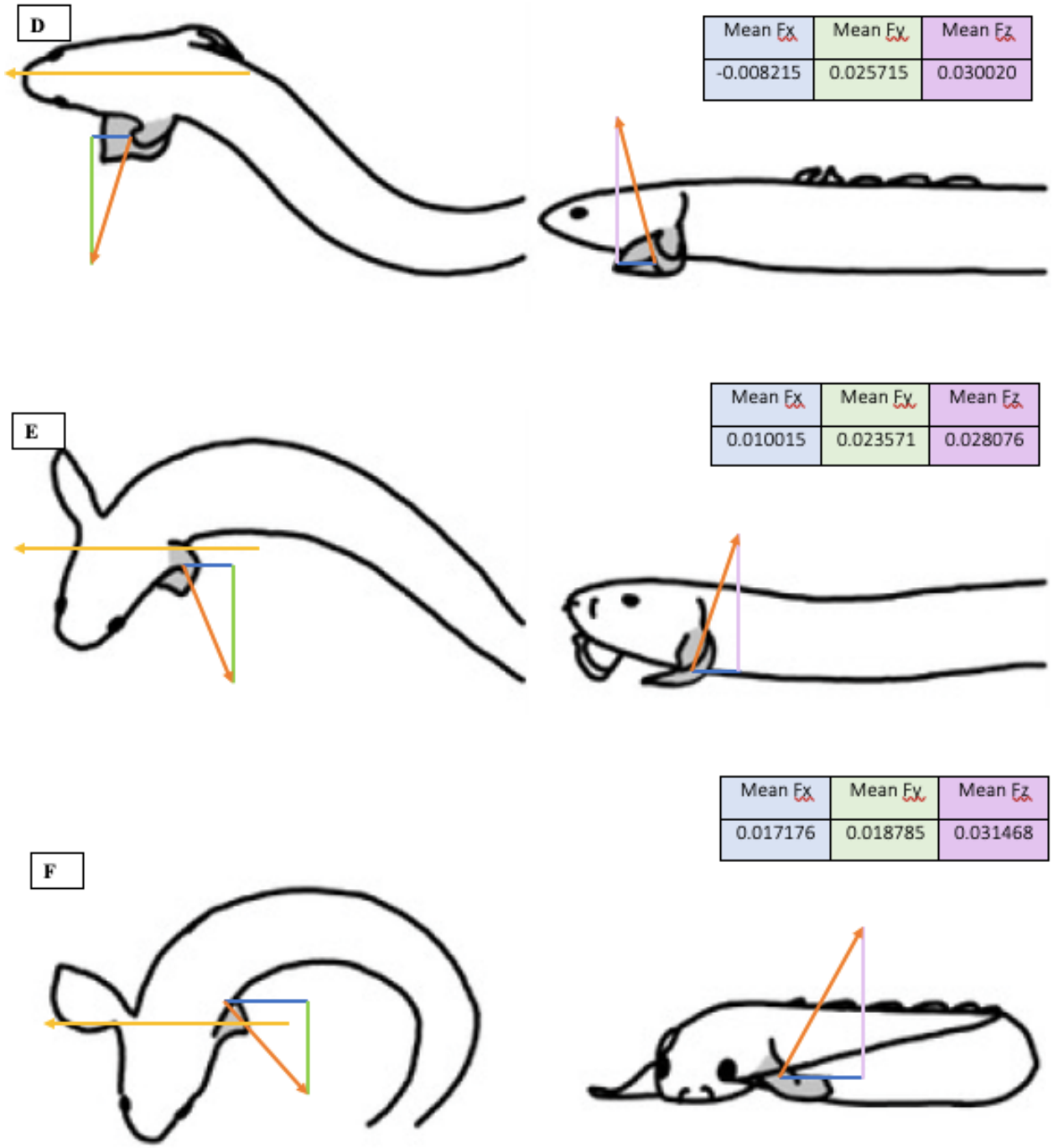

Figure A1 Force trace (A) and illustrations depicting kinematic motion, force components, and predicted resultant force vector (B-F) of step 1 (Table 2.2). Step 1 belongs to the '*special slip*' subgroup of category *slip* as it contained two periods of slip within a single step. Stance duration is depicted as percent stance. Forward (Fx), lateral (Fy), and vertical (Fz) force components are indicated by the red, green, and black lines, respectively. The resultant force magnitude is displayed by the dark blue line. This step contains a single slip phase, indicated by the pink box. Objective kinematic timings are indicated by the vertical lines and include maximum nose elevation (yellow), minimum nose elevation (dark green), minimum abduction angle (light blue), and minimum abduction angular velocity (brown). The kinematic motions illustrated were observed at the midpoint between the timings of interest, and include the onset of loading to the onset of the first slip phase (B); the onset of the first slip phase to the end of the first slip phase (C); the end of the first slip phase to the onset of the second slip phase (D); the onset of the second slip phase to the end of the second slip phase (E); and lastly, the end of the second slip phase to the end of the stance (F). The mean magnitudes of forward (Fx) (blue), lateral (Fy) (green), and vertical (Fz) (purple) forces are recorded in the tables. Arrows in orange depict the resultant force vector, and arrows in yellow illustrate the straightest path of motion as determined by the kinematics measured from the CoM.

A

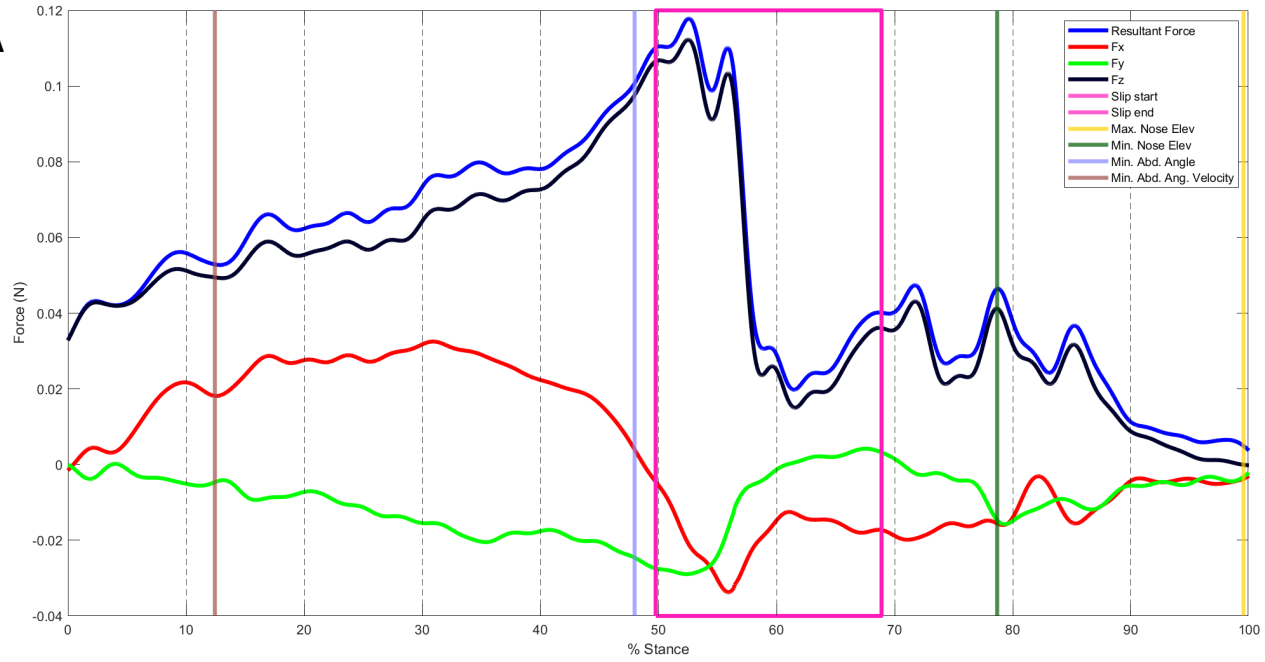

B

Mean Fx	Mean Fy	Mean Fz
0.017897	-0.01588	0.062525

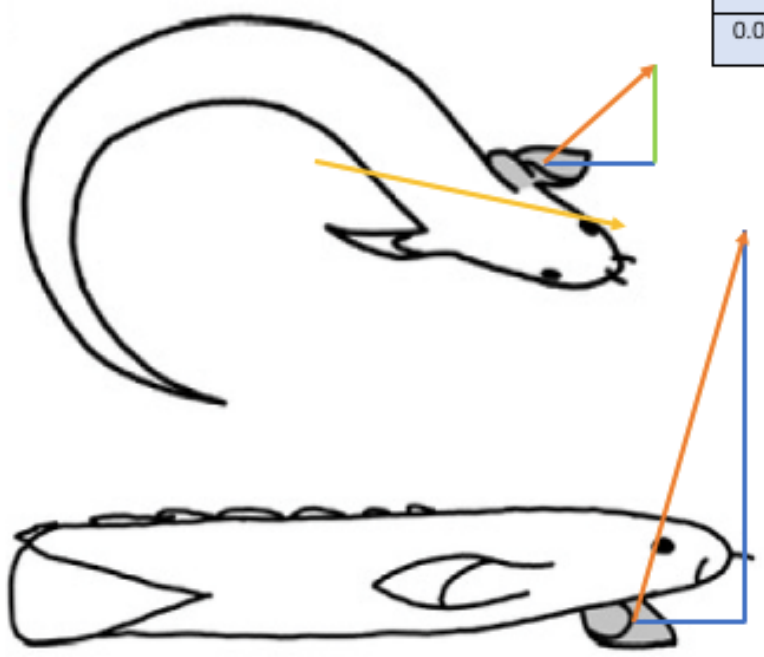

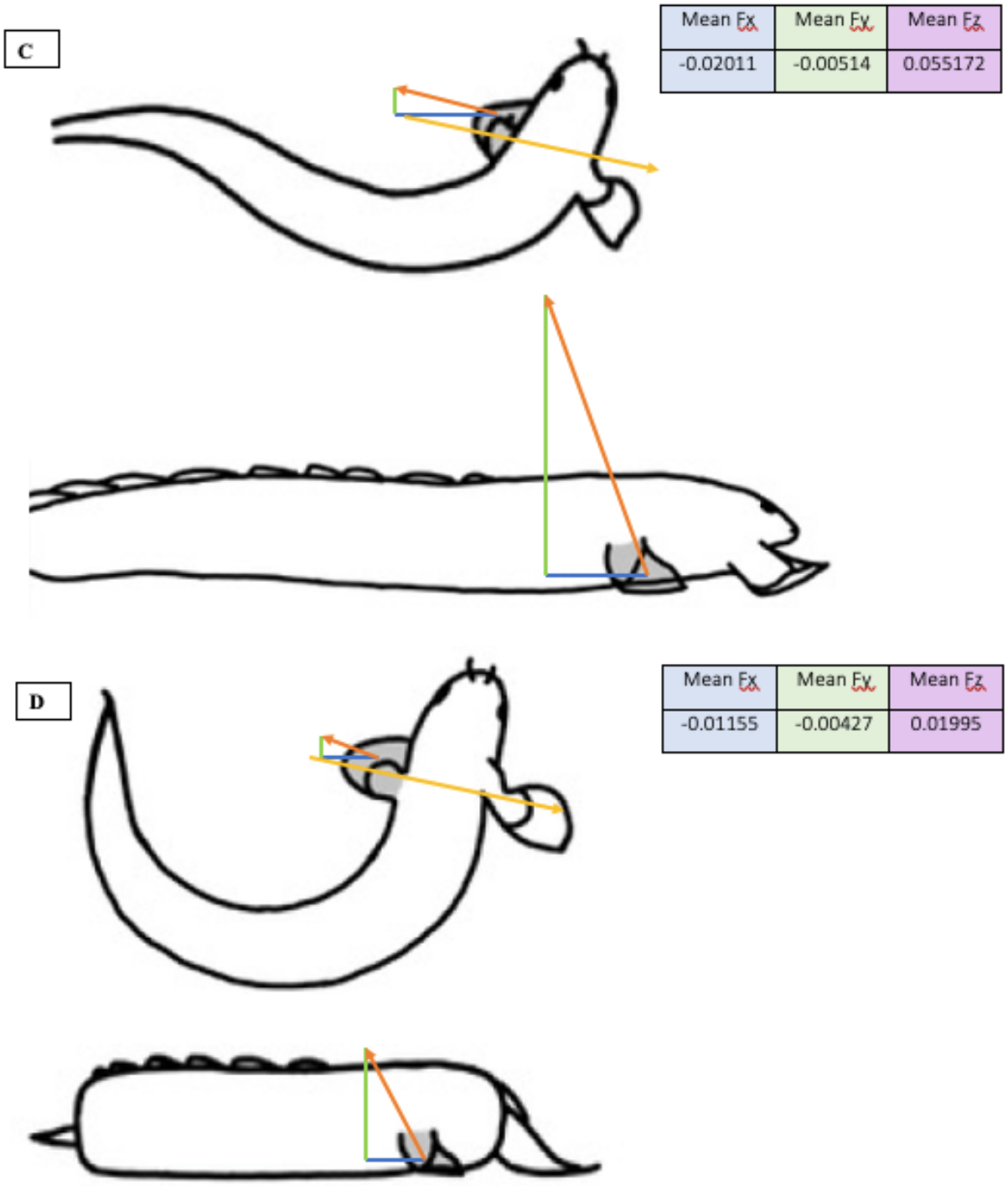

Figure A2 Force trace (A) and illustrations depicting kinematic motion, force components, and predicted resultant force vector (B-D) of step 2 (Table 2.2). Step 2 belongs to the '*mid-slip*' subgroup of category *slip.* Stance duration is depicted as percent stance. Forward (Fx), lateral (Fy), and vertical (Fz) force components are indicated by the red, green, and black lines, respectively. The resultant force magnitude is displayed by the dark blue line. This step contains a single slip phase, indicated by the pink box. Objective kinematic timings are indicated by the vertical lines and include maximum nose elevation (yellow), minimum nose elevation (dark green), minimum abduction angle (light blue), and minimum abduction angular velocity (brown). The kinematic motions illustrated were observed at the midpoint between the timings of interest, and include the onset of loading to the onset of the slip phase (B); the onset of the slip phase to the end of the slip phase (C); the end of the slip phase to the end of the stance (D). The mean magnitudes of forward (Fx) (blue), lateral (Fy) (green), and vertical (Fz) (purple) forces are recorded in the tables. Arrows in orange depict the resultant force vector, and arrows in yellow illustrate the straightest path of motion as determined by the kinematics measured from the CoM.

A

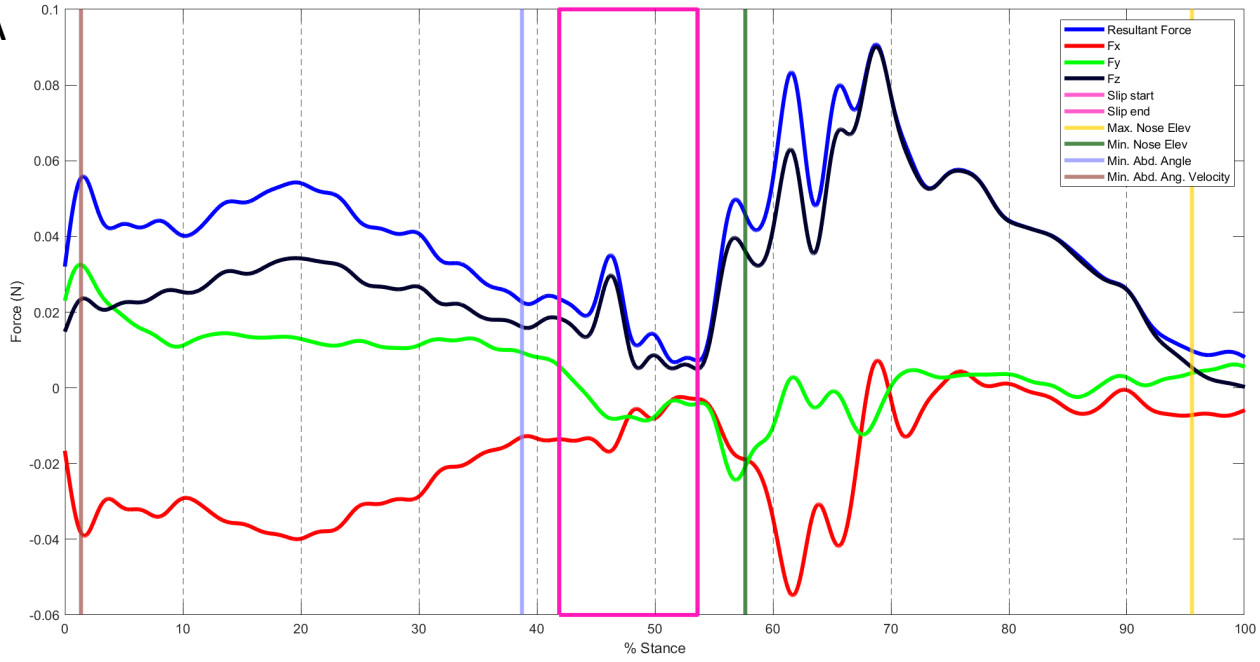

B

Mean Fx	Mean Fy	Mean Fz
-0.027202	0.017345	0.025296

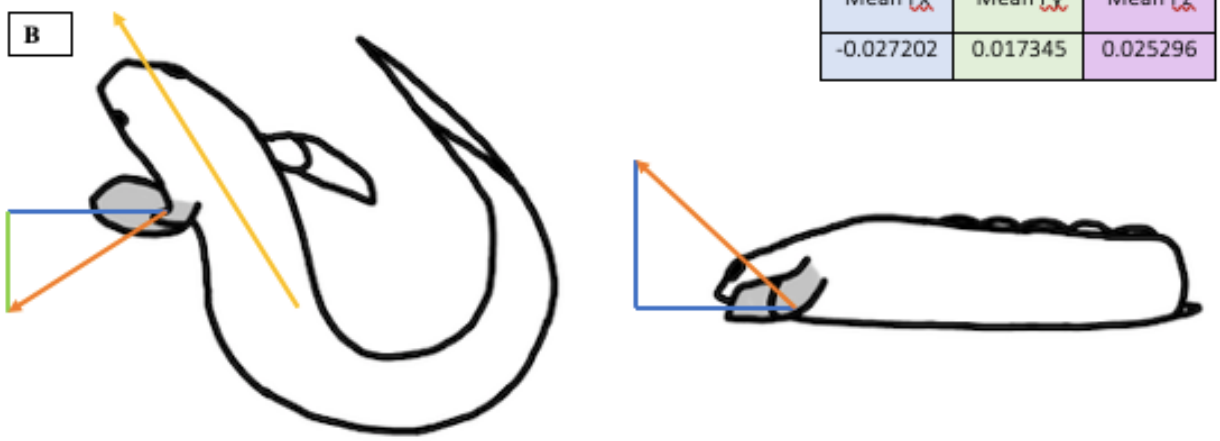

C

Mean Fx	Mean Fy	Mean Fz
-0.001255	0.010428	0.012985

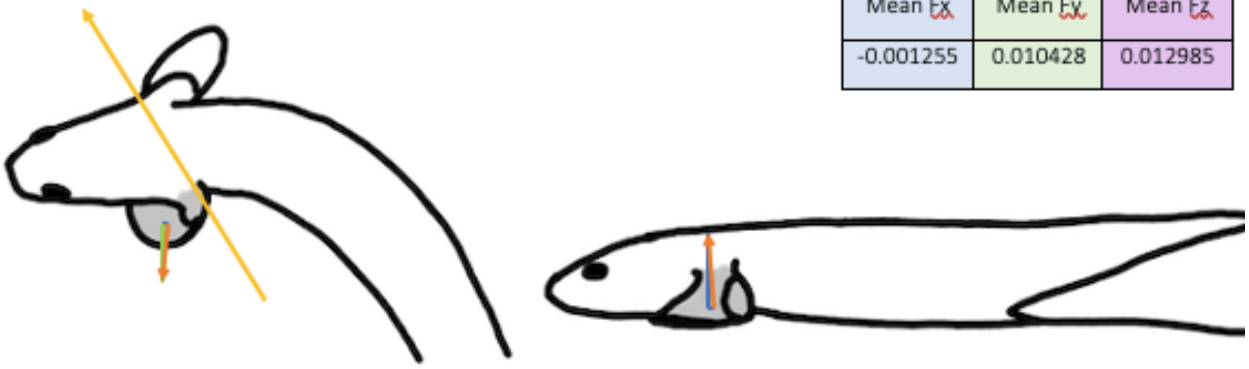

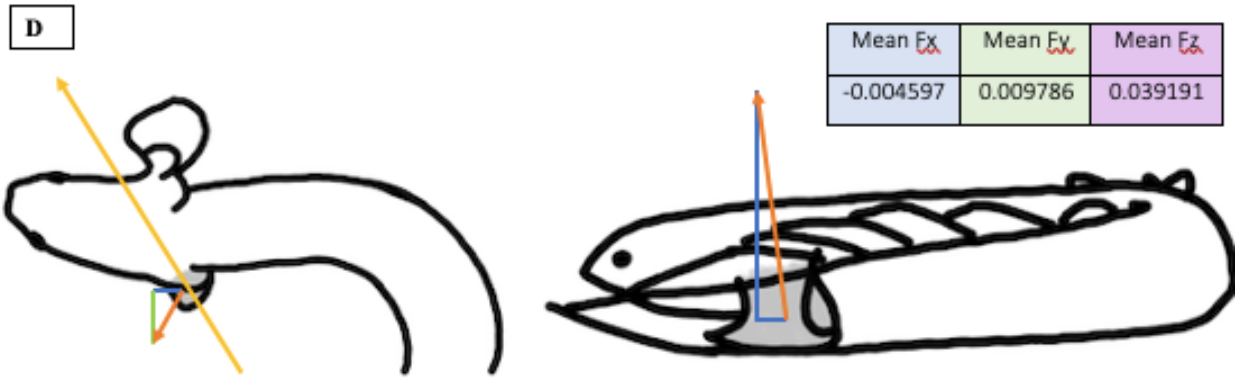

Figure A3 Force trace (A) and illustrations depicting kinematic motion, force components, and predicted resultant force vector (B-D) of step 3 (Table 2.2). Step 3 belongs to the '*mid-slip*' subgroup of category *slip.* Stance duration is depicted as percent stance. Forward (Fx), lateral (Fy), and vertical (Fz) force components are indicated by the red, green, and black lines, respectively. The resultant force magnitude is displayed by the dark blue line. This step contains a single slip phase, indicated by the pink box. Objective kinematic timings are indicated by the vertical lines and include maximum nose elevation (yellow), minimum nose elevation (dark green), minimum abduction angle (light blue), and minimum abduction angular velocity (brown). The kinematic motions illustrated were observed at the midpoint between the timings of interest, and include the onset of loading to the onset of the slip phase (B); the onset of the slip phase to the end of the slip phase (C); the end of the slip phase to the end of the stance (D). The mean magnitudes of forward (Fx) (blue), lateral (Fy) (green), and vertical (Fz) (purple) forces are recorded in the tables. Arrows in orange depict the resultant force vector, and arrows in yellow illustrate the straightest path of motion as determined by the kinematics measured from the CoM.

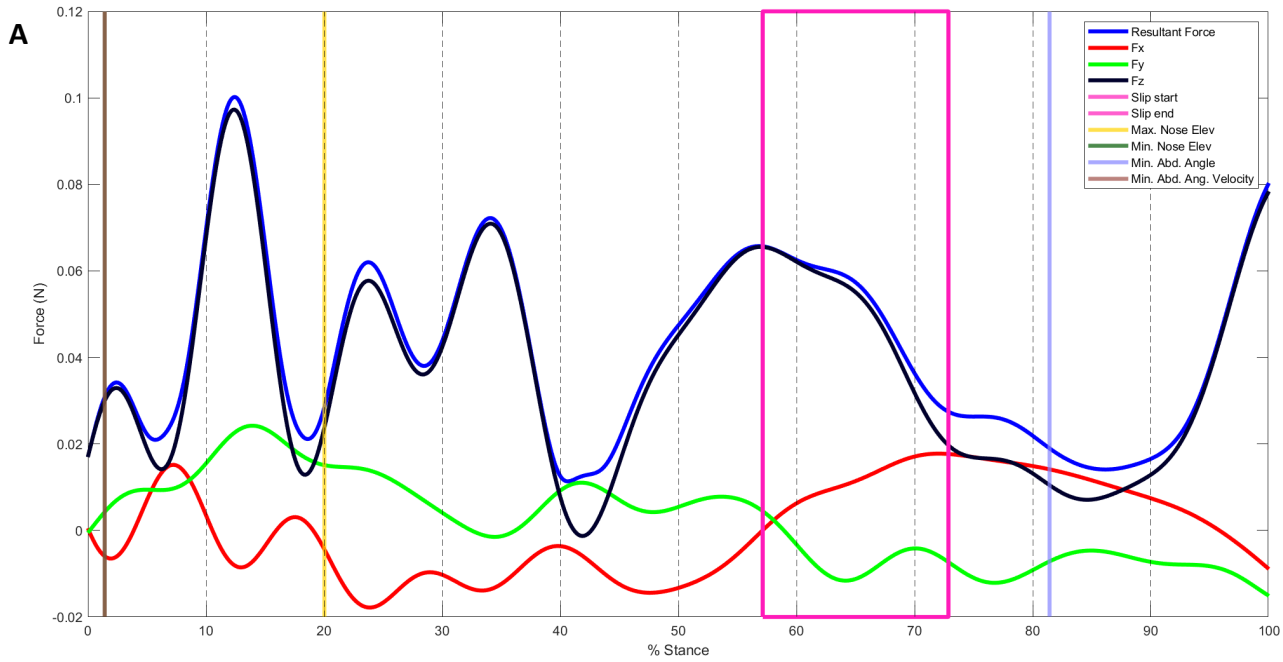

B

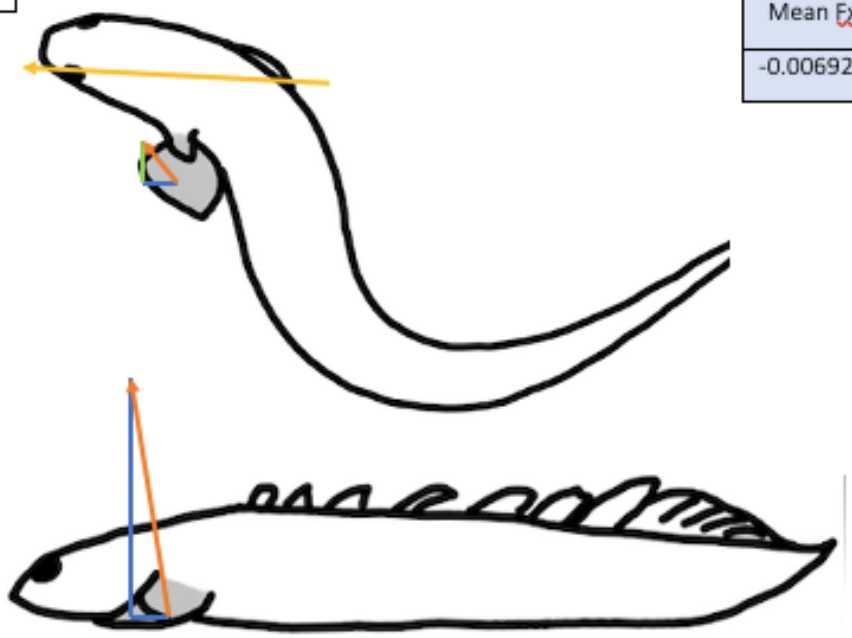

Mean Fx	Mean Fy	Mean Fz
-0.006928	-0.009127	0.041758

C

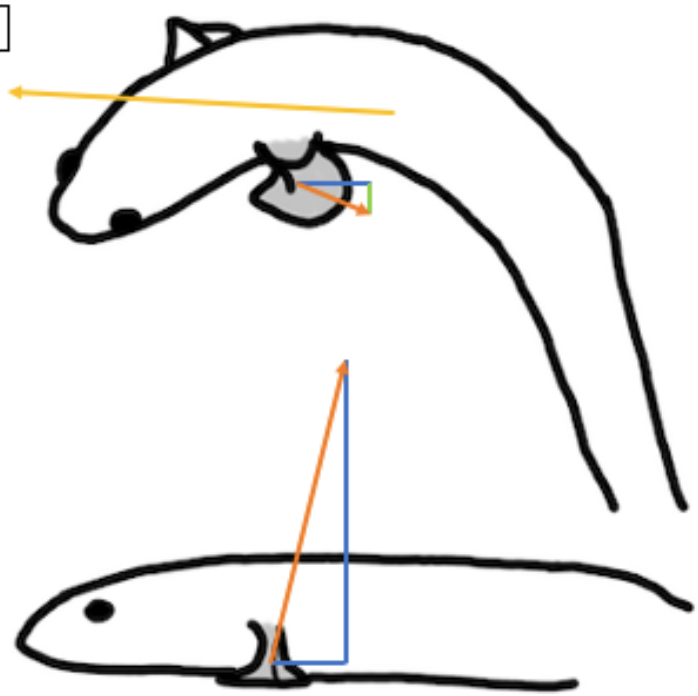

Mean Fx	Mean Fy	Mean Fz
0.011556	0.005348	0.049155

D

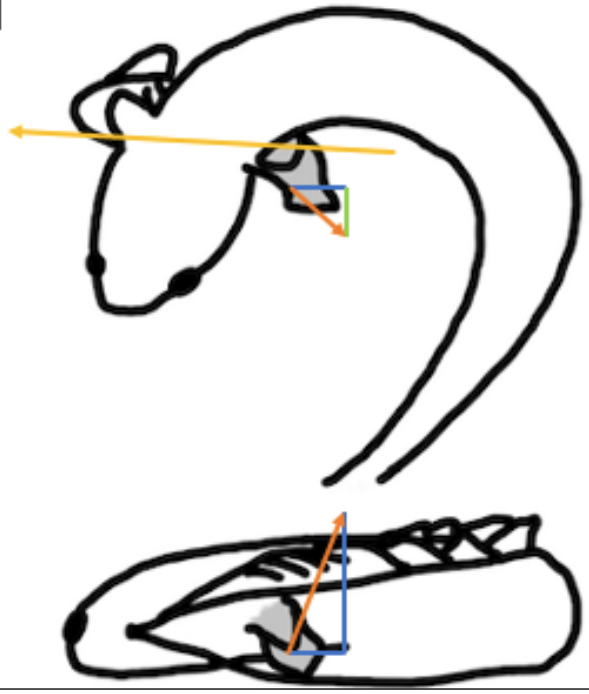

Mean Fx	Mean Fy	Mean Fz
0.009172	0.008044	0.022798

Figure A4 Force trace (A) and illustrations depicting kinematic motion, force components, and predicted resultant force vector (B-D) of step 4 (Table 2.2). Step 4 belongs to the '*variable slip*' subgroup of category *slip.* Slip occurs after 50% stance. Stance duration is depicted as percent stance. Forward (Fx), lateral (Fy), and vertical (Fz) force components are indicated by the red, green, and black lines, respectively. The resultant force magnitude is displayed by the dark blue line. This step contains a single slip phase, indicated by the pink box. Objective kinematic timings are indicated by the vertical lines and include maximum nose elevation (yellow), minimum nose elevation (dark green), minimum abduction angle (light blue), and minimum abduction angular velocity (brown). The kinematic motions illustrated were observed at the midpoint between the timings of interest, and include the onset of loading to the onset of the slip phase (B); the onset of the slip phase to the end of the slip phase (C); the end of the slip phase to the end of the stance (D). The mean magnitudes of forward (Fx) (blue), lateral (Fy) (green), and vertical (Fz) (purple) forces are recorded in the tables. Arrows in orange depict the resultant force vector, and arrows in yellow illustrate the straightest path of motion as determined by the kinematics measured from the CoM.

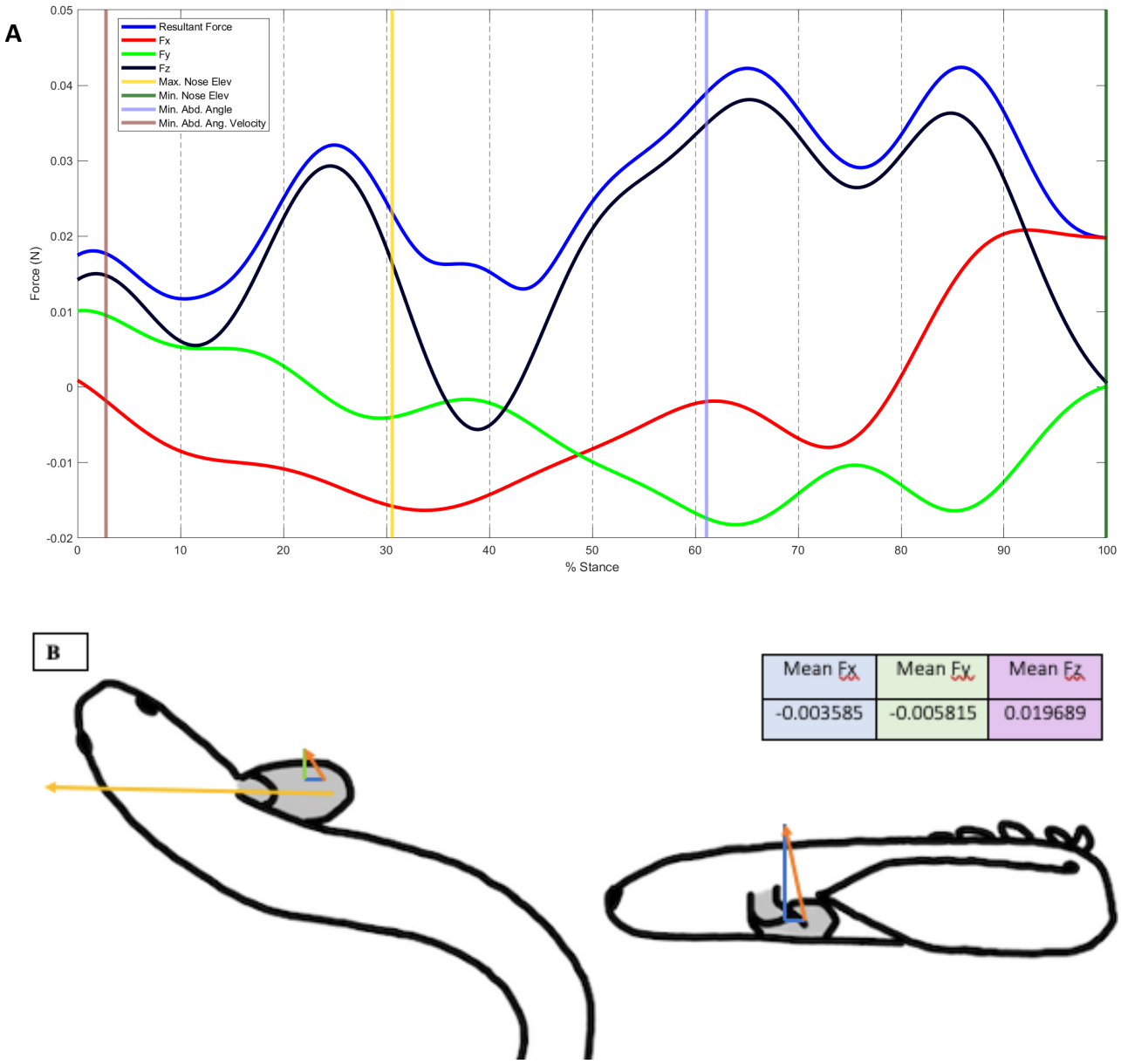

Figure A5 Force trace (A) and illustrations depicting kinematic motion, force components, and predicted resultant force vector (B) of step 5 (Table 2.2). Step 5 belongs to the '*special slip*' subgroup of category *slip.* Stance duration is depicted as percent stance. Forward (Fx), lateral (Fy), and vertical (Fz) force components are indicated by the red, green, and black lines, respectively. The resultant force magnitude is displayed by the dark blue line. This step contains a single slip phase, indicated by the pink box. Objective kinematic timings are indicated by the vertical lines and include maximum nose elevation (yellow), minimum nose elevation (dark green), minimum abduction angle (light blue), and minimum abduction angular velocity (brown). The kinematic motions illustrated were observed at the midpoint between the timings of interest, and include the onset of loading to the end of the stance (B). The mean magnitudes of forward (Fx) (blue), lateral (Fy) (green), and vertical (Fz) (purple) forces are recorded in the tables. Arrows in orange depict the resultant force vector, and arrows in yellow illustrate the straightest path of motion as determined by the kinematics measured from the CoM.

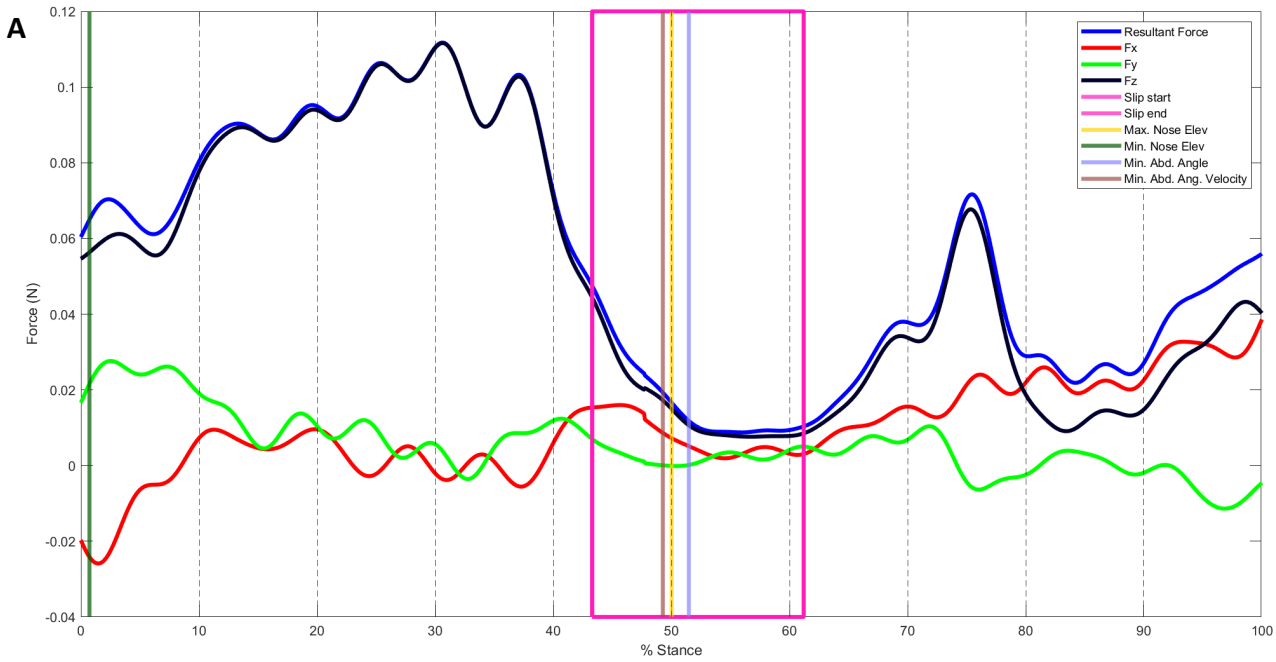

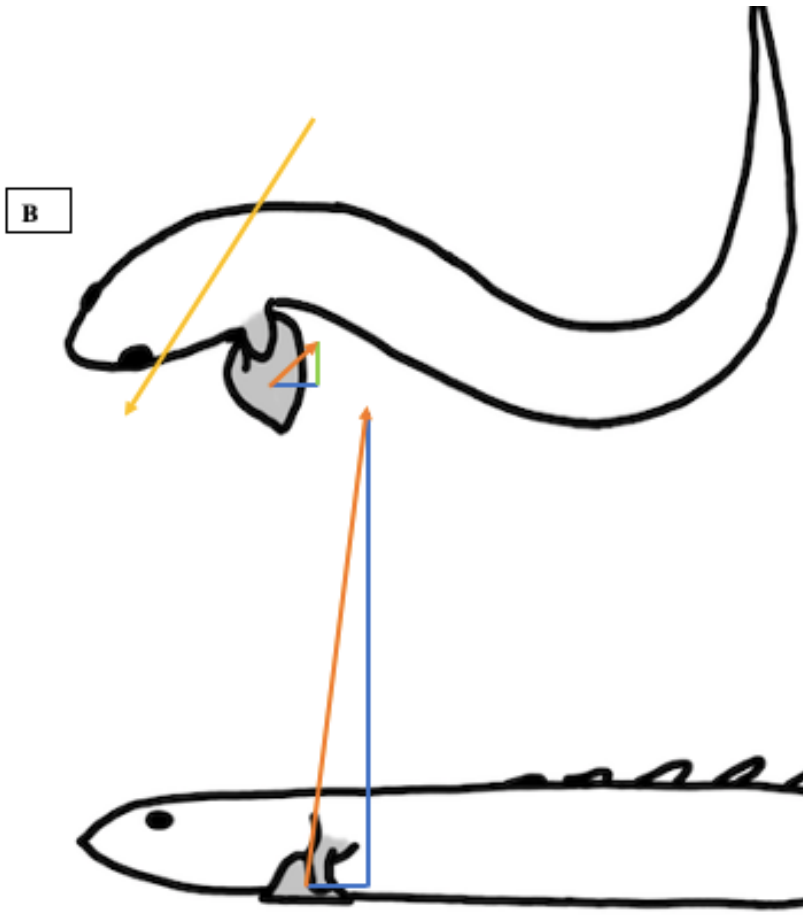

Mean Fx	Mean Fy	Mean Fz
0.009720	-0.00672	0.08399

C

Mean Fx	Mean Fy	Mean Fz
0.006334	0.004549	0.015190

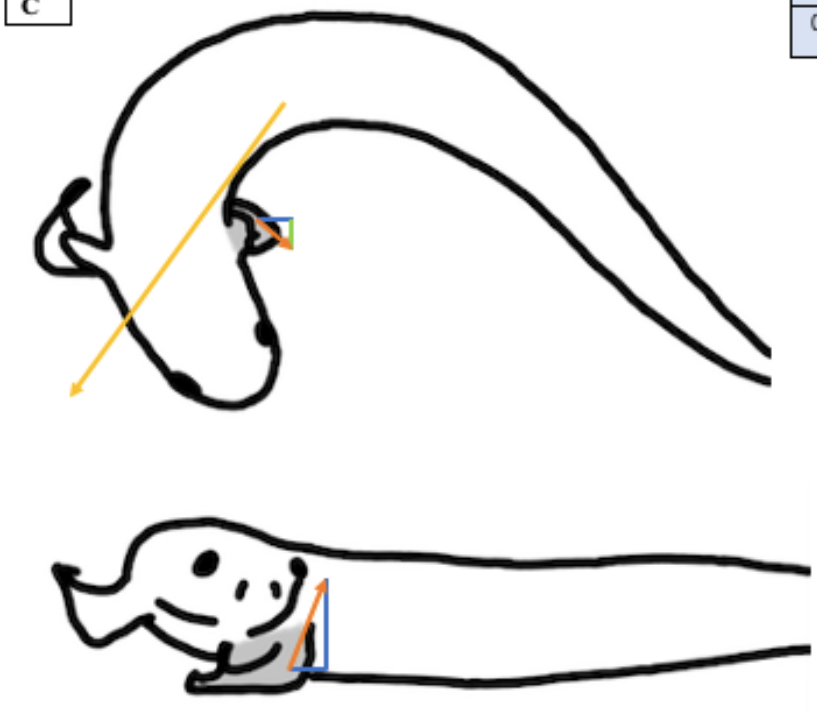

D

Mean Fx	Mean Fy	Mean Fz
0.012437	0.016346	0.027789

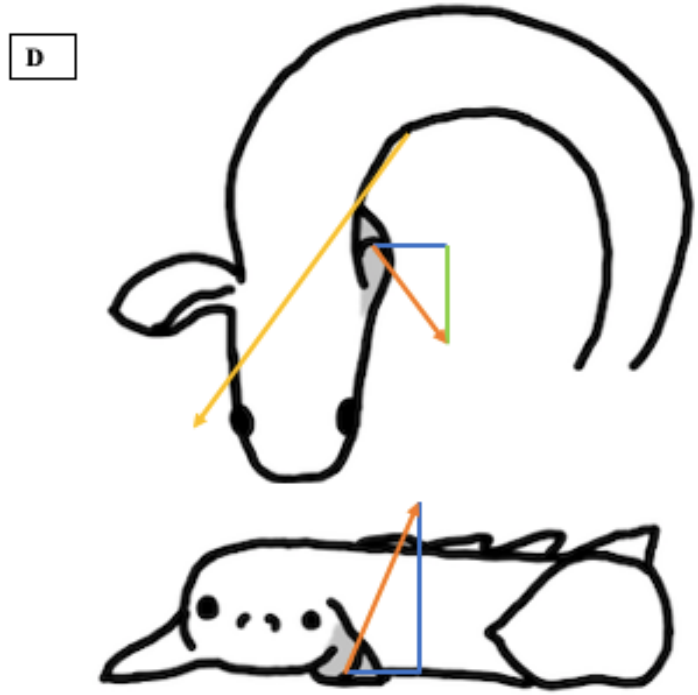

Figure A6 Force trace (A) and illustrations depicting kinematic motion, force components, and predicted resultant force vector (B-D) of step 6 (Table 2.2). Step 6 belongs to the '*mid-slip*' subgroup of category *slip.* Stance duration is depicted as percent stance. Forward (Fx), lateral (Fy), and vertical (Fz) force components are indicated by the red, green, and black lines, respectively. The resultant force magnitude is displayed by the dark blue line. This step contains a single slip phase, indicated by the pink box. Objective kinematic timings are indicated by the vertical lines and include maximum nose elevation (yellow), minimum nose elevation (dark green), minimum abduction angle (light blue), and minimum abduction angular velocity (brown). The kinematic motions illustrated were observed at the midpoint between the timings of interest, and include the onset of loading to the onset of the slip phase (B); the onset of the slip phase to the end of the slip phase (C); the end of the slip phase to the end of the stance (D). The mean magnitudes of forward (Fx) (blue), lateral (Fy) (green), and vertical (Fz) (purple) forces are recorded in the tables. Arrows in orange depict the resultant force vector, and arrows in yellow illustrate the straightest path of motion as determined by the kinematics measured from the CoM.

A

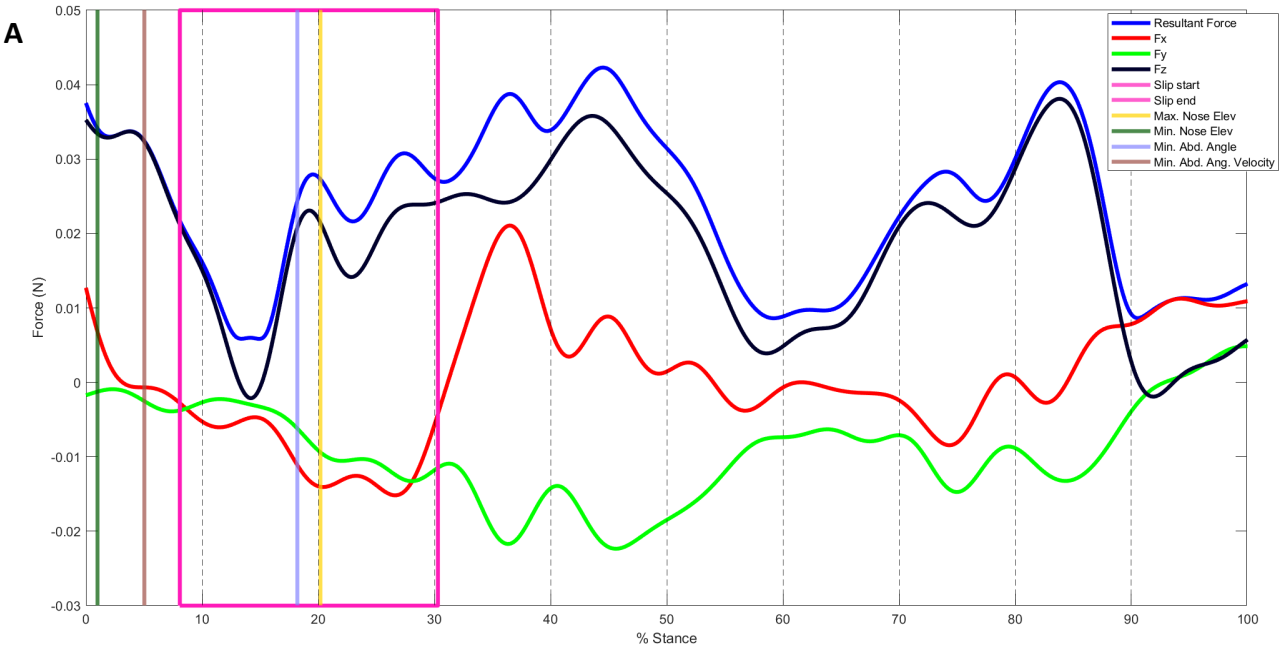

B

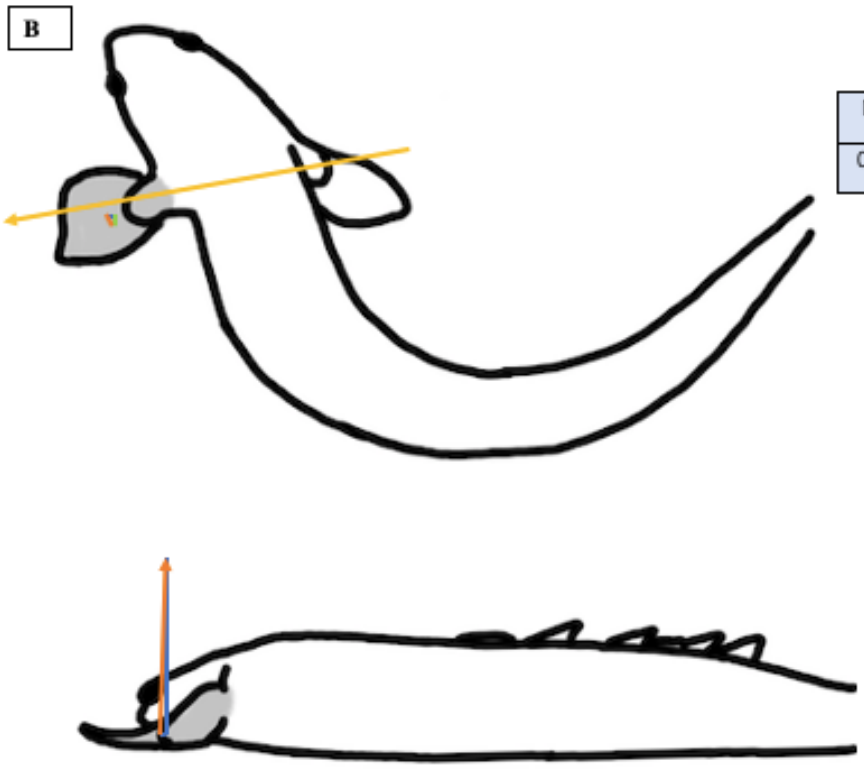

Mean Fx	Mean Fy	Mean Fz
0.000890	0.002387	0.030922

C

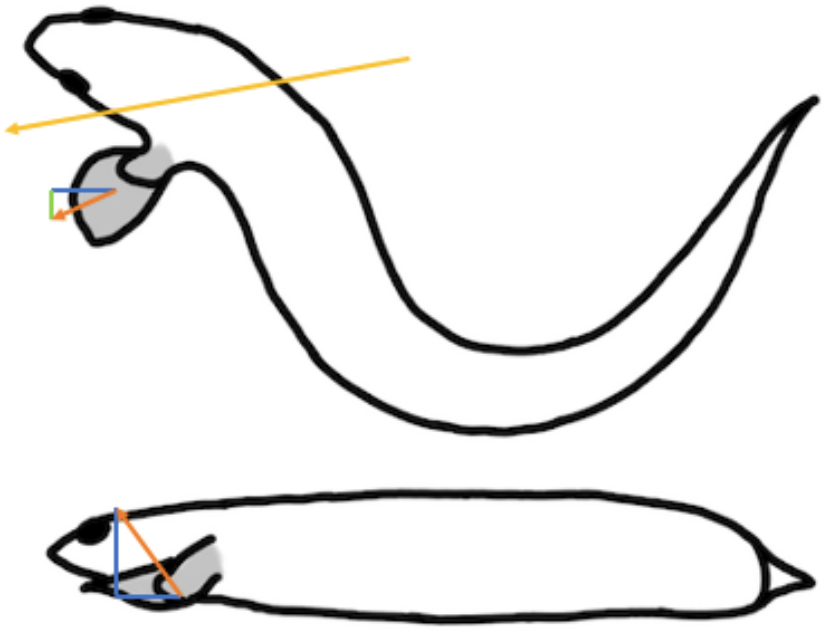

Mean Fx	Mean Fy	Mean Fz
-0.010758	0.00553	0.015078

D

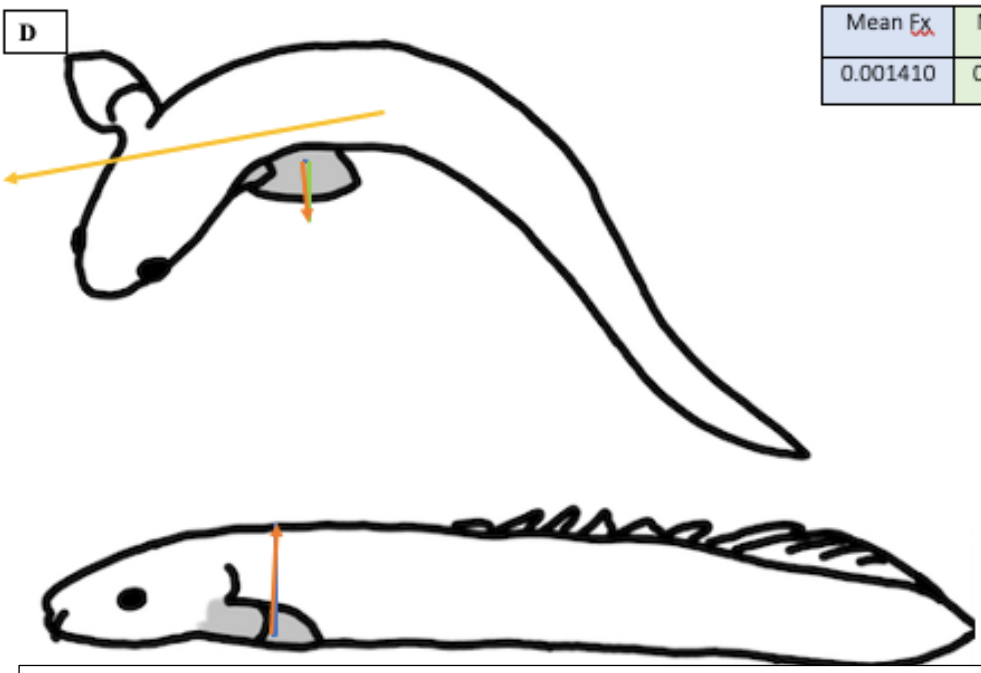

Mean Fx	Mean Fy	Mean Fz
0.001410	0.011117	0.018991

Figure A7 Force trace (A) and illustrations depicting kinematic motion, force components, and predicted resultant force vector (B-D) of step 7 (Table 2.2). Step 7 belongs to the '*variable slip*' subgroup of category *slip.* Slip occurs prior to 50% stance. Stance duration is depicted as percent stance. Forward (Fx), lateral (Fy), and vertical (Fz) force components are indicated by the red, green, and black lines, respectively. The resultant force magnitude is displayed by the dark blue line. This step contains a single slip phase, indicated by the pink box. Objective kinematic timings are indicated by the vertical lines and include maximum nose elevation (yellow), minimum nose elevation (dark green), minimum abduction angle (light blue), and minimum abduction angular velocity (brown). The kinematic motions illustrated were observed at the midpoint between the timings of interest, and include the onset of loading to the onset of the slip phase (B); the onset of the slip phase to the end of the slip phase (C); the end of the slip phase to the end of the stance (D). The mean magnitudes of forward (Fx) (blue), lateral (Fy) (green), and vertical (Fz) (purple) forces are recorded in the tables. Arrows in orange depict the resultant force vector, and arrows in yellow illustrate the straightest path of motion as determined by the kinematics measured from the CoM.

A

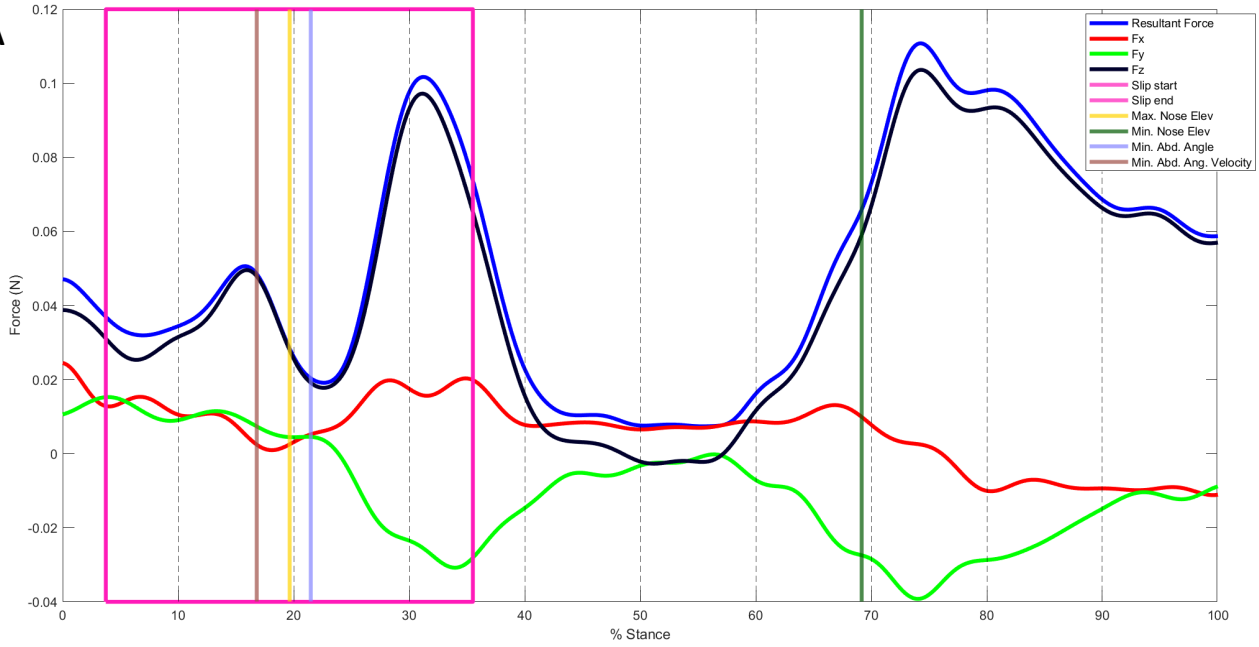

B

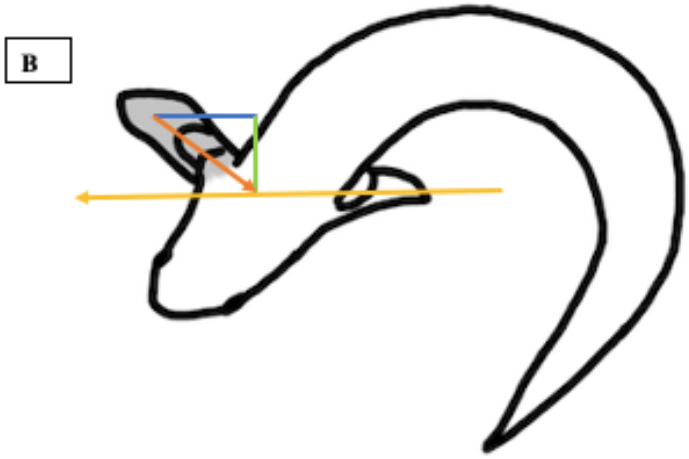

Mean Fx	Mean Fy	Mean Fz
0.018277	0.013468	0.036057

C

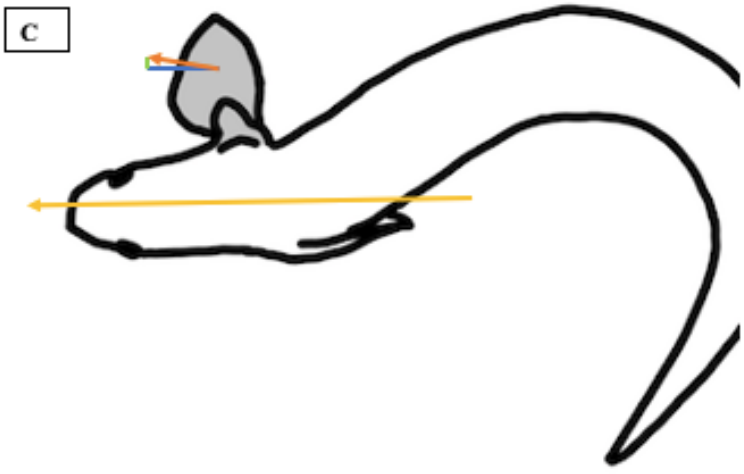

Mean Fx	Mean Fy	Mean Fz
0.011531	-0.002	0.045659

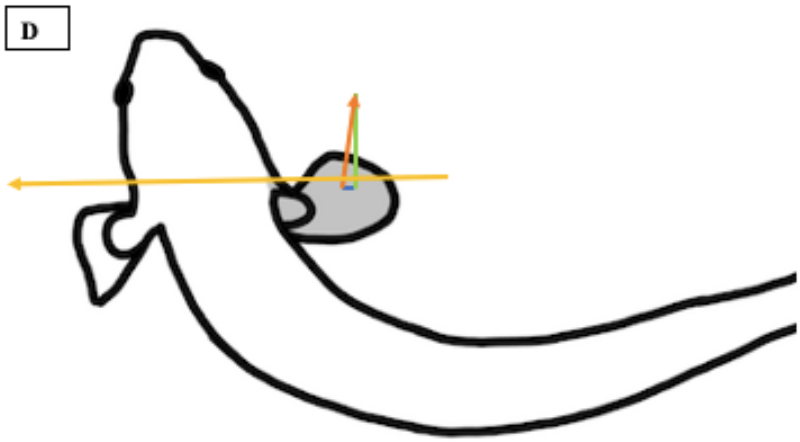

Mean Fx	Mean Fy	Mean Fz
0.002306	-0.01601	0.045376

Figure A8 Force trace (A) and illustrations depicting kinematic motion, force components, and predicted resultant force vector (B-D) of step 8 (Table 2.2). Step 8 belongs to the '*variable slip*' subgroup of category *slip.* Slip occurs prior to 50% stance. Stance duration is depicted as percent stance. Forward (Fx), lateral (Fy), and vertical (Fz) force components are indicated by the red, green, and black lines, respectively. The resultant force magnitude is displayed by the dark blue line. This step contains a single slip phase, indicated by the pink box. Objective kinematic timings are indicated by the vertical lines and include maximum nose elevation (yellow), minimum nose elevation (dark green), minimum abduction angle (light blue), and minimum abduction angular velocity (brown). The kinematic motions illustrated were observed at the midpoint between the timings of interest, and include the onset of loading to the onset of the slip phase (B); the onset of the slip phase to the end of the slip phase (C); the end of the slip phase to the end of the stance (D). The mean magnitudes of forward (Fx) (blue), lateral (Fy) (green), and vertical (Fz) (purple) forces are recorded in the tables. Arrows in orange depict the resultant force vector, and arrows in yellow illustrate the straightest path of motion as determined by the kinematics measured from the CoM.

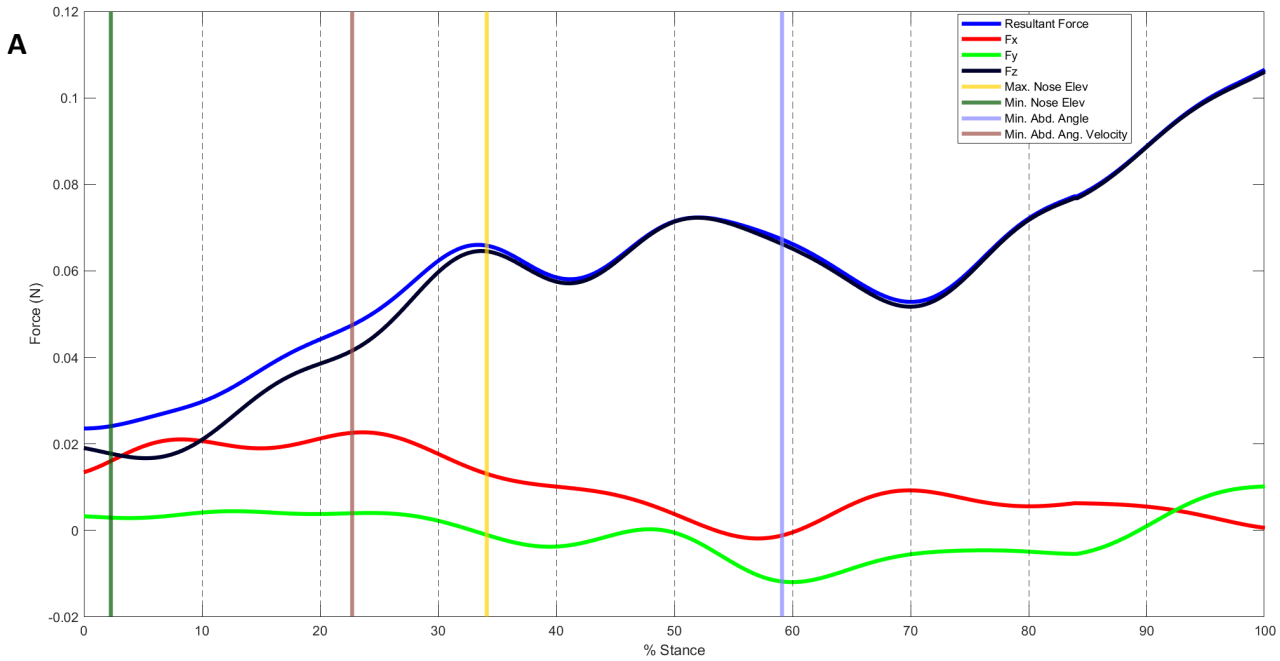

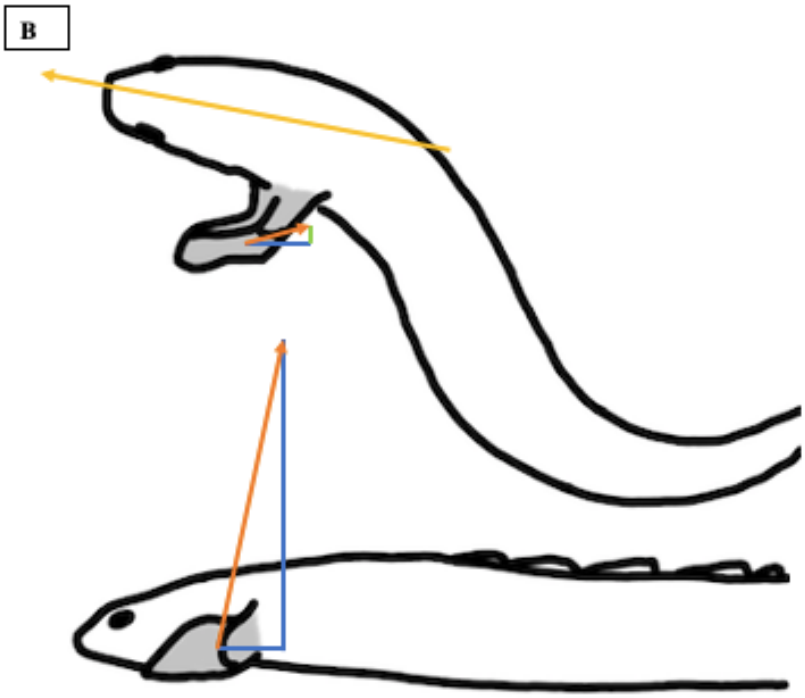

Mean Fx	Mean Fy	Mean Fz
0.011090	-0.002618	0.051633

Figure A9 Force trace (A) and illustrations depicting kinematic motion, force components, and predicted resultant force vector (B) of step 9 (Table 2.2). Step 9 belongs to the '*special slip*' subgroup of category *slip.* Stance duration is depicted as percent stance. Forward (Fx), lateral (Fy), and vertical (Fz) force components are indicated by the red, green, and black lines, respectively. The resultant force magnitude is displayed by the dark blue line. This step contains a single slip phase, indicated by the pink box. Objective kinematic timings are indicated by the vertical lines and include maximum nose elevation (yellow), minimum nose elevation (dark green), minimum abduction angle (light blue), and minimum abduction angular velocity (brown). The kinematic motions illustrated were observed at the midpoint between the timings of interest, and include the onset of loading to the end of the stance (B). The mean magnitudes of forward (Fx) (blue), lateral (Fy) (green), and vertical (Fz) (purple) forces are recorded in the tables. Arrows in orange depict the resultant force vector, and arrows in yellow illustrate the straightest path of motion as determined by the kinematics measured from the CoM.

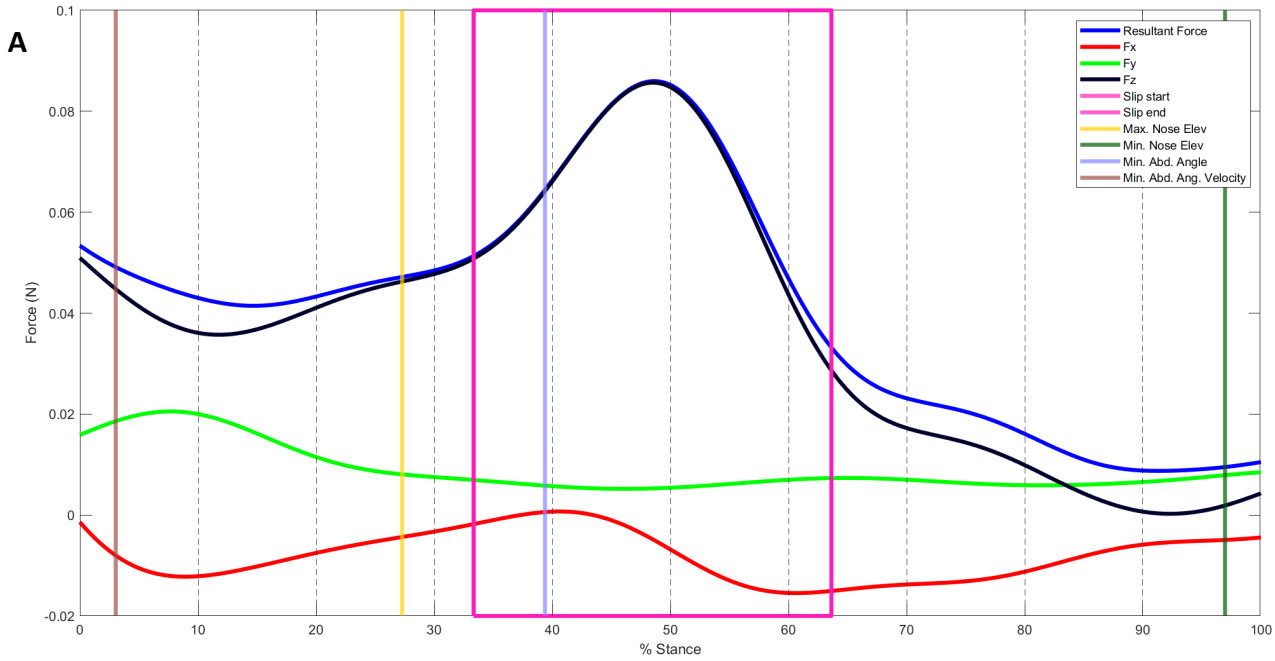

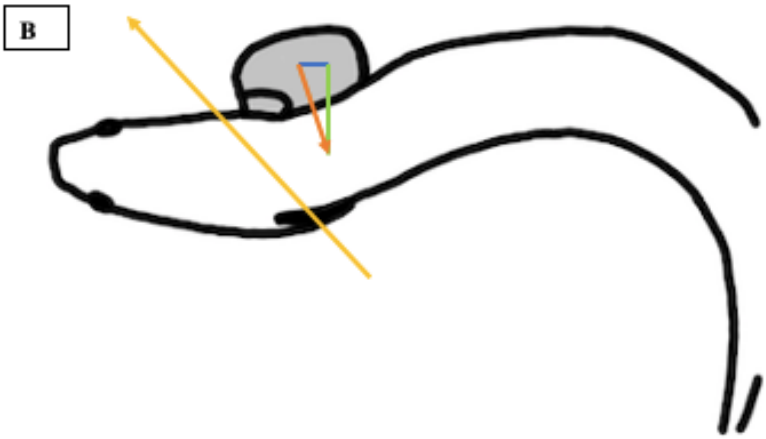

Mean Fx	Mean Fy	Mean Fz
0.004988	0.015085	0.042266

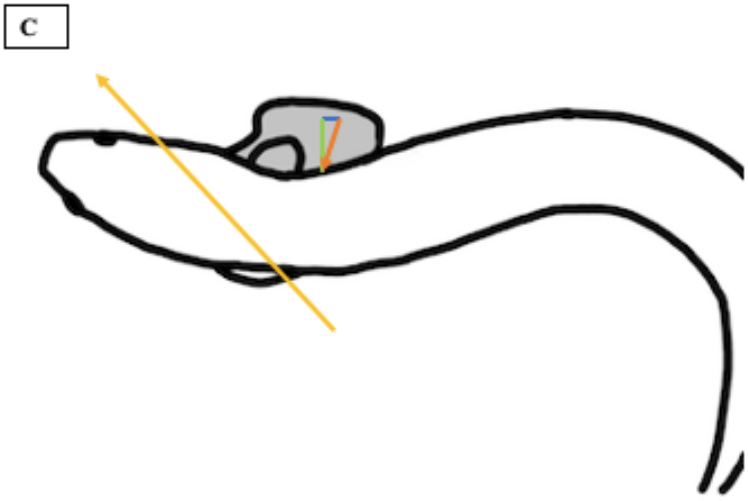

Mean Fx	Mean Fy	Mean Fz
-8.17E-05	0.008942	0.065047

D

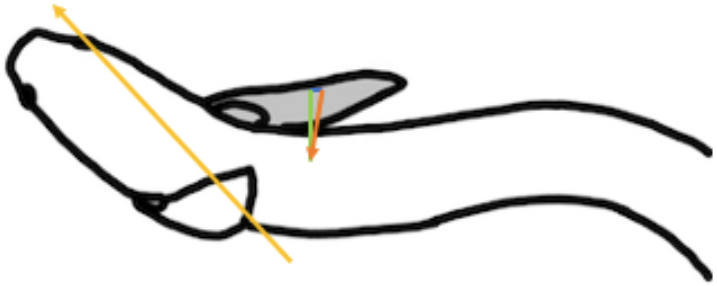

Mean Fx	Mean Fy	Mean Fz
-0.00174	0.011734	0.00935

Figure A10 Force trace (A) and illustrations depicting kinematic motion, force components, and predicted resultant force vector (B-D) of step 10 (Table 2.2). Step 10 belongs to the '*mid-slip*' subgroup of category *slip.* Stance duration is depicted as percent stance. Forward (Fx), lateral (Fy), and vertical (Fz) force components are indicated by the red, green, and black lines, respectively. The resultant force magnitude is displayed by the dark blue line. This step contains a single slip phase, indicated by the pink box. Objective kinematic timings are indicated by the vertical lines and include maximum nose elevation (yellow), minimum nose elevation (dark green), minimum abduction angle (light blue), and minimum abduction angular velocity (brown). The kinematic motions illustrated were observed at the midpoint between the timings of interest, and include the onset of loading to the onset of the slip phase (B); the onset of the slip phase to the end of the slip phase (C); the end of the slip phase to the end of the stance (D). The mean magnitudes of forward (Fx) (blue), lateral (Fy) (green), and vertical (Fz) (purple) forces are recorded in the tables. Arrows in orange depict the resultant force vector, and arrows in yellow illustrate the straightest path of motion as determined by the kinematics measured from the CoM.